CHALMERS

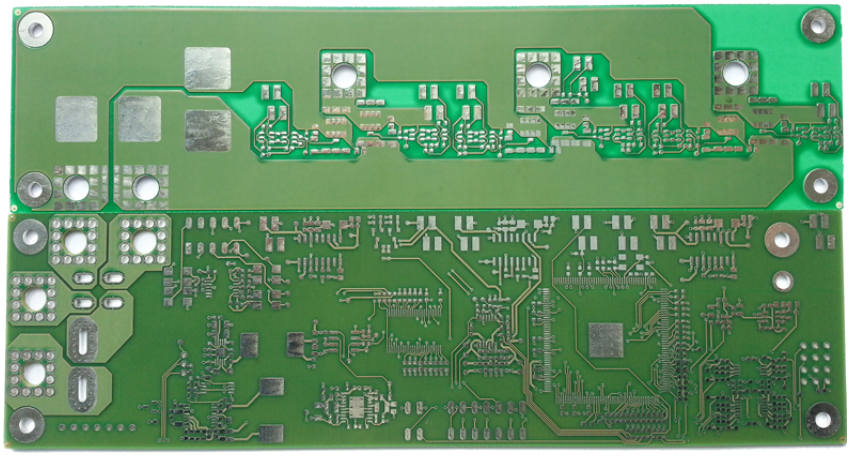

Design, Control and Evaluation of a Prototype Three Phase Inverter in a BLDC Drive System for an Ultra-Light Electric Vehicle

Master's Thesis in Electric Power Engineering

PHILIP LARSSON
NICLAS RASMUSSEN

Department of Energy and Environment
Division of Electric Power Engineering
CHALMERS UNIVERSITY OF TECHNOLOGY
Gothenburg, Sweden 2013
Master's Thesis 2013

MASTER'S THESIS IN ELECTRIC POWER ENGINEERING

Design, Control and Evaluation of a Prototype Three Phase Inverter in a BLDC Drive System for an Ultra-Light Electric Vehicle

Master's Thesis in Electric Power Engineering

PHILIP LARSSON
NICLAS RASMUSSEN

Department of Energy and Environment
Division of Electric Power Engineering
CHALMERS UNIVERSITY OF TECHNOLOGY
Gothenburg, Sweden 2013

Design, Control and Evaluation of a Prototype Three Phase Inverter in a BLDC Drive System for an Ultra-Light Electric Vehicle

PHILIP LARSSON
NICLAS RASMUSSEN

Master's Thesis 2013
ISSN 1652-8557
Department of Energy and Environment
Division of Electric Power Engineering
Chalmers University of Technology
SE-412 96 Gothenburg
Sweden
Telephone: + 46 (0)31-772 1000

Chalmers Reproservice
Gothenburg, Sweden 2013

Design, Control and Evaluation of a Prototype Three Phase Inverter in a BLDC Drive System for an Ultra-Light Electric Vehicle

Master's Thesis in Electric Power Engineering
PHILIP LARSSON
NICLAS RASMUSSEN
Department of Energy and Environment
Division of Electric Power Engineering
Chalmers University of Technology

Abstract

With an evolving vehicle industry there has been an increase in the demand for light electric vehicles. This thesis was conducted in order to gain further knowledge within the field of sensorless BLDC motor control for light electric vehicles.

A three phase inverter was modeled and simulated in Simulink with sensorless BLDC motor control. A requirement specification for a three phase inverter in a drive system for a light electric vehicle was made. From the requirement specification a three phase inverter with two different sensorless control approaches was designed in Altium Designer. The PCB was manufactured and software control algorithms as well as drivers were implemented.

The three phase inverter and its control algorithms were tested and evaluated. The three phase inverter operates successfully with sensorless control at a motor speed above $300RPM$ and fits into a light electric vehicle.

Keywords: BLDC, Design, Drive System, Electric Vehicle,Light Electric Vehicle, Motor Control, PCB, Sensorless

Acknowledgements

We would like to express our appreciation to our supervisor *Peter Dahlin* at QRTECH AB and our examiner *Prof. Torbjörn Thiringer* at Chalmers for their guidance and support throughout this thesis project.

Our coworkers at QRTECH AB also deserve our gratitude for all of their contribution and interest in the project. A special thanks to *Dr. Andreas Magnusson* for his advice and expertise.

We would also like to sincerely thank QRTECH AB for believing in our project and also for the necessary funds and equipment that were provided during the project.

Lastly we would like to thank our girlfriends and family for their support throughout our five years at Chalmers University of Technology.

Gothenburg 2013
Philip Larsson & Niclas Rasmussen

Abbreviations

ADC	Analog-to-Digital Converter
Back-EMF	Back Electromotive Force
BLDC	Brushless DC
CCS	Code Composer Studio
DSP	Digital Signal Processor
EMI	Electromagnetic Interference
GPIO	General Purpose Input/Output
IC	Integrated circuit
JTAG	Joint Test Action Group
LED	Light-Emitting Diode
MOSFET	Metal Oxide Semiconductor Field Effect Transistor
PCB	Printed Circuit Board
PI	Proportional-Integral
PMSM	Permanent Magnet Synchronous Motor
PWM	Pulse-Width Modulation
QEP	Quadrature Encoder Pulse

Contents

1 Introduction

The vehicle industry is rapidly evolving. With many different aspects coinciding such as depletion of fossil fuels, global warming, air pollution, carbon emission reduction legislation and new up and coming battery technologies there is a gradual increase in demand for electric vehicles.

With new technology and a growing market, there are many new kinds of electric vehicle topologies developing. There are also many old vehicle topologies such as bicycles and scooters that are being electrified. The high efficiency of electric drive systems which on average is 85 % compared to the regular drive systems with an internal combustion engine which has an average efficiency of 12-20 % , make it possible to design and build much lighter vehicles with the same power ratings as the heavier vehicles with an internal combustion engine [1], [2].

There are many different electric motor types with different features available. For the application of driving light electric vehicles there are two very similar motor types that stand out from the others because of their high power versus size and weight characteristics, those are the Brushless DC (BLDC) Motor and the Permanent Magnet Synchronous Motor (PMSM).

The battery is only capable of supplying a DC voltage, while the BLDC- and the PMSM- motors require a three phase voltage. In order to solve this problem an interweaving stage that converts the DC voltage to a three phase voltage is required. The conversion is made by a three phase inverter which also adds the ability to control the motor by having the ability to adjust the voltage input to the motor.

1.1 Problem Background

QRTECH is a consultancy firm within the field of hardware and software research and development. With many customers within the automotive sector they have developed a lot of embedded electronic solutions for vehicles. One such solution is a high end controller for a PMSM motor in a light electric vehicle. With already having a solution for the PMSM motor they now want an equivalent solution for a BLDC motor. In order to improve reliability and reduce cost they also want the BLDC controller to be able to operate without a positioning sensor. Having solutions for both of the motor technologies will make it possible to evaluate and provide the best solution depending on the customer needs.

1.2 Purpose

The thesis work was conducted with the purpose of developing a three phase inverter in a BLDC-motor drive system for an ultra-light vehicle. This was done in order to have a prototype platform which can be evaluated and lay as a basis for future decision making and quotation when offering customers new solutions.

Further the thesis was carried out in order to increase theoretical knowledge about BLDC-motor drive systems and in order for the authors to gain knowledge and skill of how to realize the theoretical acquired knowledge into a construction of a real working product.

The main focus of the conducted work was on the realization, construction and software implementation of a three phase inverter which is able to control a BLDC-motor with both sensored- and different sensorless- control strategies.

1.3 Delimitations

In order to be able to complete the project within a timeframe of 20 weeks a few delimitations have been made. Only one sensored and two different sensorless control approaches based on back-EMF measurement will be implemented. Only a rather modest model for the motor simulation will be implemented, with the main purpose of evaluating the sensored and senorless control algorithms. The three phase inverter will only be built and tested in a lab environment during the period of the thesis. Support for a third party solution for wireless control will be implemented instead of adding an additional RF circuit to the three phase inverter.

1.4 Outline

The project started with a theoretical study on previous work within the field. The study kept on throughout the project. A Simulink model of a BLDC drive system was implemented which provided a platform that allowed for experimenting with different sensorless control techniques. Power requirement simulations were also made in order to determine the requirement specifications of the inverter. Once this was done and finalized the work on the circuit layout started. When all components had been selected the design of the Printed Circuit Board (PCB) started simultaneously with the software development for the Digital Signal Processor (DSP). When the PCB had been manufactured and all of the components had been mounted, short circuit tests and circuit functionality tests were conducted. Lastly motor control tests with the different control algorithms were carried out. The results were evaluated and compared to the simulated results.

2 Technical Background

This chapter introduces the BLDC motor and the three phase inverter. It also presents the inverter control techniques such as sensored and sensorless control. The chapter also give some technical background to the gate driver.

2.1 BLDC Motor

The BLDC motor seen in Figure 2.1 is a permanent magnet AC synchronous motor. It is characterized by ideally having a trapezoidal back Electromotive Force (back-EMF) which is presented in Figure 2.2 and that it is driven by square shaped currents. These are the major differences from the PMSM which has a sinusoidal shaped back-EMF and is driven with sinusoidal phase currents. The BLDC motor is usually constructed in single-phase, two-phase and three phase configurations, where the three phase configuration is the most common. Motors with more than three phases can be manufactured but are however uncommon since the number of power electronic devices increases with the number of phases which increases manufacturing cost [3].

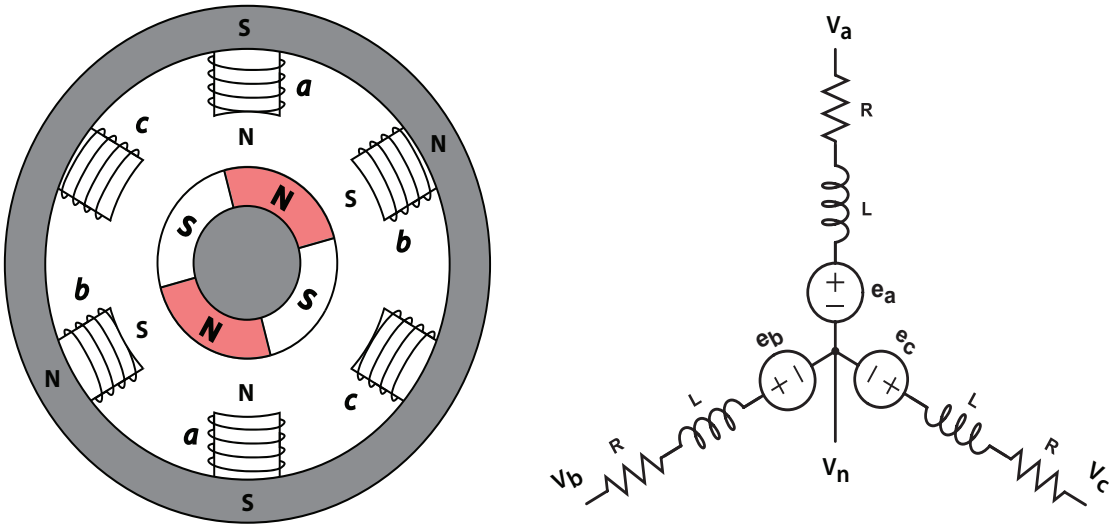

Figure 2.1: A three phase BLDC motor with its circuit diagram

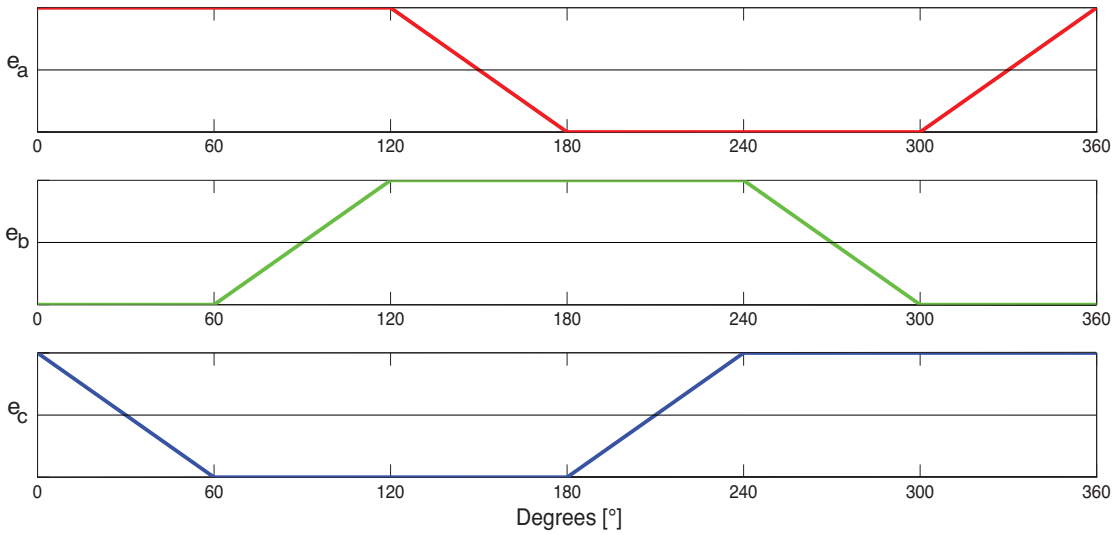

Figure 2.2: Ideal back-EMF voltages , e_a, e_b and e_c of the BLDC motor

The stator is made out of stacked steel laminations and is constructed in a very similar way to that of the induction motor. The rotor is made out of permanent magnet pairs with the north pole and south pole in consecutive order. Since it is a synchronous motor, the stator and rotor rotate at the same frequency. This means that there is no slip between the stator and rotor in the BLDC motor which is the case for the induction motor. The three phase BLDC motor is driven by applying a positive current to one of the motor phases and a negative current to another while having no current going through the third phase leaving it at floating potential. Since torque is produced by the interaction between the field generated in the stator and by the permanent magnets on the rotor, the motor starts to rotate. To keep the permanent magnets of the rotor from aligning with the stator in a static condition, the current through the stator which gives rise to the magnetic field needs to be commutated in a specific way. The current commutation is controlled so that the rotor field keeps trying to align with the stator field and thereby the motor continues to rotate. The current is switched in six different commutation steps for each electrical rotation. The BLDC-motor in comparison to a brushed DC motor has a lot of advantages which are presented in Table 2.1. The major disadvantage of the BLDC motor is that it needs a more advanced controller in order for it to operate [4].

Table 2.1: The BLDC Motor Compared to the Brushed DC Motor [4], [5]

Property	BLDC Motor	Brushed DC Motor
Maintenance	Low rate of maintenance required.	The brushes need consistent maintenance.
Speed Range	A very wide speed range since there are no mechanical brushes that limits the speed at higher RPM.	Medium. This is mainly due to that there is a mechanical limitation which is caused by the increased wearing of brushes at higher speeds.
Power Versus Size	Very high because of the very good thermal characteristics. This is because the windings are located in the stator, which is connected to the case, which in turn gives a better heat dissipation.	Moderate to Low. The armature current will increase the temperature in the air gap which limits the output power.
Rotor Inertia	Low. The permanent magnets are lighter than regular rotor windings made out of copper.	Higher since the copper weigh more than permanent magnets.
Efficiency	Very high, since there are no copper losses in any rotor windings.	Lower because of the voltage drop in the brushes.
Lifespan	Very long.	Shorter since the brushes will wear out.
Torque Versus Speed Characteristics	Flat.	Flat until reaching higher speeds where friction will increase due to the brushes.
Electromagnetic Interference	Low.	The brushes will generate noise.
Commutation	Electrical commutation inside an inverter.	Mechanical commutation in the brushes.
Control	Requires digital controlled inverter in order to run.	Simple control, can run at fixed speed without the need of a controller, inexpensive.
Manufacturing Cost	Easy to manufacture, however the material cost is high due to the high material cost of the permanent magnets.	More complex to manufacture because of the mechanical brushes. Has a cheaper material cost, since no expensive permanent magnets are required.

2.2 Motor Control with a Three Phase Inverter

A three-phase inverter technically is three sections of half bridge inverters. Each inverter stage is able to produce an output 120° displaced with respect to the other. The half-bridge sections are usually referred to as legs with a three phase inverter consisting of three legs, one for each phase, see Figure 2.3.

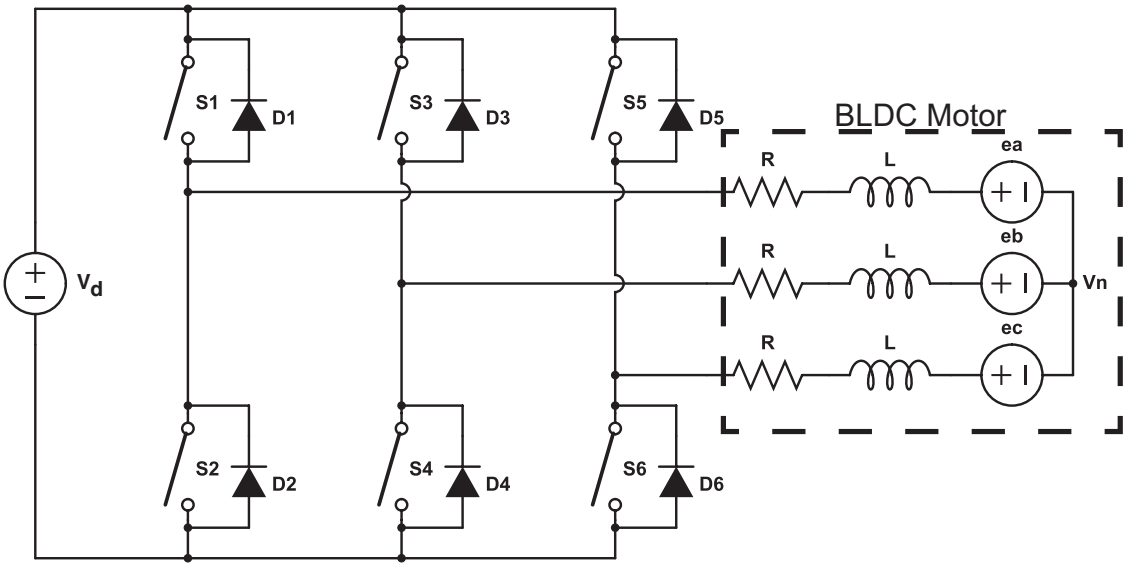

Figure 2.3: Three phase inverter with a connected BLDC motor

Since the BLDC motor is characterized by only having two phases energized at the same time, only three out of the six switches of the inverter will be active for each switching sequence. One of the three phase inverter legs will be Pulse Width Modulated (PWM) with the lower transistor inversely switched with respect to the upper transistor and in another leg the lower transistor will conduct. This is performed in a periodical six-step commutation sequence, which can be seen in Table 2.2 [6], [7]. If reverse rotation is desired the sequences needs to be reversed as well.

Table 2.2: Switching sequences

Sequence	Rotor position, θ_e	Switching		Phase current		
		PWM	ON	A	B	C
1	$0-60°$	Q1,$\overline{Q2}$	Q4	DC+	DC-	OFF
2	$60-120°$	Q1,$\overline{Q2}$	Q6	DC+	OFF	DC-
3	$120-180°$	Q3,$\overline{Q4}$	Q6	OFF	DC+	DC-
4	$180-240°$	Q3,$\overline{Q4}$	Q2	DC-	DC+	OFF
5	$240-300°$	Q5,$\overline{Q6}$	Q2	DC-	OFF	DC+
6	$300-360°$	Q5,$\overline{Q6}$	Q4	OFF	DC-	DC+

Unlike brushed DC motors where a commutator and brushes are used to change current polarity the BLDC motor usually use semiconductors with feedback from the rotor position to change current polarity. Hence to be able to know when to

commutate each phase of the BLDC motor the position needs to be known. This could be done in many different ways, either by sensored or sensorless techniques. During the last decade many new sensorless methods have been developed. There are mainly two reasons for this, the high cost of positioning sensors and that of increased reliability since sensors can fail during operation. In certain applications such as flooded compressors or pumps it is not even possible to use sensors. There are however also drawbacks to the different sensorless techniques, for example that it is generally hard to control the motor at low speeds [4].

2.2.1 Sensored Motor Control

Hall effect sensors are normally used in order to determine the motor rotor position. They can either be mounted on the surface of the stator or be embedded into the stator. Typically three hall sensors are mounted with a 120° phase shift between them. These make it possible to determine in which of the six sequences the rotor currently is in and when to commutate [8].

Other sensors such as encoders and resolvers could however also be used. The encoder transmits two digital pulses and measures the distance and time between them which makes it possible to calculate the speed and the angle of the rotor. Resolvers produce a sinusoidal and a cosinusoidal signal which both are used in order to indicate the position within a 360° revolution [9].

2.2.2 Sensorless Motor Control

There are many different sensorless control techniques that can be implemented for a BLDC motor. One method in order to estimate the rotor position is by measuring the back-EMF of the motor. This can effortlessly be done by measuring the terminal voltages of the phases. The back-EMF voltage is generated in the non-driven winding by the permanent magnets when the motor rotate. The magnitude of the voltage is proportional to the rotor speed and for this reason it is difficult to control the motor at low speed. The back-EMF method can be implemented since one of the phases is not energized during each of the commutation sequences [6]. For the case when phase C is the phase that is not fed by the inverter the phase voltages will be

$$V_a = Ri_a + L\frac{di_a}{dt} + e_a + V_n \tag{2.1}$$

$$V_b = Ri_b + L\frac{di_b}{dt} + e_b + V_n \tag{2.2}$$

$$V_c = e_c + V_n \tag{2.3}$$

where V_n is the motor neutral voltage with reference to ground. Since current only flows through the motor from phase A to phase B the current in those phases will be equal but opposite. This gives

$$i_a = -i_b \tag{2.4}$$

By adding (2.1)-(2.4) the following expression is obtained

$$V_a + V_b + V_c = e_a + e_b + e_c + 3V_n \tag{2.5}$$

and from the back-EMF waveforms shown in Figure 2.4 it can realized that the sum of the back-EMFs at a zero crossing point is equal to zero. This reduces (2.5) to

$$\frac{V_a + V_b + V_c}{3} = V_n \tag{2.6}$$

and is used in order to determine when the back-EMF crosses the virtual ground of the motor in each phase.

The next step in the commutation sequence occurs 30° after the zero crossing point which also can be seen in Figure 2.4. So by measuring the phase potentials and implementing an algorithm it is possible to estimate the rotor position and the needed switching state in the sequence.

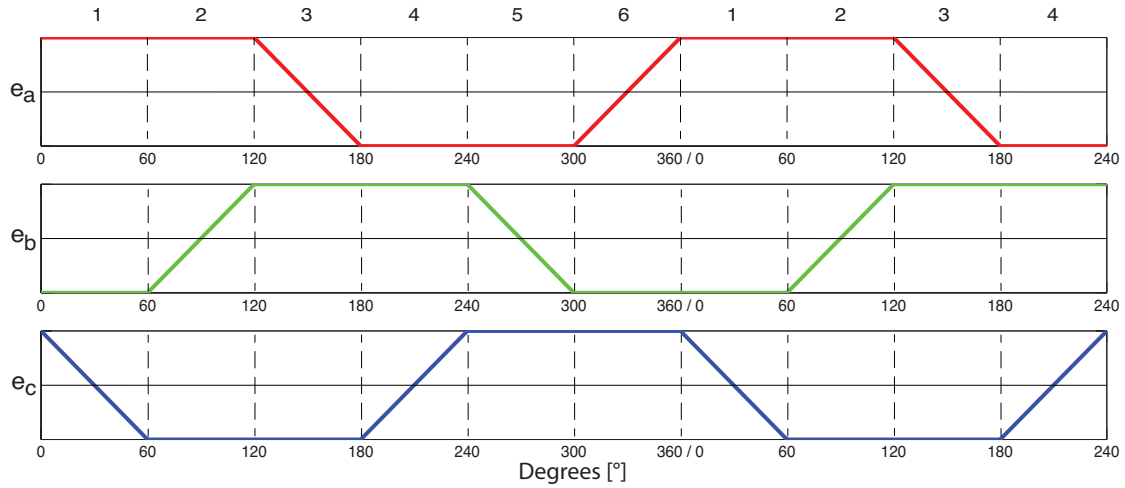

Figure 2.4: Ideal back-EMF voltages

2.3 Gate Driver

The N-channel Metal Oxide Semiconductor Field Effect Transistor (MOSFET) needs a gate-source voltage in the magnitude of $10 - 12\ V$ in order to fully behave like a switch. This imposes a problem for the upper switch in each of the half bridge sections of the three phase inverter since the source potential will be equal to the input voltage. One way to solve this problem is by using a gate driver with a bootstrap capacitor. This method is quite simple and effective but it has certain limitations [10]. One such limitation is that the duty cycle and the on-time of the MOSFET cannot be too large due to the fact that the bootstrap capacitor recharges during the off-time of the MOSFET. If a very high duty cycle is required a charge pump circuit which makes it possible to recharge the capacitor during the on-time of the transistor can be implemented [11].

The gate driver is used as a power amplifier between the Integrated Circuit (IC) which is acting as a controller, such as a DSP, and the power MOSFET. It makes sure that there is sufficient current in order to charge and recharge the gate capacitance of the MOSFET. A typical connection of a gate driver IC can be seen in Figure 2.5, where CB is the bootstrap capacitor. A bootstrap circuit consists of a capacitor and a diode. The capacitor is charged through the diode when the lower MOSFET is on, which means that V_s is connected to ground. When the upper MOSFET should be turned on the lower MOSFET is turned off and the negative side of the capacitor is then connected to V_s and the positive side is connected to the gate, VOA, through the gate driver circuit. This will provide the needed gate voltage to turn on the upper MOSFET [11].

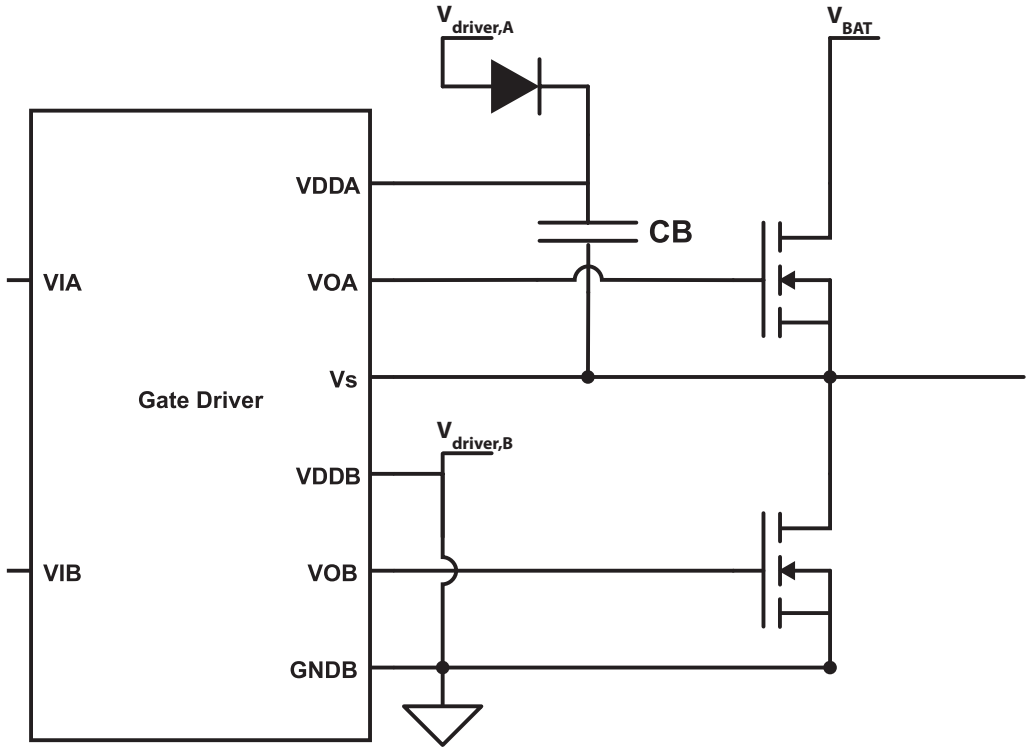

Figure 2.5: A typical connection of a high-side/low-side gate driver IC with a bootstrap capacitance, CB

The value of the bootstrap capacitor is proposed to be

$$C_{BS,min} = \frac{\Delta Q_{BS,min}}{\Delta V_{BS,max}} \tag{2.7}$$

where $\Delta Q_{BS,min}$ is the minimum charge the capacitor must supply to turn the MOSFET on and $\Delta V_{BS,max}$ is the maximum allowed voltage dip in the capacitor. The minimum charge is calculated by

$$\Delta Q_{BS,min} = Q_G + Q_{LS} + \frac{I_{QBS,max}}{f_s} + \frac{I_{CBS,leak}}{f_s} \tag{2.8}$$

where Q_G is the required gate charge of the MOSFET, Q_{LS} is the level shift charge required by the driver, $I_{QBS,max}$ is the maximum current that is required by the floating section of the driver, $I_{CBS,leak}$ is the leakage current of the bootstrap capacitor and f_s is the switching frequency. The maximum allowed voltage dip is calculated by

$$\Delta V_{BS,max} = \big(V_{DD} - V_f - V_{LS}\big) - V_{GS,min} \tag{2.9}$$

where V_{DD} is the positive supply voltage, V_f is the voltage drop across the bootstrap diode, V_{LS} is the voltage drop across the lower MOSFET and $V_{GS,min}$ is the minimum required gate-source voltage to turn the MOSFET on. $\big(V_{DD} - V_f - V_{LS}\big)$ is the voltage which the capacitor will be charged to.

In order to have a safety margin from this worst case voltage drop the rule of thumb is that the value obtained in (2.7) is multiplied by 15.

3 Modeling and Simulation

In this chapter the motor model and three phase inverter model are introduced. The models are used to simulate the three phase inverter with a BLDC motor in Simulink. In order to define the design framework a requirement specification was formulated.

3.1 BLDC Motor Model

The mathematical model which was used in order to simulate the BLDC motor consisted of an electrical- and a mechanical-part.

If the mutual inductance is assumed to be constant when the motor rotates the voltage in the stator windings can be expressed as

$$V_a = Ri_a + L\frac{di_a}{dt} + e_a \tag{3.1}$$

$$V_b = Ri_b + L\frac{di_b}{dt} + e_b \tag{3.2}$$

$$V_c = Ri_c + L\frac{di_c}{dt} + e_c \tag{3.3}$$

where V_a, V_b, V_c is the terminal voltage, R is the stator resistance, i_a, i_b, i_c is the stator phase current, L is the stator inductance and e_a, e_b, e_c is the induced back-EMF in each phase.

The trapezoidal back-EMF in a 3-phase BLDC motor is related to a function of rotor position where each phase is 120° phase shifted and given by

$$e_a = K_e\omega_m F(\theta_e) \tag{3.4}$$

$$e_b = K_e\omega_m F(\theta_e + \frac{2\pi}{3}) \tag{3.5}$$

$$e_c = K_e\omega_m F(\theta_e + \frac{4\pi}{3}) \tag{3.6}$$

where K_e is the motor back-EMF constant, ω_m is the rotor speed, θ_e is the electrical rotor angle and F is the trapezoidal shape reference function with respect to rotor position, with boundaries between +1 and -1.

$$F(\theta_e) = \begin{cases} 1 & 0 \leq \theta_e < \frac{2\pi}{3} \\ 1 - \frac{6}{\pi}(\theta_e - \frac{2\pi}{3}) & \frac{2\pi}{3} \leq \theta_e < \pi \\ -1 & \pi \leq \theta_e < \frac{5\pi}{3} \\ -1 + \frac{6}{\pi}(\theta_e - \frac{5\pi}{3}) & \frac{5\pi}{3} \leq \theta_e < 2\pi \end{cases} \tag{3.7}$$

Since there is no wire connected to the motor's neutral phase the phase-to-phase voltage equations are used in order to control the motor. The phase-to-phase voltage equations are derived from (3.1)-(3.3) and turn into

$$V_{ab} = R(i_a - i_b) + L\frac{d}{dt}(i_a - i_b) + e_{ab} \tag{3.8}$$

$$V_{bc} = R(i_b - i_c) + L\frac{d}{dt}(i_b - i_c) + e_{bc}. \tag{3.9}$$

Only (3.8) and (3.9) will be needed since the third phase-to-phase voltage will be a combination of the other two. In order to obtain the state space model (3.8) and (3.9) are combined together with the fact that the sum of all phase currents simultaneously will be zero, $i_a + i_b + i_c = 0$, which gives

$$\frac{di_a}{dt} = -\frac{R}{L}i_a + \frac{2}{3L}(V_{ab} - e_{ab}) + \frac{1}{3L}(V_{bc} - e_{bc}) \tag{3.10}$$

$$\frac{di_b}{dt} = -\frac{R}{L}i_b - \frac{1}{3L}(V_{ab} - e_{ab}) + \frac{1}{3L}(V_{bc} - e_{bc}) \tag{3.11}$$

The last of the currents is given by the following equation

$$i_c = -i_a - i_b \tag{3.12}$$

The total electric torque produced by the BLCD motor is the summation of the electric torque produced in each phase.

$$T_e = T_a + T_b + T_c = \frac{e_a i_a + e_b i_b + e_c i_c}{\omega_m} \tag{3.13}$$

The mechanical part is represented by the following equation

$$T_e = \beta\omega_m + J\frac{d\omega_m}{dt} + T_L \tag{3.14}$$

where B is a constant of friction, J is the rotor and coupled shaft inertia and T_L is the load torque.

The Simulink model of the ideal BLDC motor is then obtained by (3.10)-(3.12) together withs (3.13) and (3.14).

3.2 Three Phase Inverter Model

Simulating an inverter of a BLDC motor in Simulink has been proven to be a bit difficult due to the complications in simulating the freewheeling diodes. Baldursson [12] proposed a method in order to solve this problem. It simulates the freewheeling diodes as voltage sources in order to make sure that the freewheeling currents only can flow in one direction. The diode model is implemented into a Matlab function. This function is then implemented in Simulink which uses the phase currents, back-EMF, rotor position and dc-source voltage as inputs. For each of the different position intervals showed in Table 2.2 the function will output different voltages to the motor.

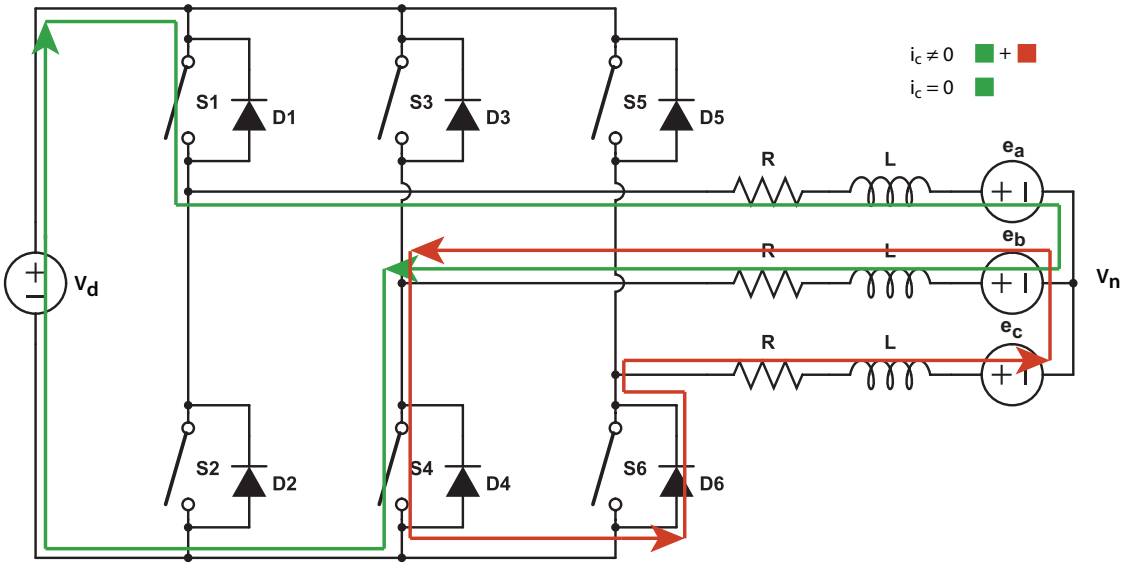

Figure 3.1: Current path through the three phase inverter for the interval $0-60°$ where the green path represents the current through the active phases and the red path represents the commutating current from the previous switching sequence

Figure 3.1 represent the interval between $0-60°$ where the different output voltages can be derived for the case when there is a current through the freewheeling diode, in this case D6. When the current through the freewheeling diode is zero, blocking, the diode will be represented by a voltage source, in this case V_{bc}, to make sure that the current only flows in one direction. A simplified case can be seen in Figure 3.2 for the interval between $0-60°$.
When $i_c \neq 0$ the three phase-to-phase voltages can easily be derived from Figure 3.1

$$V_{ab} = V_d \tag{3.15}$$

$$V_{bc} = 0 \tag{3.16}$$

$$V_{ca} = -V_d \tag{3.17}$$

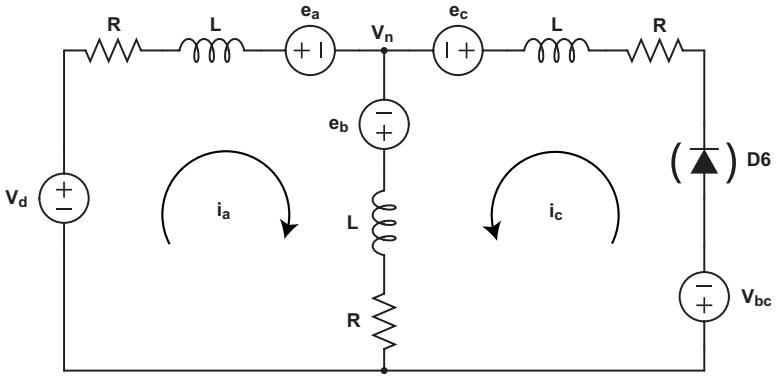

Figure 3.2: Circuit topology for the case $0-60°$, where V_{bc} represents the voltage over the reversed biased diode, $D6$

When $i_c = 0$ Kirchhoff's voltage law are applied around each mesh in Figure 3.2 to obtain the three phase-to-phase voltages

$$V_d - Ri_a - L\frac{di_a}{dt} - e_a + e_b - L\frac{d(i_a + i_c)}{dt} - R(i_a + i_c) = 0 \tag{3.18}$$

$$-V_{bc} - Ri_c - L\frac{di_c}{dt} - e_c + e_b - L\frac{d(i_a + i_c)}{dt} - R(i_a + i_c) = 0 \tag{3.19}$$

when $i_c = 0$

$$V_d - 2Ri - e_a - 2L\frac{di}{dt} - e_a + e_b = 0 \tag{3.20}$$

$$-V_{bc} - e_c + e_b - L\frac{di}{dt} - Ri = 0 \tag{3.21}$$

(3.20) and (3.21) gives

$$V_{bc} = \frac{1}{2}(-V_d + e_a + e_b - 2e_c) \tag{3.22}$$

So the three phase-to-phase voltages will be

$$V_{ab} = V_d \tag{3.23}$$

$$V_{bc} = \frac{1}{2}(-V_d + e_a + e_b - 2e_c) \tag{3.24}$$

$$V_{ca} = \frac{1}{2}(-V_d - e_a - e_b + 2e_c) \tag{3.25}$$

The same derivation is applied for the rest of the switching sequences and result in Table 3.1. The calculations for the five remaining cases are presented in Appendix A.

Table 3.1: Inverter output voltages

θ_e	Diode current	V_{ab}	V_{bc}	V_{ca}
$0-60°$	$i_c \neq 0$	V_d	0	$-V_d$
	$i_c = 0$	V_d	$\frac{1}{2}(-V_d + e_a + e_b - 2e_c)$	$\frac{1}{2}(-V_d - e_a - e_b + 2e_c)$
$60-120°$	$i_b \neq 0$	0	V_d	$-V_d$
	$i_b = 0$	$\frac{1}{2}(V_d + e_c + e_a - 2e_b)$	$\frac{1}{2}(V_d - e_c - e_a + 2e_b)$	$-V_d$
$120-180°$	$i_a \neq 0$	$-V_d$	V_d	0
	$i_a = 0$	$\frac{1}{2}(-V_d - e_b - e_c + 2e_a)$	V_d	$\frac{1}{2}(-V_d + e_b + e_c - 2e_a)$
$180-240°$	$i_c \neq 0$	$-V_d$	0	V_d
	$i_c = 0$	$-V_d$	$\frac{1}{2}(V_d + e_a + e_b - 2e_c)$	$\frac{1}{2}(V_d - e_a - e_b + 2e_c)$
$240-300°$	$i_b \neq 0$	0	$-V_d$	V_d
	$i_b = 0$	$\frac{1}{2}(-V_d + e_c + e_a - 2e_b)$	$\frac{1}{2}(-V_d - e_c - e_a + 2e_b)$	V_d
$300-360°$	$i_a \neq 0$	V_d	$-V_d$	0
	$i_a = 0$	$\frac{1}{2}(V_d - e_b - e_c + 2e_a)$	$-V_d$	$\frac{1}{2}(V_d + e_b + e_c - 2e_a)$

3.3 Requirement Specification

In order to be able to define a framework for the design criterias of the drive system, such as selection of motor, battery technology and the controller specifications, several models and simulations are required. This needs to be done in order to be able to determine the maximum power, speed, current and voltage as well as the total energy needed for the system. Vehicle dynamics can be modeled in intricate ways, however a longitudinal vehicle road serves well for the purpose of determine the maximum limits of a drive system [13].

3.3.1 Longitudinal Vehicle Dynamic Model

In the longitudinal vehicle dynamic model the vehicle and the forces acting upon it can be described with a free body diagram represented in Figure 3.3. In this model the vehicle's center of mass where all of its weight is concentrated is used as a reference point. The forces that will be taken into account for are the force of gravity, the force of friction due to the rolling resistance exerted by the road and wheel interaction, the aerodynamic drag force and the propulsive force exerted by the electric motor at the wheel. The sum of the forces in the system will determine acceleration or deceleration of the vehicle [13].

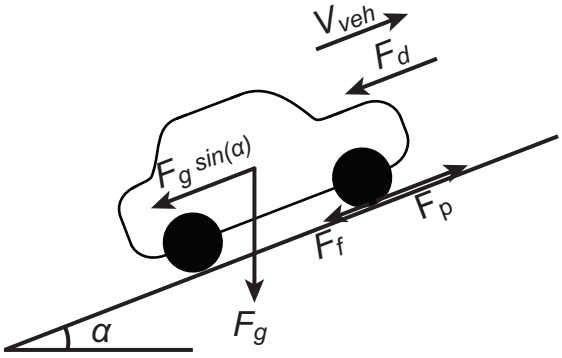

Figure 3.3: Free body diagram

The system can be modeled as

$$F_p = m_{veh}\frac{dv_{veh}}{dt} + F_d + F_f + F_g sin(\alpha) \tag{3.26}$$

where F_p is the force of propulsion exerted by the motor, F_d is the aerodynamic drag force, F_f is the frictional force between the road and the wheels, F_g is the gravitational force α is the slope angle and m_{veh} is the total vehicle mass. The tractive power needed to be exerted by the motor is given by (3.27)

$$P_p = F_p v_{veh} = m_{veh}\frac{dv_{veh}}{dt}v_{veh} + F_d v_{veh} + F_f v_{veh} + F_g sin(\alpha) v_{veh} \tag{3.27}$$

$$P_p = m_{veh}\frac{dv_{veh}}{dt}v_{veh} + P_d + P_f + P_g \tag{3.28}$$

where P_d is the power exerted on the vehicle due to the aerodynamic friction also known as the drag power, which is described by (3.29), P_f is the frictional power

between the wheels and the road, which is shown in (3.30), and P_g is the power exerted by gravitation which is described in (3.31).

$$P_d = F_d v_{veh} = \frac{1}{2} C_d A_f \rho_a v_{eff}^2 v_{veh} \tag{3.29}$$

where C_d is the drag coefficient, A_f is the effective area of the vehicle perpendicular to the direction of motion, ρ_a is the density of air, v_{eff} is the velocity of the vehicle relative to air and $v_{veh} + v_{air}$.

$$P_f = F_f v_{veh} = C_{rr} F_N v_{veh} \tag{3.30}$$

where C_{rr} is the coefficient of rolling resistance and F_N is the normal force.

$$P_g = F_g v_{veh} = m_{veh} g sin(\alpha) v_{veh} \tag{3.31}$$

where g is the acceleration due to gravity.

3.3.2 Drive System Requirement Specification

Several drive cycle models were made in order to calculate the current and the power output needed in the different drive cycle scenarios. In order to determine the maximum peak power and current needed, a worst case drive cycle was implemented. This was realized into a slope with a 15° incline where the vehicle accelerated from stationary to full speed in five seconds. To determine the necessary current during regular driving condition, a drive cycle on flat surface was implemented. A worst case scenario was implemented in order to determine the maximum amount of power needed. It was calculated to approximately 2 kW when accelerating from stationary to full speed, 20 km/h, at an incline of 15° in 5 seconds.

In addition the battery technology and battery voltage needs to be selected. The battery voltage is set in discrete steps by the number of battery cells chosen and by their nominal voltage. For the purpose of driving a light electric vehicle weight and size has to be minimized. To reduce the weight and the size, a high power density is needed. In order to be economically viable the high power density must come at a low cost. From these design criteria's a six cell lithium polymer battery (LiPO) with a nominal cell voltage of 3.7 V and especially thin design and was chosen. With the nominal battery voltage set to 22.2 V it is possible to determine the maximum current to 90 A and to select a BLDC motor which is able to handle the voltage and currents up to at least 90 A for a short period.

4 Inverter Design

The inverter layout was divided into two different PCBs, a Control PCB and a Power PCB. This was done in order to separate the high power components from the low power components. A four layer FR-4 PCB was used for the control circuits and a one-layer aluminum PCB was used for the power circuits. The aluminum was used in order obtain an improved cooling performance for the transistors.

Due to layout optimization and the component shape the current sensor and the gate drives were placed on the Control PCB although they usually are placed on the Power PCB.

An electronic design software called Altium Designer from Altium where used to draw both the schematics and PCBs.

4.1 Control PCB Schematic

The control PCB consists of low voltage logic components which are necessary for the control of the electronic commutation of the motor. An overview over the control PCB can be seen in Figure 4.1 where every major circuit is divided into a block. All of the circuit schematics for the Control PCB can be seen in Appendix B.

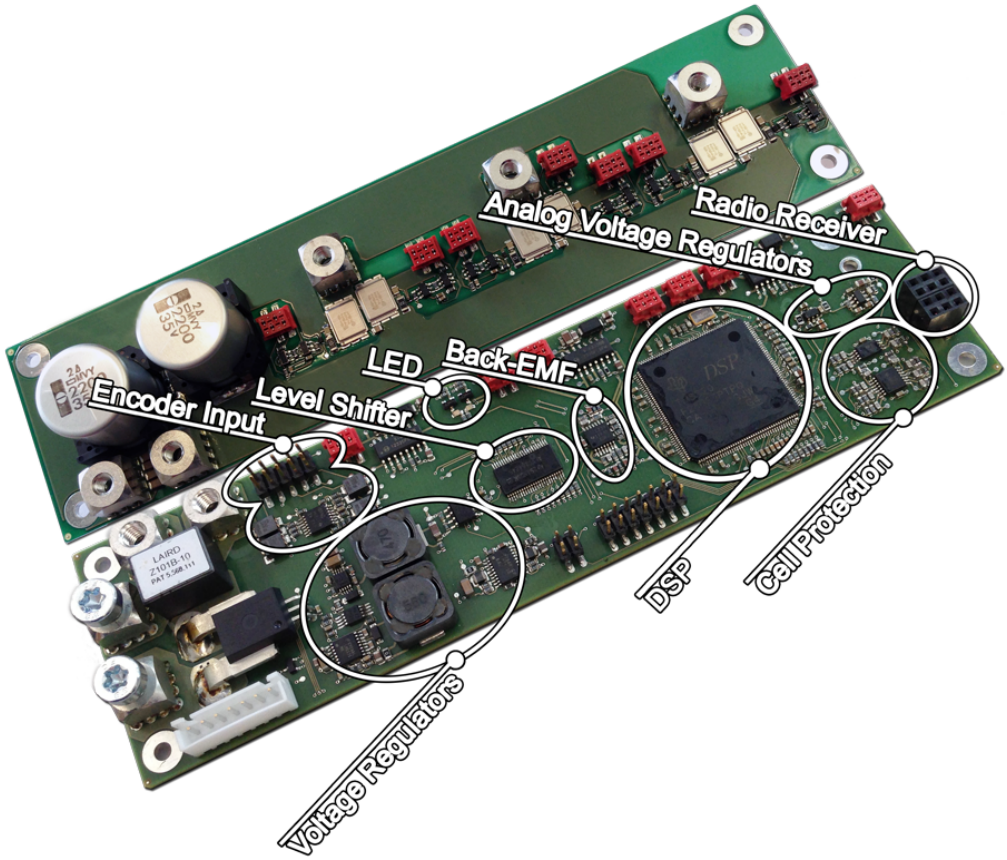

Figure 4.1: Overview of the different blocks in the PCB

All of the different blocks will be described in more detail in the following sections.

4.1.1 Voltage Regulators

The voltage regulator block converts the battery voltage down into four different voltage levels. The voltage values were 10 V, 5.0 V, 3.3 V and 1.9 V where 3.3 V and 1.9 V also were used as analog voltages.

To transform the battery voltage down to 10 V a buck converter was used. The 10 V was used in order to supply the high and the low side driver outputs of the gate drivers with power. The voltage was also used in a gate amplifying stage in order to maintain a good gate signal to the MOSFETs on the power PCB.

The 5.0 V voltage level was also acquired by using a buck converter. This voltage level was used in order to supply, the radio receiver, the encoder, the level shifter and the gate driver with power.

A buck regulator with dual outputs was used in order to attain the digital 3.3 V and 1.9 V from the digital 5.0 V. Both of the voltages were used to supply the DSP and the 3.3 V was also used to supply two Light-Emitting Diodes (LEDs), the level shifter and the back-EMF circuits. The same analog voltages were obtained by using linear power regulators with the 5.0 V as input. These voltages where used to supply the DSP and the current sensor.

A supervision circuit with dual inputs was used in order to detect power fails of the voltages, which supply the DSP. This was implemented as a safety function to protect the DSP and the critical components supplied by the same voltage.

4.1.2 Radio Receiver

The radio receiver block consists only of a connector for a radio receiver with three analog inputs which are connected to the DSP and a 5.0 V output. The radio receiver and the transmitter were third-party components which normally are used for radio-controlled cars. The purpose of this circuit was to be able to control the vehicle wirelessly in the future.

4.1.3 Cell Protection

Since a lithium polymer battery was used as power supply the voltages from each of the cells needed to be monitored by the DSP. This was done to reduce the risk of damaging the cells under running operation. An input header for the balance connector of the battery was mounted along with six differential amplifiers to obtain the different cell voltages. The voltage protection circuit is limited to only measuring six cells due to the design with six differential amplifiers. The nominal cell voltage is 3.7 V and the voltage of each cell should be in the range from 4.2V to 2.7 V in order to protect the cell from taking any damaged because of an under or over voltage. This gives a nominal voltage of 22.2 V for the input supply voltage to the inverter. The gain of the differential amplifiers was set to 0.62 to be able to sample within the full signal range with the Analog-to-Digital Converter (ADC).

4.1.4 LED

The LED block consists of two LEDs, one green and one red, and two MOSFETs which are used to switch the LEDs on and off. The LEDs act as indicator lights for the DSP to show if the controller is working and in order to make the debugging process easier.

4.1.5 Encoder

A quadrature encoder was used for verification and comparison of the two different sensorless methods. The outputs from the encoder were A, B and index pulse along with their inverted signals. All of these signals were used to obtain an accurate position of the rotor and rotor direction. The A and $\overline{A}$ signals were filtered with a common mode choke and amplified in a differential amplifier to achieve a more stable and reliable A-signal. The B signals and the index signals where filtered and amplified in the same way. These three signals were then sent to the DSP in order to calculate the position.

4.1.6 DSP

The DSP functions as a brain for the three phase inverter. It is here all of the input and output signals are processed in order to make it possible to control the switching sequences. All of the signals used by the three phase inverter can be seen in Table 5.1 and Table 5.2. Filters were connected to each of the DSP's analog inputs to reduce signal noise. This improved the signal quality and made it easier to use the signals in the software. A Joint Test Action Group (JTAG) connector was also connected and used for programming and debugging the DSP.

4.1.7 Back-EMF

In the back-EMF block, the phase potentials were measured in order to be used by the two sensorless methods. The signals were filtered to reduce noise from the PWM switching and scaled down to use the full range of the ADC conversion. Back-EMF A, back-EMF B and back-EMF C, were measured with the DSPs analog inputs which can be seen in Figure 4.2. Three resistors from each phase were connected in parallel in order to recreate the potential of the motor neutral. The motors virtual neutral was also measured by the DSP ADC. These four analog input signals along with a digital sensorless algorithm, were used for one of the sensorless methods.

The other sensorless method which was implemented used a similar approach, but instead of analog signals it used three digital signals as input to the DSP. The signals, Zero Cross A, Zero Cross B and Zero Cross C, was obtained from three comparators, which also can be seen in Figure 4.2.

When the phase potential is higher than the virtual neutral the output of the comparator will be high and when the phase potential is low, vice versa. The shapes of these signals were very similar to the ones from a hall sensor. An algorithm was also used in this case to estimate the next needed switching state. Both of the algorithms are based on the equations in Section 2.2.2.

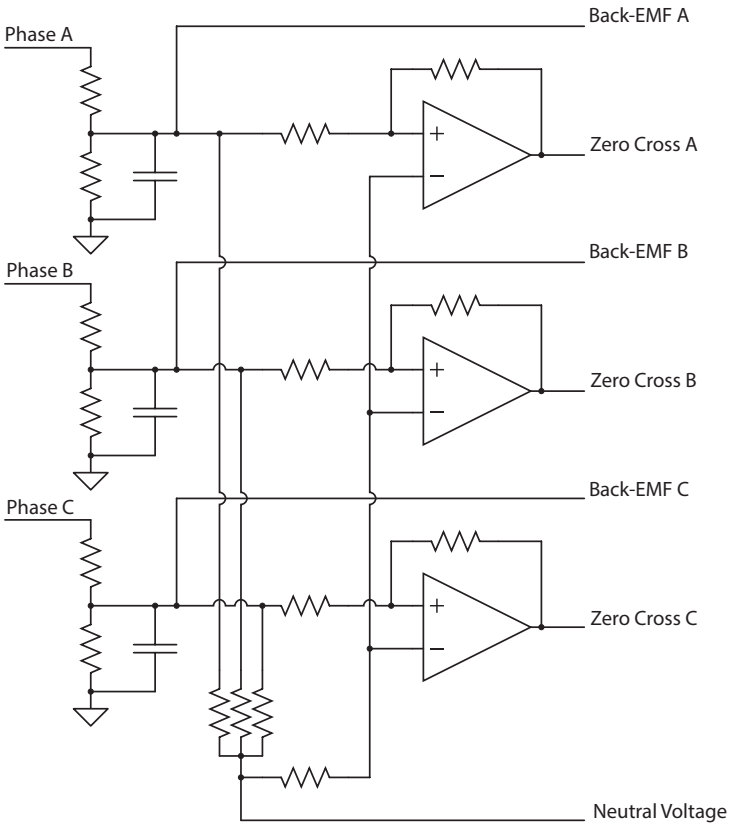

Figure 4.2: Schematic overview of the back-EMF block

4.1.8 Level Shifter

The level shifter was used to connect digital circuits which used different voltage levels. For example the output signals from the encoder were shifted down from 5.0 V to 3.3 V, which the DSP is able to measure. In the other direction, the PWM outputs from the DSP were shifted up from 3.3 V, to 5.0 V, which was required for the gate driver.

4.2 Power PCB Schematic

An overview over the power PCB with all of the major parts divided into different blocks can be seen in Figure 4.3. All of the circuit schematics for the power PCB can be seen in Appendix C.

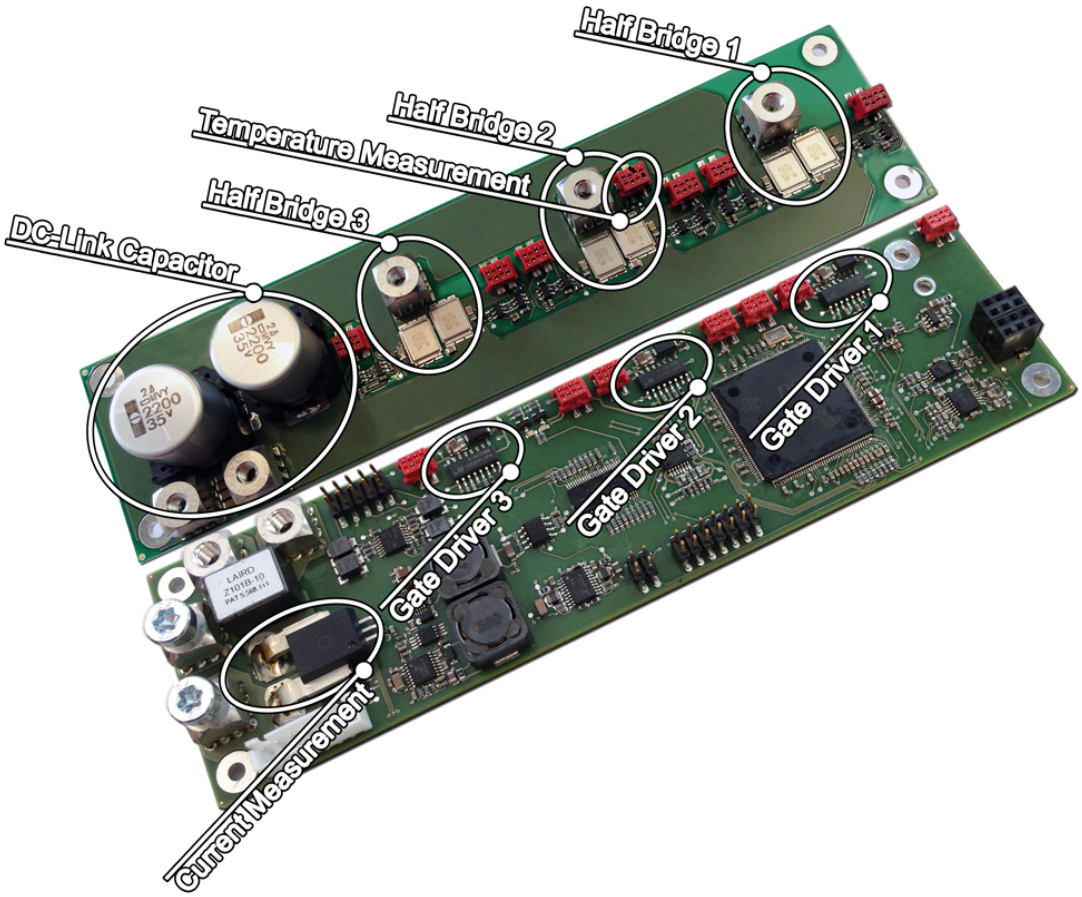

Figure 4.3: Overview of the different blocks in the PCB

All the blocks will be described more detailed in the following subsections.

4.2.1 Gate Driver

The gate driver that was used had both a high-side and a low-side driver along with a bootstrap capacitor and a bootstrap diode at the upper MOSFET, which can be seen in Figure 4.4. In order to achieve independent control of the MOSFETs both the low side and high side input were used with an individual PWM signal. The PWM output signals from the DSP with a voltage level of 3.3 V goes through a level shifter to adjust the voltage level to 5.0 V. The adjusted voltage is compatible with the gate driver inputs VIA and VIB.

The distances between the output signals of the gate driver and the input signals to the MOSFETs need to be as short as possible in order to reduce parasitic inductance in the traces. The inductance decrease the instantaneous current which in turn decreases the speed of the switching [14]. This phenomenon lead to that an amplifying stage was placed in front of the MOSFET gate.

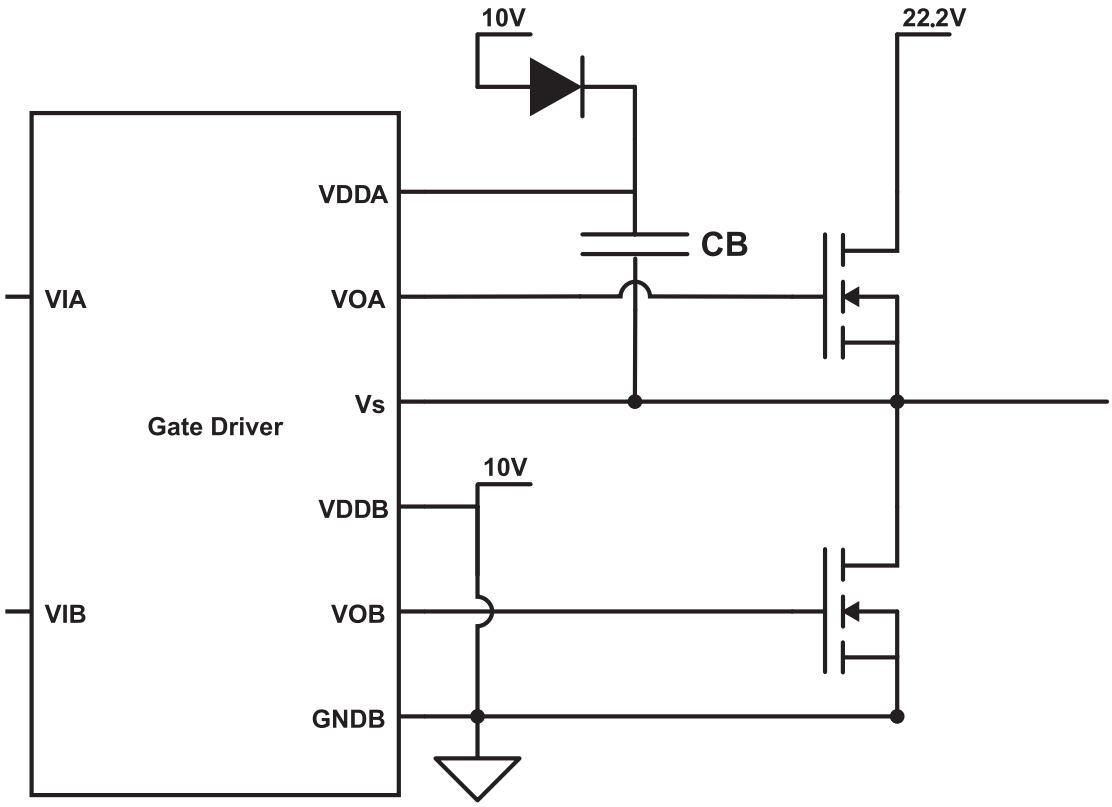

Figure 4.4: The high-side/low-side gate driver IC with a bootstrap capacitance, CB

The bootstrap capacitor, CB was selected according to (2.7)-(2.9). A fast recovery diode was chosen as the bootstrap diode in order to reduce the timeframe in which the bootstrap capacitor can discharge into V_{DD}.

4.2.2 Half Bridge

There are three half bridge blocks, Half Bridge 1, Half Bridge 2 and Half Bridge 3, which together compose the three phase inverter. Each block consist of two MOSFETs, one upper and one lower MOSFET which are connected to one common gate driver IC.

The MOSFET switching scheme for BLDC motor control is presented in Table 2.2 and from this table it can be seen that two switches always are on except for the dead time between the PWM pulses. Dead time is used in order to avoid that both the upper switch and the lower switch are on at the same time. During the dead time, the current will freewheel through the body diode of the MOSFET. So the power dissipation of the MOSFETs in the three phase inverter will be

$$P_{total} = 2P_{cond}\big(1 - T_{dead}\big) + 2P_{switch} + 2P_{cond,diode}T_{dead} \tag{4.1}$$

where P_{cond} and $P_{cond,diode}$ are the conduction losses of the MOSFET and P_{switch} are the switching losses of the MOSFETs. Which are

$$P_{cond} = I_{on}^2 R_{ds(on)} \tag{4.2}$$

$$P_{switch} = \frac{V_{ds} I_{on} f_s}{2} \left(t_r + t_f \right) \tag{4.3}$$

$$P_{cond,diode} = V_f I_{on} \tag{4.4}$$

where $R_{ds(on)}$ is the on state resistance of the MOSFET, I_{on} is the conduction current, V_{ds} is the drain to source voltage when the MOSFET is off, t_r and t_f is the turn on and turn off times, f_s is the switching frequency and V_f is the diode forward voltage drop [15].

The power dissipation during a worst case scenario was calculated to be 32 W, which correspond to a loss of 1.6 %. The current used in this worst case was $90A$, from Section 3.3.2, and the nominal battery voltage of 22.2 V. The selected MOSFETs were specified to handle these parameters.

4.2.3 DC-Link Capacitors

A capacitor bank consisting of two electrolytic capacitors and four ceramic capacitors were connected in parallel and placed between the battery and the three half bridges in order to obtain a steady bus voltage. The two electrolytic capacitors filter the low frequency voltage ripple and the four ceramic capacitors filter the high frequency voltage ripple. The following expression was used to calculate the minimum value of the electrolytic capacitor

$$C_{min} = \frac{I_{motor,peak}}{\Delta V f_s} \tag{4.5}$$

where $I_{motor,peak}$ is the peak motor current, ΔV is the maximum allowed voltage ripple and f_s is the switching frequency [16].

4.2.4 Current Measurement

Current control was used in order to regulate the motor output power. This makes it necessary to measure the current continuously. Since the BLDC motor only has one active current at the time, two phases conducting, there is no need to measure all three phase currents. Instead one current sensor was mounted between the battery and the three phase inverter.

A hardware shutdown function consisting of two comparators where used as a safety function in case of a software or external failure. The two comparators were set to trigger on two different currents, one for maximum allowed positive current and one for maximum allowed negative current with the analog current sensor signal used as an input.

4.2.5 Temperature Measurement

Near one of the half bridges a negative temperature coefficient resistor was mounted to be able to measure temperatures. The temperature was monitored by the DSP as a software safety function and is able to trig a shutdown when the temperature becomes too high.

4.3 PCB Layout

Circuit noise and disturbances are a common problem when realizing a schematic circuit layout into a PCB layout. This is was mainly due to the fact that the components are not ideal and that the signal traces cannot be made infinitely short and thereby give rise to phenomena's such as Electromagnetic Interference (EMI) because of unwanted coupling to other circuits caused by capacitive, inductive or conductive coupling. A first approach in order to reduce those unwanted effects when designing a PCB is to follow PCB design guidelines. Those help the designer to make general layout decisions without having to stop and analyze each and every step and thereby speed up the design process significantly. This makes the guidelines a very cost efficient tool in order to reduce EMI instead of having to rely upon expensive containers such as metallic enclosures [17], [18]. There are however almost as many guidelines as there are design engineers. It is therefore necessary to be critical and investigate if the guidelines are up to date and in which specific case each guideline apply [17].

4.3.1 Control PCB Layout

The Control PCB layout was influenced by a number of aspects of which the major ones will be discussed in this section. The first aspect was to determine the PCB dimensions. Since the application is light electric vehicles this is a crucial factor since it needs to be able to fit and to be mounted in a good way. The two PCBs, the Control PCB and the Power PCB were placed beside each other, instead of on top of each other, because of the definite height constraint of the application.

The control PCB was decided to be a multilayer PCB and to have four layers made out of the regular glass epoxy panel FR-4 with copper foil laminated on each layer. The four layers made it possible to have a ground plane, a power plane and two signal layers. The four layer structure was a very cost effective approach in order to reduce current loops and trace inductances that can cause EMI and signal noise [17].

Circuits with similar noise characteristics were grouped together such as the different switching voltage regulators and the encoder signal input interface. The analog circuits, the DSP's analog inputs and the linear regulators, were put far from the switched regulators in order to reduce the risk of noise coupling with the analog measurements. A separate ground for the analog circuits was also realized with the same intention.

The components within a block were placed close to each other with the main focus on minimizing the signal current loop area. Having a ground plane also reduce the signal current loop area since it provides the signals with a close and low-impedance path [17].

The different power planes were placed on a single layer which prevents coupling between two different power buses. This also allows for an efficient design since devices with same voltage rating could be grouped together. To further minimize EMI, decoupling capacitors were placed as close to the power supply pins as possible with direct via holes down to the ground plane.

All of the connectors onto and from the PCB were located at the edges of the

board in order to minimize the length of the connector cables. Connector headers leading to the Power PCB were aligned with the corresponding connector headers to allow for short wiring between the circuit boards.

4.3.2 Power PCB Layout

The Power PCB is a single layer PCB made out of aluminum which gives it significantly better thermal conductivity properties than a regular PCB such as FR4 made out of glass epoxy panel. The aluminum PCB is composed of a three layer structure of, a circuit layer made out of a copper foil, a dielectric insulation layer with good thermal conductivity properties and a metal substrate [19]. The thermal conductivity of the aluminum PCB is 2.2 W/mK which is six times higher than the thermal conductivity for the FR4 material [20].

The component placement became even more critical since only one circuit layer was available and components needed to act as bridges for the traces in order to be able to minimize the current loops effectively. The conduction traces where made into planes in order to support the high currents of up to 90 A.

5 Software Implementation

The DSP which was used to control the motor was a Texas Instruments TMS320F28335. It is a 32-bit floating-point processor with a clock rate of up to 150 MHz. It has floating-point capability which makes the processor well suited for motor control in relation to fixed-point because of its capability of having a wider range of values and more accurate measurements. The DSP is equipped with both on-board Random Access Memory (RAM) and internal flash memory for standalone control. There are 16 ADC inputs with a 12-bit resolution with an input range of $0-3.0\ V$. There are also 88 General Purpose Input/Output (GPIO) pins where some of them have special features such as PWM and Encoder support. It is also possible to make interrupts with different types of trigger signals. The different pins and software functions that are being used are further explained in this section.

An overview over the system can be seen in Figure 5.1, where the different functions are represented in different blocks.

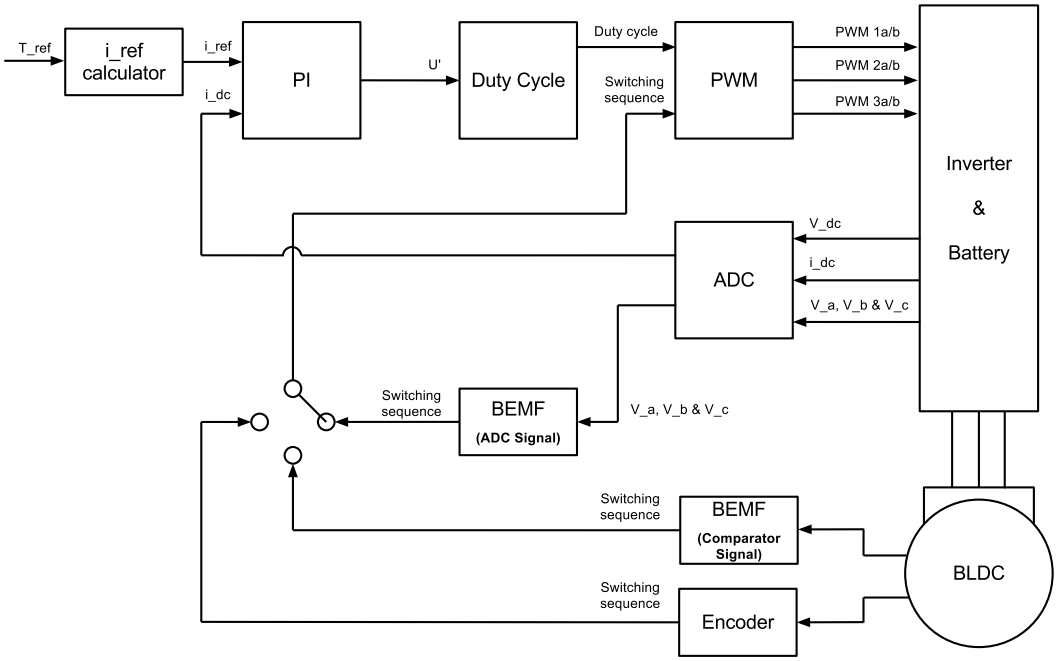

Figure 5.1: DSP block layout overview

For the software implementation Code Composer Studio™ v5 (CCS) with libraries from ControlSUITE™ for C2000™ was used.

The DSP operation procedure starts with a hardware initialization where the processor first resets and then initialize functions like stack pointers, registers, clocks and watchdog [21]. After the hardware initialization is done the software initialization starts and settings are loaded to the RAM. Examples of settings are the PWM switching frequency, assigning the PWM outputs and other features for the GPIO pins and the ADC channels. An overview of the pinouts can be seen in Table 5.1 and Table 5.2. The software goes into a waiting loop after the initializations is done and wait for trigger signals for interrupts. The trigger signal

for the interrupt was set at the end of every PWM cycle, which has a switching frequency of 20 kHz. Flow chart for the startup can be seen in Figure 5.2.

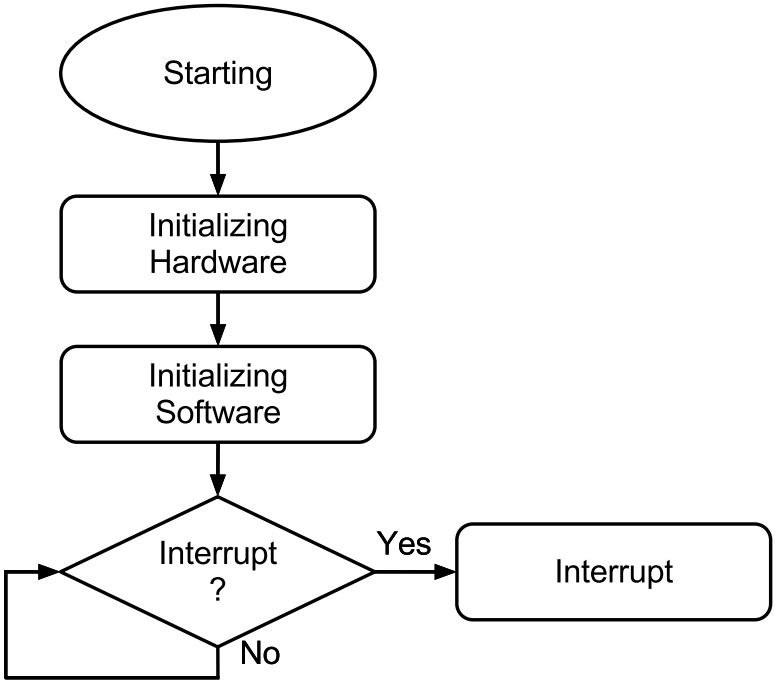

Figure 5.2: Main procedure flow chart

The algorithms that need to be run in real time are placed in the interrupt block. The flow chart of the most necessary functions in the interrupt block can be seen in Figure 5.3.

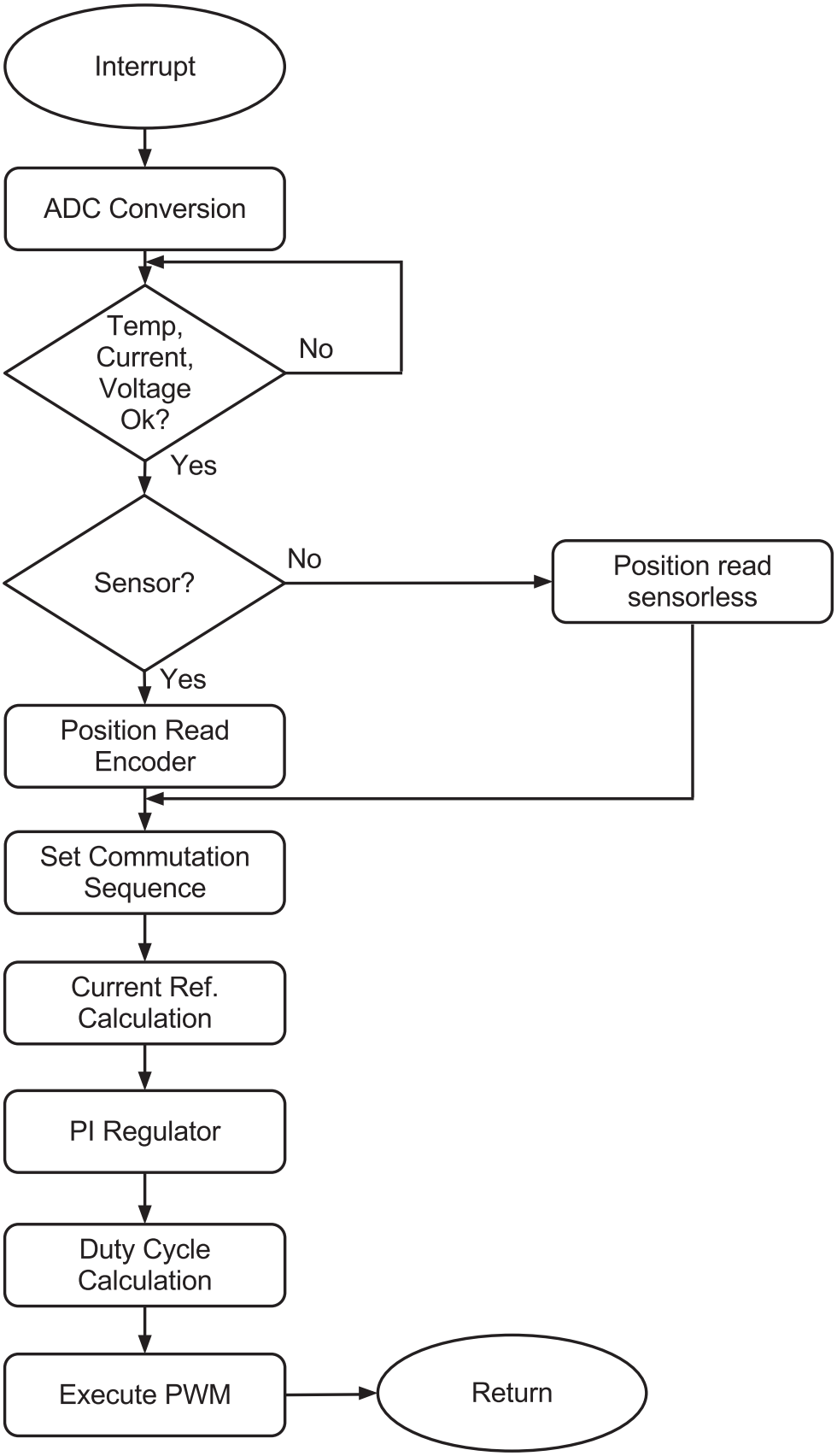

Figure 5.3: Interrupt procedure flow chart

All of the ADC channels were set to sample simultaneously with the PWM signal as trigger. The input voltages were then attained with the following formula

$$D = \frac{4095}{3.0} V_{in} \tag{5.1}$$

where D is the digital number converted from the ADC and V_{in} is the input voltage to the DSP. 4095 is the resolution of an ADC with 12-bits and 3.0 is the range of the input voltage. The digital numbers are then scaled with different factors, depending on the hardware, to determine the true voltages. The signals which are sampled by the ADC are represented in Table 5.1 together with a short description.

Table 5.1: Input signals to the ADC module

Input	Name	Description
ADC A0	I_meas	DC-link current
ADC A1	Radio_ref	Torque reference from radio control
ADC A2	Torque_ref	Torque reference wired
ADC A3	Temp-NTC	Temperature from the three phase inverter
ADC A4	Back-EMF A	Voltage potential in phase A
ADC A5	Back-EMF B	Voltage potential in phase B
ADC A6	Back-EMF C	Voltage potential in phase C
ADC A7	Virtual_n	Virtual neutral point of the motor
ADC B0	Cell voltage 1	Voltage battery cell 1
ADC B1	Cell voltage 2	Voltage battery cell 2
ADC B2	Cell voltage 3	Voltage battery cell 3
ADC B3	Cell voltage 4	Voltage battery cell 4
ADC B4	Cell voltage 5	Voltage battery cell 5
ADC B5	Cell voltage 6	Voltage battery cell 6
ADC B6	Ch 1 ext	Extra channel from radio control (Not in use)
ADC B7	Ch 3 ext	Extra channel from radio control (Not in use)

There are two different methods implemented to estimate the rotor position, one using ADC channels which samples the phase voltage potential and another using the digital inputs with a comparator triggering on the zero crossing of the back-EMF. For the method using the ADC the signal value is continuously compared to the value of the virtual neutral point, which is obtained from a resistor network with three resistors connected in parallel with the motor, see Section 4.1.7. All the signals have digital filters implemented in order to reduce high-frequency switching noise. When the back-EMF value and the neutral point value are equal, the DSP indicates that a zero-cross event has occurred. The time difference compared to the previous zero-crossing event is also calculated. This time divided by two is then used to delay the output of the commutations sequence estimator with 30°. This is done because of the zero-cross event occuring 30° before the next commutation sequence should start, which can be seen in Figure 2.2. The motor direction is obtained by comparing in which order the zero-cross events occurs.

Six of the input signals to the ADC were used to measure the cell voltages of the battery pack. If one of these cells exceeds its upper or lower voltage limits the program will shut down the controller. The same will happen if the input voltage to the converter exceeds its upper or lower voltage limits. This is a safety function for the battery to minimize the risk to damage the cells. Other safety functions that were implemented were temperature measurement and over current protection, with both hardware and software.

The digital input and output pins that are being used are represented in Table 5.2 together with a short description.

Table 5.2: Input and output signals of the DSP

Pin	Input/Output	Name	Description
GPIO 0	Output	PWM-1a	PWM signal for S1
GPIO 1	Output	PWM-1b	PWM signal for S2
GPIO 2	Output	PWM-2a	PWM signal for S3
GPIO 3	Output	PWM-2b	PWM signal for S4
GPIO 4	Output	PWM-3a	PWM signal for S5
GPIO 5	Output	PWM-3b	PWM signal for S6
GPIO 10	Input	PSC PFO	Power fail input
GPIO 11	Output	PSC WDI	Watchdog timer output
GPIO 12	Input	$\overline{\text{I\_trip}}$	Hardware current trip
GPIO 20	Input	QEP-A	Encoder A pulse
GPIO 21	Input	QEP-B	Encoder B pulse
GPIO 23	Input	QEP-I	Encoder I pulse
GPIO 26	Input	ON/OFF	On/Off button for the sensor
GPIO 27	Output	Disable	Disable the gate drivers when high
GPIO 29	Input	Zero cross A	Signal from back-EMF comparator, phase A
GPIO 30	Input	Zero cross B	Signal from back-EMF comparator, phase B
GPIO 31	Input	Zero cross C	Signal from back-EMF comparator, phase C
GPIO 76	Output	Led 1	Red LED
GPIO 77	Output	Led 2	Green LED

The other method which is implemented to estimate the rotor position works in a similar way to the one which is sampled by the ADC. The difference is that the zero-cross event is detected with comparators. So when the back-EMF voltage is higher than the neutral point, the comparator output will be high and when the back-EMF voltage is lower than the neutral point, the output will be low. In this way the direction of the rotation and the commutation sequence can be calculated.

Encoder support was implemented to be able to evaluate the sensorless methods. The enhanced Quadrature Encoder Pulse (QEP) register and special pins reserved for this purpose where used to calculate the angle, the direction of the rotation and the speed.

Another register which was used in the DSP was the register of the enhanced PWM. This register controls the PWM output signals, which is varied to change the speed and the torque of the motor. The output depends on which of the switching sequences the rotor is in and of the duty cycle. These two parameters

are the inputs to the PWM function. The switching sequence is received from either one of the two sensorless algorithms or the encoder and the duty cycle is received from the Proportional-Integral (PI) regulator, see Figure 5.1. Table 5.3 represents the PWM switching of the transistors depending on the switching sequence.

Table 5.3: Commutation states for the three phase inverter

Sequence	S1	S2	S3	S4	S5	S6
1	**PWM**	$\overline{\textbf{PWM}}$	OFF	**ON**	OFF	OFF
2	**PWM**	$\overline{\textbf{PWM}}$	OFF	OFF	OFF	**ON**
3	OFF	OFF	**PWM**	$\overline{\textbf{PWM}}$	OFF	**ON**
4	OFF	**ON**	**PWM**	$\overline{\textbf{PWM}}$	OFF	OFF
5	OFF	**ON**	OFF	OFF	**PWM**	$\overline{\textbf{PWM}}$
6	OFF	OFF	OFF	**ON**	**PWM**	$\overline{\textbf{PWM}}$

6 Verification and Evaluation of Results

In this section the simulation and laboratory measurement results will be presented and evaluated.

6.1 Board Verification

A major part of the project was put into functionality verification. Already at an early stage of the inverter design process, jumper resistors were used in order to simplify the validation and troubleshooting procedure. They also reduce the damage of circuit errors and the short-circuit failures, since they isolate an error within a specific circuit function, for example one of the switched power regulators. This made the troubleshooting process more structured and significantly reduced the risk of damaging components. It also saved a lot of time since the error was isolated within a smaller circuit and not the whole circuit board. The LED lights also proved to be very valuable for the purpose of troubleshooting. By receiving direct visual feedback the process went much faster.

All the power levels were verified to their specified value. This was an important and necessary result in order to have any functionality at all from any of the components. The next major step was the validation of the onboard DSP, this included; establishing a connection to the DSP, compiling to its flash memory and verifying the input and output signals. The PWM output signals were measured in order to verify that the PWM control registers had been setup correctly. The measured PWM outputs of the switches S1, S2, S5 and S6 which corresponds to the ones in Table 5.3 is illustrated in Figure 6.1.

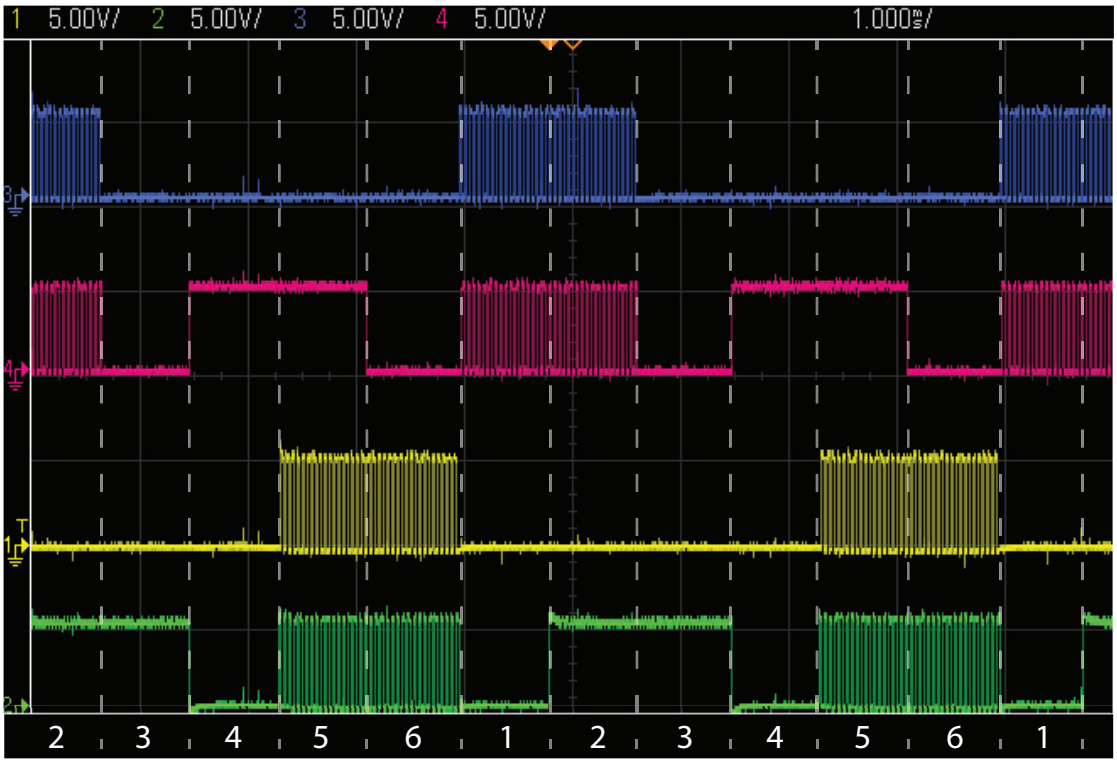

Figure 6.1: PWM outputs from the DSP with a 50 % duty cycle with motor in no load operation, blue S1, magenta S2, yellow S5 and green S6 at [5 V/div] and [1 ms/div]

The measured signals corresponds correctly to the desired state in Table 5.3. There is however also a dead time on the measured PWM outputs which is not visible in Figure 6.1. The dead time is necessary in order to protect the three phase inverter from a shoot through in one of the half bridges.

The gate driver output signal was measured in order to validate that the amplification of the PWM signal worked as intended. The signal for the same four switches after the gate driver amplification stage is presented in Figure 6.2.

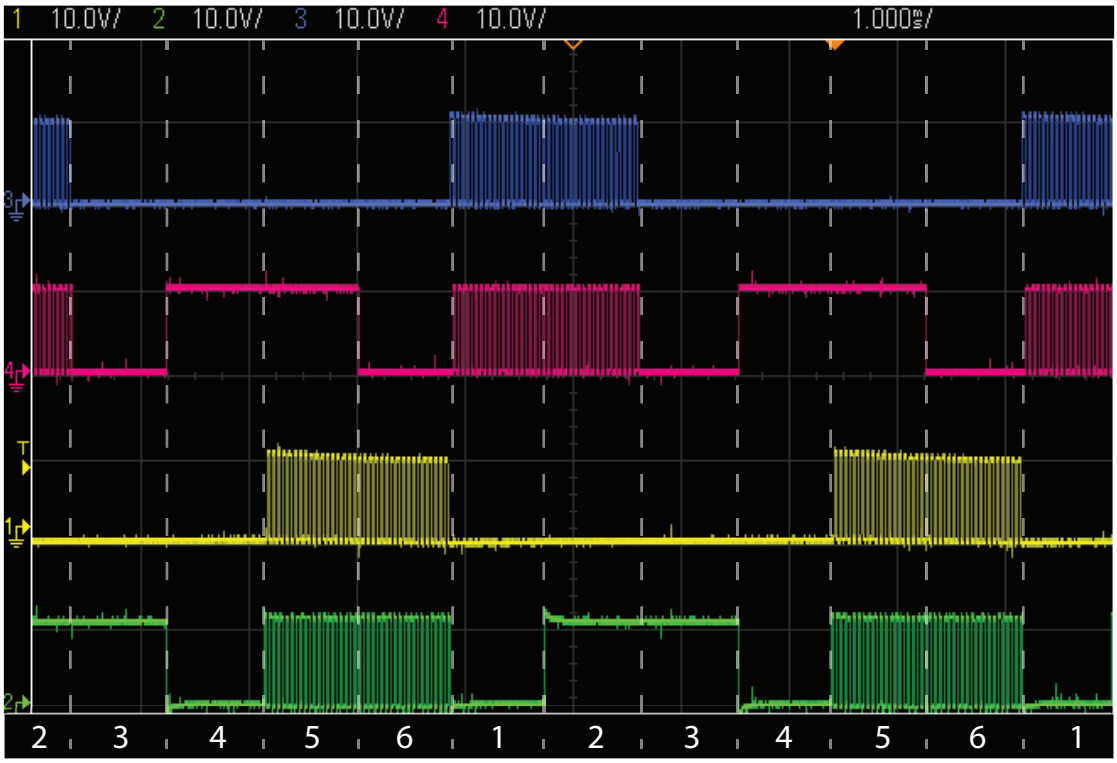

Figure 6.2: PWM outputs from the gate driver with a 50 % duty cycle with motor in no load operation, blue S1, magenta S2, yellow S5 and green S6 at [10 V/div] and [1 ms/div]

The similarities of Figure 6.1 and Figure 6.2 shows that the gate driver properly amplifies the PWM input signals. In this case 3.3 V is amplified to 5.0 V through the level shifter and then amplified to 10 V through the gate driver. The safety shutdown functionality of the gate drivers was also tested and validated.

The output signals of the encoder, the A pulse and the $\overline{A}$ pulse, is presented in Figure 6.3 along with output from the differential amplifier.

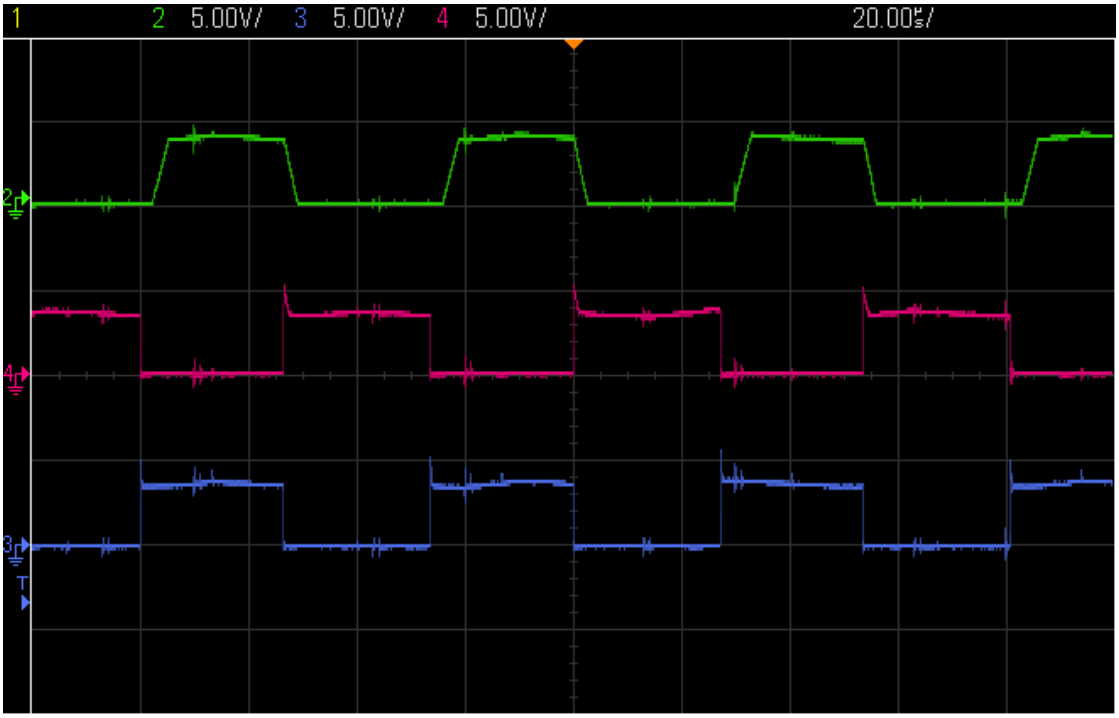

Figure 6.3: Encoder output signals, green differential amplifier, magenta A, blue $\overline{A}$, [100 mV/div] and [20 $\mu s/div$]

The encoder signals from the measurement presented in Figure 6.3 has a very good looking shape without any noise and would be able to function well without the differential amplifying stage. The measurements were however conducted in a lab environment and not in a real field test with a lot of exterior noise. In a case with a lot of external disturbances the differential stage can improve the reliability. The differential amplifiers chosen for this stage were a bit slow and if replaced, they could probably give a considerably faster response.

The current measurement signal presented in Figure 6.4 has some noise on top of the actual signal. This was mainly caused by the necessary placement of the current sensor, close to battery connectors. This was however also close to the switched power regulators which gives rise to a lot of noise. This signal is of major importance in order for current control to be able to function as intended. The noise level was a lot higher than the current measurement sensitivity. This problem was solved by using a digital filter.

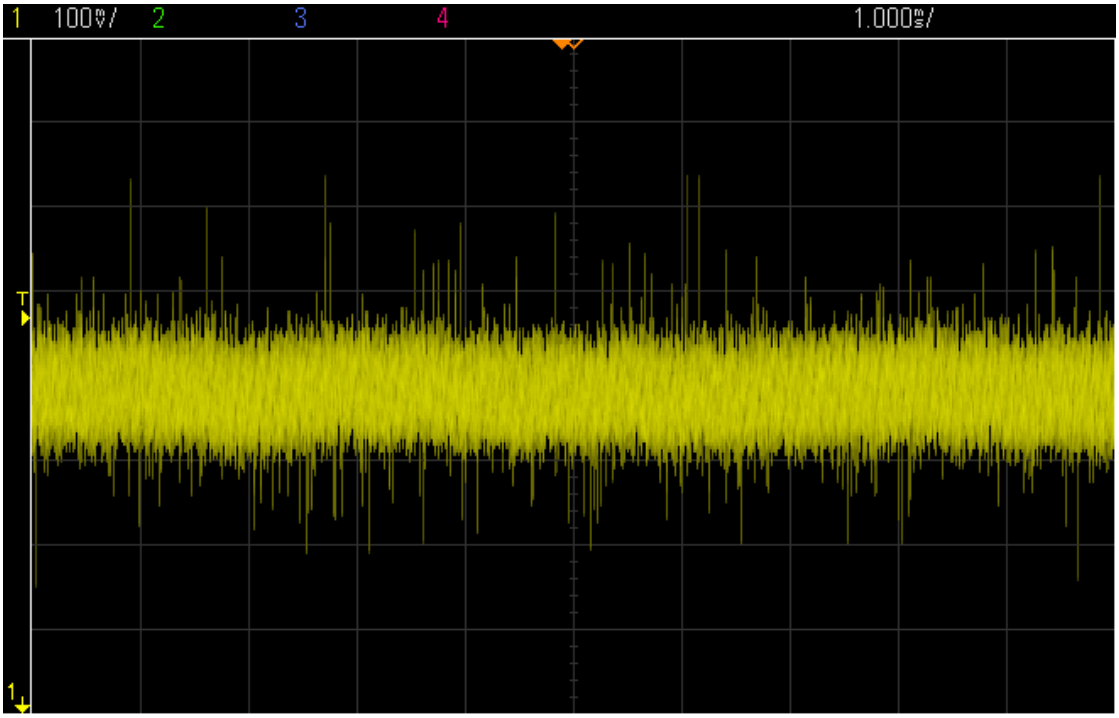

Figure 6.4: Current sensor analog output voltage with circuit noise [100 mV/div] and [1 ms/div]

6.2 Sensored and Sensorless Evaluation

The Simulink motor model was used in order to be able to confirm that the sensorless control algorithms functioned as intended. To be able to have a reference model, a sensored control was first implemented. The back-EMF of the simulated BLDC motor in sensored operation is shown in Figure 6.5 and the corresponding result from the in lab BLDC motor is shown in Figure 6.7.

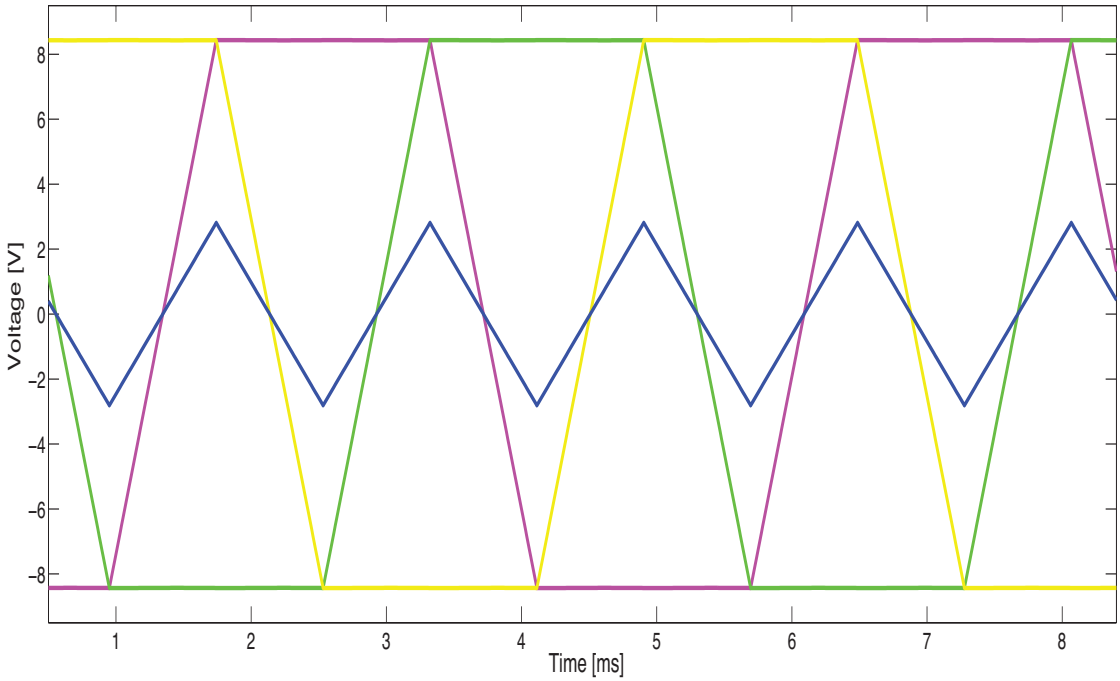

Figure 6.5: Back-EMF of a simulated BLDC motor in sensored operation, yellow Phase A, magenta Phase B, green Phase C and blue virtual ground

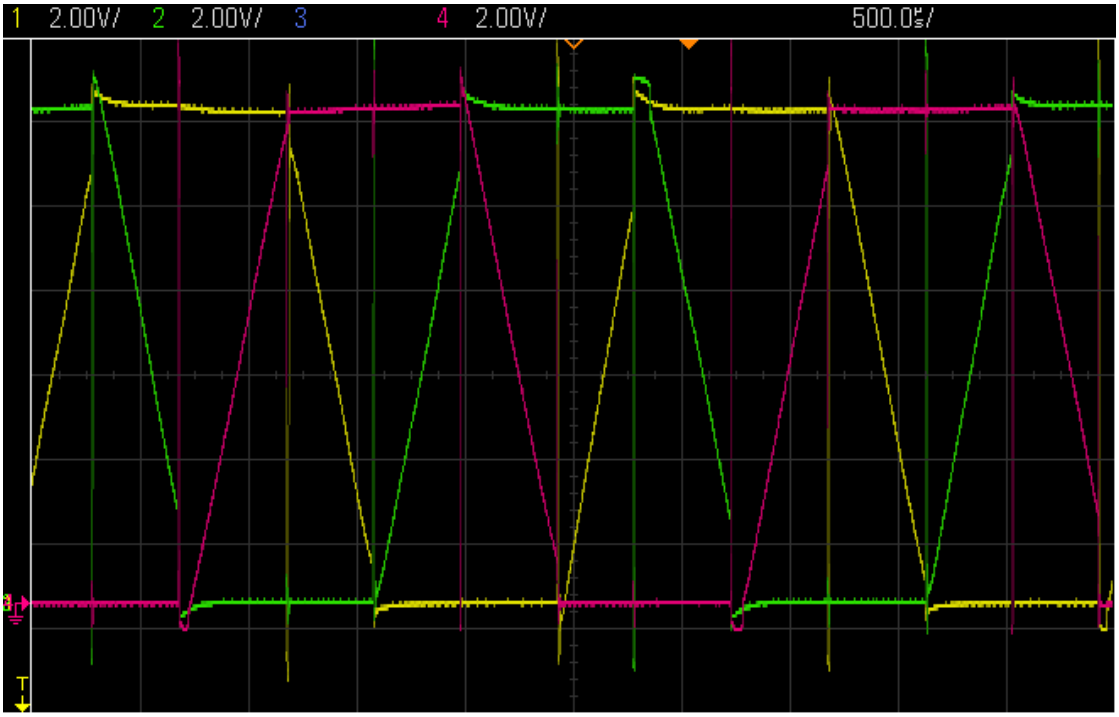

Figure 6.6: Measured phase potential of a BLDC motor in sensored operation at a 100 % duty cycle, yellow Phase A, magenta Phase B and green Phase C, [2 V/div] and [500 $\mu s/div$]

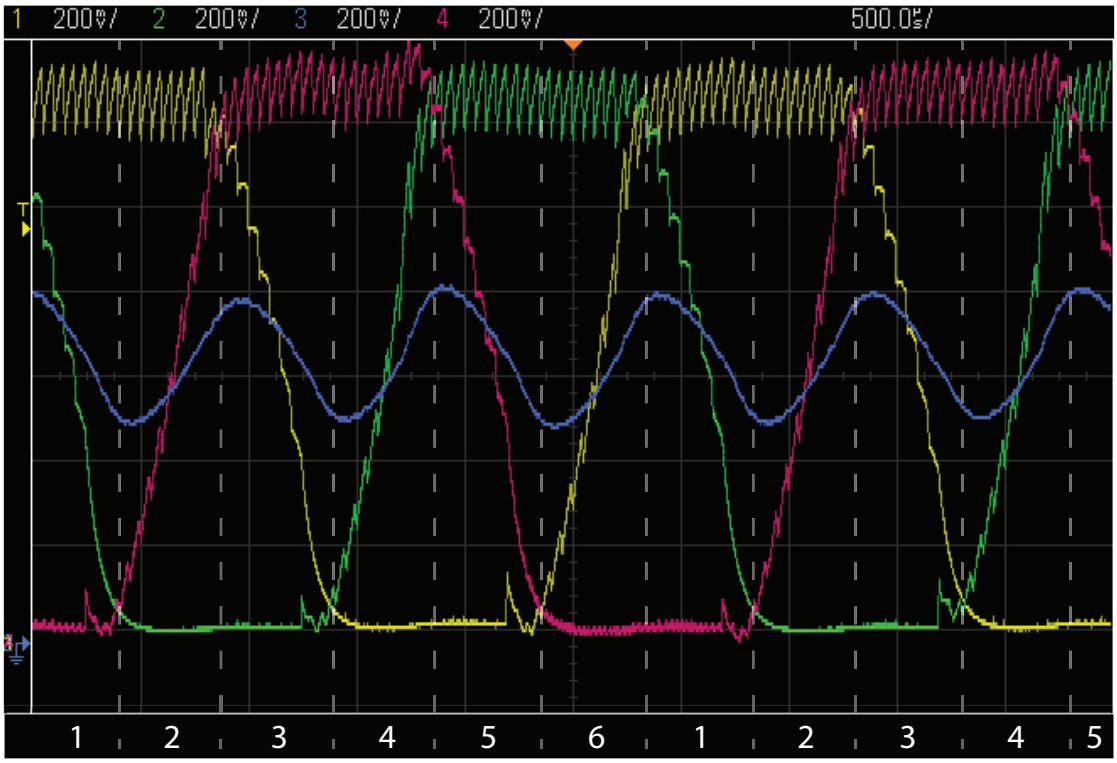

Figure 6.7: Measured filtered phase potential of a BLDC motor in sensored operation at a 50 % duty cycle, yellow Phase A, magenta Phase B, green Phase C and blue virtual ground, [200 mV/div] and [500 $\mu s/div$]

The unfiltered phase potential in Figure 6.6 and the voltage divided and filtered phase potential in Figure 6.7 are both very similar to the simulated back-EMF in Figure 6.5. This is because the phase potential is equal to the back-EMF in every third switching sequence for each phase. For example in phase A in Figure 6.7 the back-EMF is visible during switching sequence three and six. This is when the phase is not being driven. The filtered signal in Figure 6.7 has a trapezoidal shape, with a PWM noise of 20 kHz.

The simulated model controlled with the sensorless algorithm gave the same result as with the sensored operation presented in Figure 6.5. This was expected because of the ideal characteristics of the model. The major difference was that the simulated motor could not start in sensorless operation since it needs a back-EMF to estimate the position.

The phase potential of a BLDC motor was measured with the three phase inverter operating in the two different sensorless modes. The measurements are presented in Figure 6.8 and in Figure 6.9. The first one uses comparators for detection of the zero crossing of the back-EMF and the later one uses the analog inputs of the DSP and digitally detects the zero crossing.

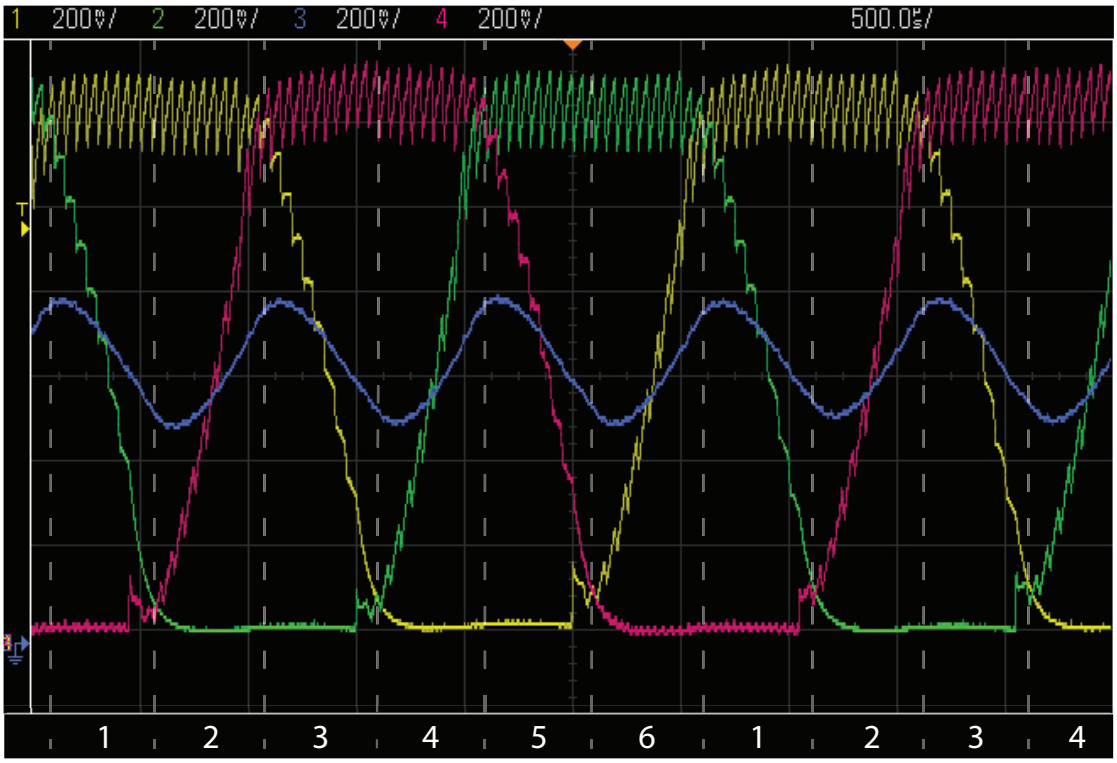

Figure 6.8: Measured filtered phase potential of a BLDC motor in sensorless operation using comparators at a 50 % duty cycle, yellow Phase A, magenta Phase B, green Phase C and blue virtual ground, [200 mV/div] and [500 $\mu s/div$]

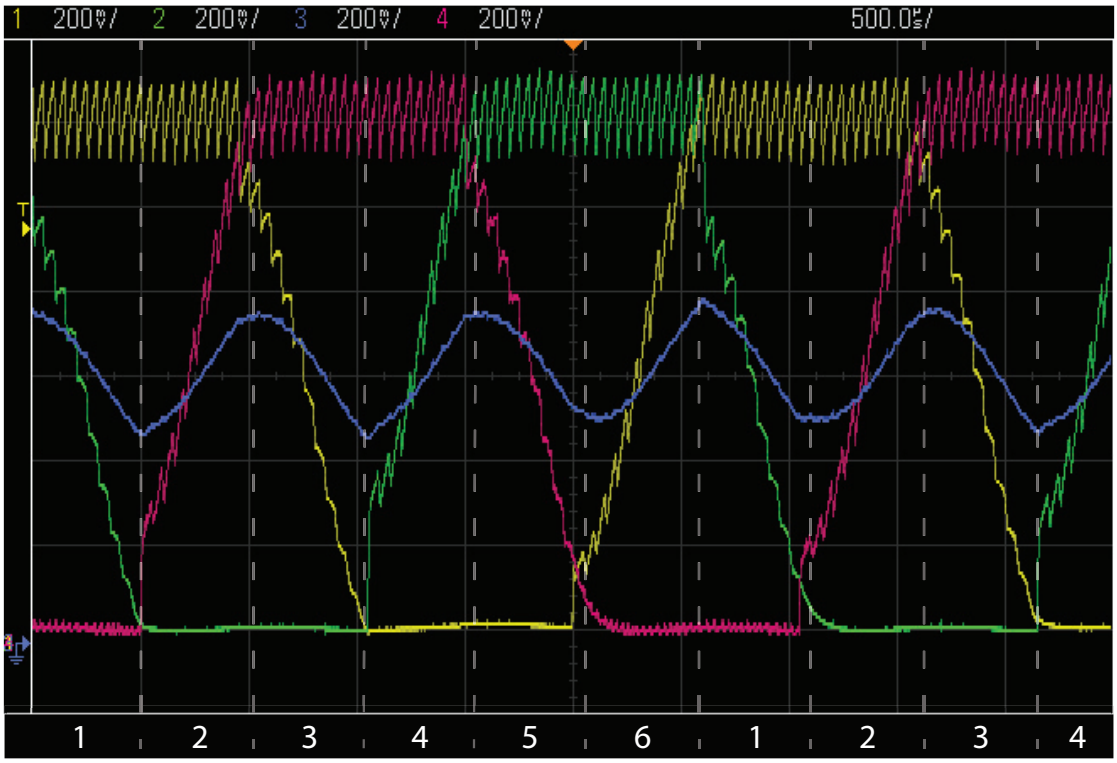

Figure 6.9: Measured filtered phase potential of a BLDC motor in sensorless operation using analog inputs at a 50 % duty cycle, yellow Phase A, magenta Phase B, green Phase C and blue virtual ground, [$200mV/div$] and [500 $\mu s/div$]

The sensorless methods are fully functional however they both require a minimum motor RPM in order to be able to operate. The threshold RPM was measured to approximately 600 RPM for the method with comparators and roughly 300 RPM for the method which measures the phase potential and virtual motor neutral with analog inputs. The difference between the results is due to that the hysteresis which is set to reduce the impact of noise is not adjustable for the comparators. However the method which uses the ADCs is able to adjust the hysteresis depending on the motor speed which gives the increased performance. When the signal has been sampled it can be digitally filtered which also gives an increased performance. The 300 RPM measurement is presented in Figure 6.10. For light electric vehicles the required initial speed usually is not a problem since it can be supplied by the driver.

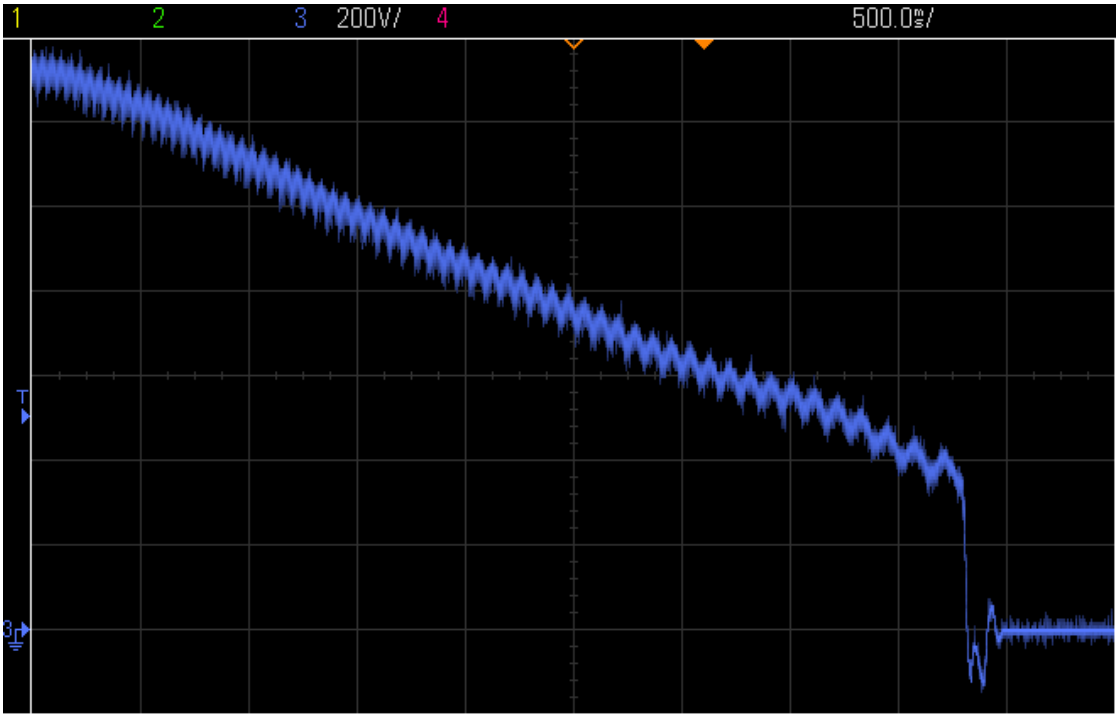

Figure 6.10: Speed [200 RPM/div] versus Time [500 ms/div]

The simulated comparator output signal and the measured comparator output signal presented in Figure 6.11 and Figure 6.12 looks very similar.

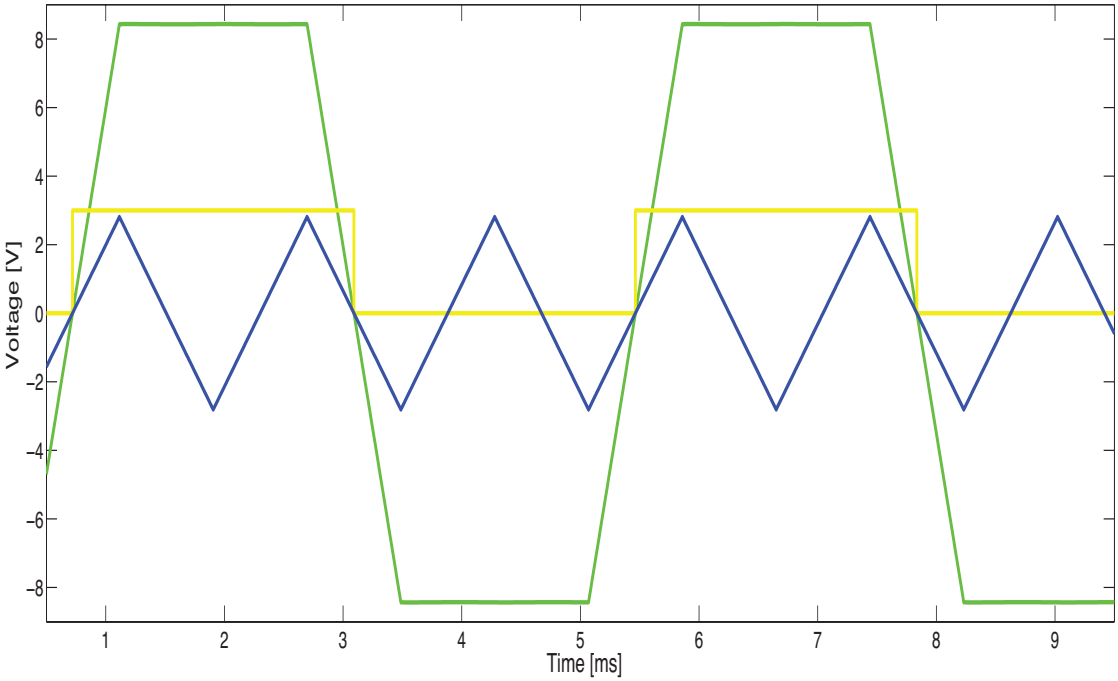

Figure 6.11: Simulated back-EMF in phase C, green, with the comparator output signal, yellow, and the virtual ground, blue

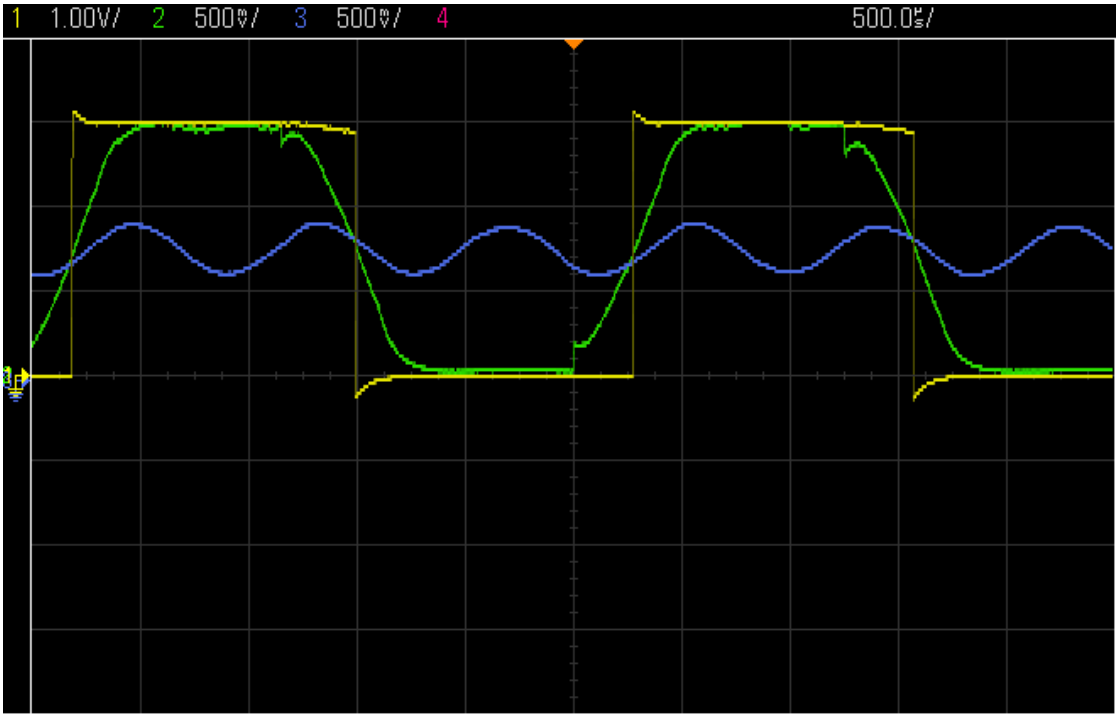

Figure 6.12: Measured phase potential in phase C, green [0.5 V/div], with the comparator output signal, yellow [1 V/div], and the virtual ground, blue [0.5 V/div], at [500 $\mu s/div$]

The comparator triggers correctly when the back-EMF crosses the virtual ground. The same also applies for the two other phases. The three comparator outputs give a similar signal sequence as corresponding hall sensors would.

6.3 Further evaluation

The phase A current during simulated motor operation and motor operation were measured and presented in Figure 6.13 and Figure 6.14. The simulated and the measured current have similar looking shapes.

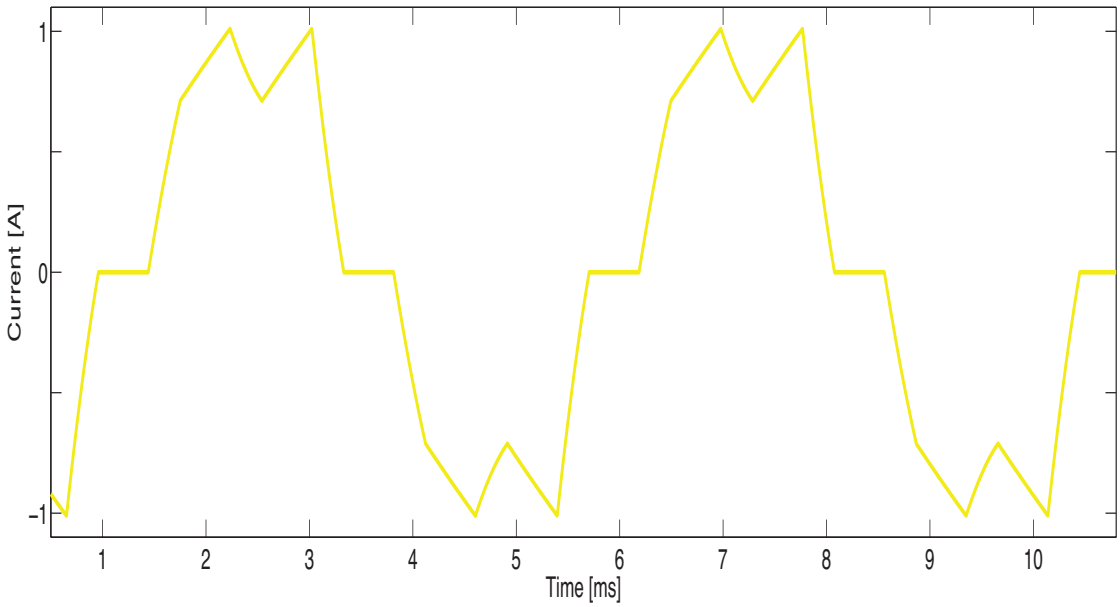

Figure 6.13: Simulated current in phase A

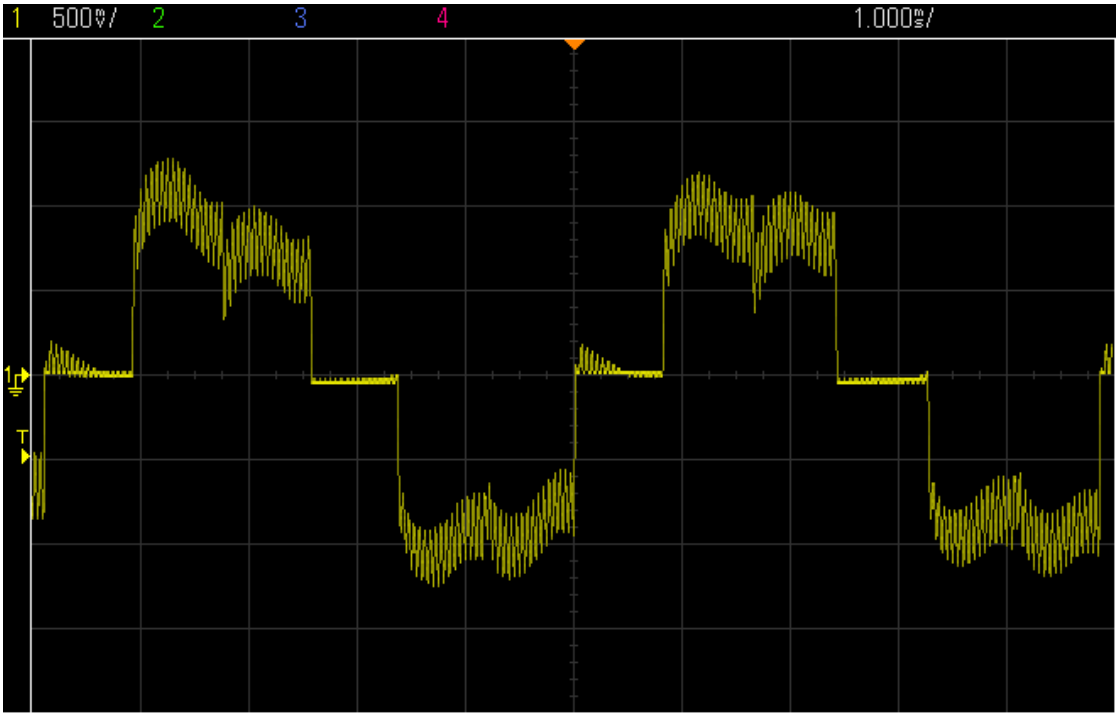

Figure 6.14: Measured current in phase A, 1 V corresponds to 10 A, [500 mV/div] , [ms/div]

The phase currents have a small dip at the top and bottom which is because of the current commutation due to the motor inductance when going from one switching sequence to the other in the three phase inverter. For phase A the positive current dip occurs between switching sequence one and two and the negative current dip occurs between switching sequence four and five from Table 5.3.

The implemented current regulator operates as expected and keeps the current constant when changing loads. Current control is especially well suited for electric vehicles since the current is proportional to the motor torque and thereby gives the driver the same feedback experience as it would from a regular car throttle.

The battery cell protection circuit is verified to be operational with an emulated battery. However a test with a real lithium ion battery with its balance connector connected to the cell protection circuit needs to be conducted in order to fully verify its functionality. A draw back with this circuit is that in its present state it can only handle up to six cells. The circuit solution is also redundant since each of the battery cells uses an analog input; these are usually few and expensive on DSPs. A better solution to this problem would be to use a battery cell monitoring solution that only communicates with the DSP through digital inputs and outputs. If a low manufacturing cost is the prominent design factor then it is possible to measure only a few of the cell voltages which are more likely to suffer from an over- or under- voltage.

7 Closure

This section presents the conclusions as well as introducing some potential future work.

7.1 Conclusion

The thesis purpose was to design and develop a three phase inverter for an ultra-light electric vehicle with sensorless BLDC motor control and to evaluate the result. A three phase inverter has been simulated, designed, built and evaluated. The purpose has been fulfilled since the three phase inverter has been verified to function as intended.

The three phase inverter supports two different sensorless algorithms based on back-EMF measurement as well as support for sensored control. The two sensorless algorithms give similar results however they require different surrounding components as well as DSP inputs. The method using ADCs is preferred in this case since the DSP had ADCs available and it required less surrounding components compared to the one using comparators.

The three phase inverter has been made small enough to fit in an ultra-light vehicle in its present state and is able to independently control a BLDC drive system.

7.2 Future Work

From the knowledge acquired throughout the project there are a lot of design improvements that can be made. One example is using fewer power levels which would make it possible to remove a lot of components and another is only using one position feedback method which also would allow for a smaller design. A DSP with only the necessary functionality and inputs and outputs would also allow for an improved and more efficient design.

Evaluation of the necessary cooling for the MOSFETs remains. Proper measurements could determine if the aluminum PCB is required or if the design could be fitted on only one PCB. This would make it possible to remove all connectors between the two PCBs as well as the extra amplifying stages at the MOSFET gates.

In order to improve the drive system reliability a connector for motor temperature measurement should be implemented. Another cell protection circuit that is able to protect more cells without using any of the ADC inputs should be implemented.

References

[1] S.S Williamson el al., "Comprehensive Drive Train Efficiency Analysis of Hybrid Electric and Fuel Cell Vehicles Based on Motor-Controller Efficiency Modeling," in Transactions on Power Electronics, 2006 , pp. 730-740.

[2] P. Waide and C.U. Brunner, "Energy-Efficiency Policy Opportunities for Electric Motor-Driven Systems," International Energy Agency, France, 2011.

[3] D. Hanselman, *Brushless Permanent Magnet Motor Design*, 2 nd. Ohio: Magna Physics Publishing, 2006.

[4] *AN885 - Brushless DC (BLDC) Motor Fundamentals*, Microchip Technology Inc., Chandler, AZ, 2003.

[5] A. Hughes, *Electric Motors and Drives*, 3 rd. Oxford, Great Britain: Elsevier, 2006.

[6] *AN1083 - Sensorless BLDC Control With Back-EMF Filtering*, Microchip Technology Inc., Chandler, AZ, 2007.

[7] N. Mohan, T.M. Undeland, and W.P. Robbins, *Power Electronics - Converters, Application and Design*, 3 rd. Hoboken: John Wiley and Sons Inc., 2003.

[8] K.A. Coke and S.D. Sudhoff, "A Hybrid Observer for High Preformance Brushless DC Motor Drives," in Transactions on Energy Conversion, 1996, pp. 318-323.

[9] M. Konghirum, "Automatic Offset Calibration of Quadrature Encoder Pulse Sensor for Vector Controlled Drive of Permanent Magnet Synchronous Motors," in TENCON, Melbourne, 2005, pp.1-5.

[10] P. Dwane et al., "A Resonant High Side Gate Driver for Low Voltage Applications," in Power Electronics Specialists Conference, Recife, 2005.

[11] *Bootstrap Component Selection For Control IC's*, International Rectifier, El Segundo, CA, 2001.

[12] S. Baldursson, "BLDC Motor Modelling and Control - A Matlab®/Simulink® Implementation," M.S. thesis, Dept. Elect. Eng., Chalmers Univ., Gothenburg, Sweden, 2005.

[13] P. Suntharalingam el al., "Gear Locking Mechanism to Extend the Consistent Power Operating Region of the Electric Motor to Enhance Acceleration and Regenerative Braking Efficiency in Hybrid Electric Vehicles," in Vehicle Power and Propulsion Conference, Dearborn, MI, 2009, pp.103-108.

[14] L. Balogh, "Design And Application Guide For High Speed MOSFET Gate Drive Circuits," Texas Instruments Inc., 2012.

[15] S.A Hossain and P. Reis, "Effect of BLDC Motor Commutation Schemes on Inverter Power Loss," in International Conference on Electrical Machines, Vilamoura, 2008, pp. 1-5.

[16] S.A Hossain and R. Pedro, "Effect of BLDC Motor Commutation Schemes on Inverter Capacitor Size Selection," in International Conference on Electrical Machines, Rome, 2010, pp. 34-36.

[17] T. Hubing, "PCB EMC Design Guidelines: A Brief Annotated List," in International Symposium on Electromagnetic Compatibility, 2003. 2003.

[18] S. Muralikrishna and S. Sathyamurthy, "An Overview of Digital Circuit Design and PCB Design Guidelines - An EMC Perspective," in Electromagnetic Interference and Compatibility, Bangalore, 2008, pp. 567-573.

[19] J.K Park et al., "Formation of Through Aluminum Via for Noble Metal PCB and Packaging Substrate," in Electronic Components and Technology Conference, Lake Buena Vista, FL, 2011, pp. 1787-1790.

[20] *Thermal Clad - HT-04503*, The Bergquist Company, Chanhassen, MN, 2009.

[21] *TMS320F28335 Digital Signal Controllers - Data Manual*, Texas Instruments Inc., 2012.

A Calculation of Inverter Output Voltage

A.1 Case $60 - 120°$

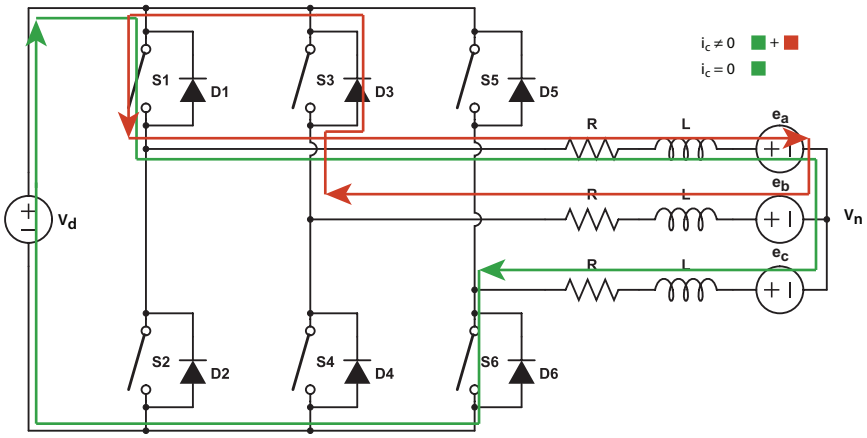

Figure A.1: Current path through the three phase inverter for the interval $60 - 120°$ where the green path represents the current through the active phases and the red path represents the commutating current from the previous switching sequence

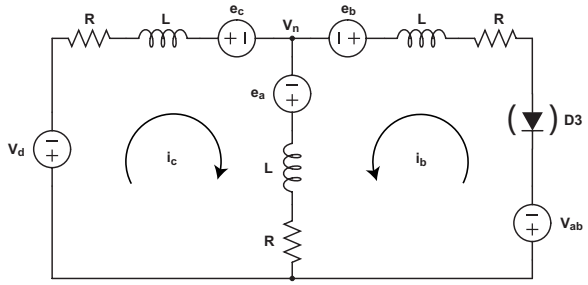

Figure A.2: Circuit topology for the case $60 - 120°$, where V_{bc} represents the voltage over a reversed biased diode

$i_b \neq 0$

$$V_{ab} = 0 \tag{A.1}$$

$$V_{bc} = V_d \tag{A.2}$$

$$V_{ca} = -V_d \tag{A.3}$$

When $i_b = 0$ Kirchhoff's voltage law are applied around each mesh in Figure A.2 to obtain the three phase-to-phase voltages

$$-V_d - Ri_c - L\frac{di_c}{dt} - e_c + e_a - L\frac{d(i_c + i_b)}{dt} - R(i_c + i_b) = 0 \tag{A.4}$$

$$-V_{ab} - Ri_b - L\frac{di_b}{dt} - e_b + e_a - L\frac{d(i_c + i_b)}{dt} - R(i_c + i_b) = 0 \tag{A.5}$$

when $i_b = 0$

$$-V_d - 2Ri - 2L\frac{di}{dt} - e_c + e_a = 0 \tag{A.6}$$

$$-V_{ab} - e_b + e_a - L\frac{di}{dt} - Ri = 0 \tag{A.7}$$

(A.6) and (A.18) gives

$$V_{ab} = \frac{1}{2}(V_d + e_c + e_a - 2e_b) \tag{A.8}$$

so the three phase-to-phase voltages will be

$$V_{ab} = \frac{1}{2}(V_d + e_c + e_a - 2e_b) \tag{A.9}$$

$$V_{bc} = \frac{1}{2}(V_d - e_c - e_a + 2e_b) \tag{A.10}$$

$$V_{ca} = -V_d \tag{A.11}$$

A.2 Case $120 - 180°$

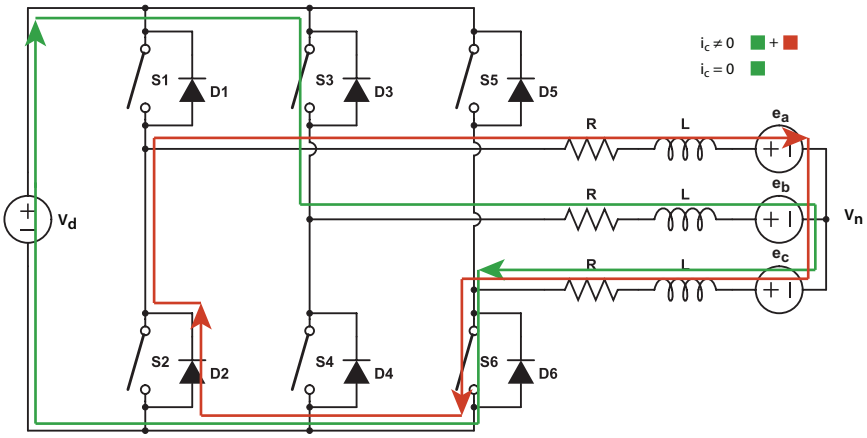

Figure A.3: Current path through the three phase inverter for the interval $120 - 180°$ where the green path represents the current through the active phases and the red path represents the commutating current from the previous switching sequence

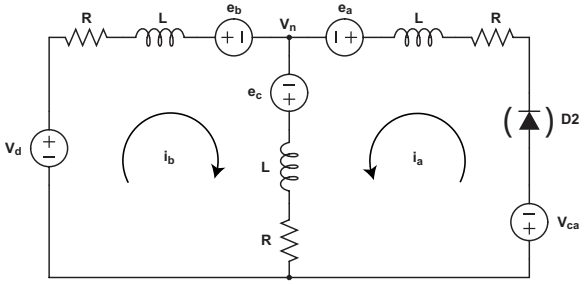

Figure A.4: Circuit topology for the case $120 - 180°$, where V_{bc} represents the voltage over a reversed biased diode

$i_a \neq 0$

$$V_{ab} = -V_d \tag{A.12}$$

$$V_{bc} = V_d \tag{A.13}$$

$$V_{ca} = 0 \tag{A.14}$$

When $i_a = 0$ Kirchhoff's voltage law are applied around each mesh in Figure A.4 to obtain the three phase-to-phase voltages

$$V_d - Ri_b - L\frac{di_b}{dt} - e_b + e_c - L\frac{d(i_b + i_a)}{dt} - R(i_b + i_a) = 0 \tag{A.15}$$

$$-V_{ca} - Ri_a - L\frac{di_a}{dt} - e_a + e_c - L\frac{d(i_b + i_a)}{dt} - R(i_b + i_a) = 0 \tag{A.16}$$

when $i_a = 0$

$$V_d - 2Ri - 2L\frac{di}{dt} - e_b + e_c = 0 \tag{A.17}$$

$$-V_{ca} - e_a + e_c - L\frac{di}{dt} - Ri = 0 \tag{A.18}$$

(A.17) and (A.18) gives

$$V_{ca} = \frac{1}{2}(-V_d + e_b + e_c - 2e_a) \tag{A.19}$$

so the three phase-to-phase voltages will be

$$V_{ab} = \frac{1}{2}(-V_d - e_b - e_c + 2e_a) \tag{A.20}$$

$$V_{bc} = V_d \tag{A.21}$$

$$V_{ca} = \frac{1}{2}(-V_d + e_b + e_c - 2e_a) \tag{A.22}$$

A.3 Case $180 - 240°$

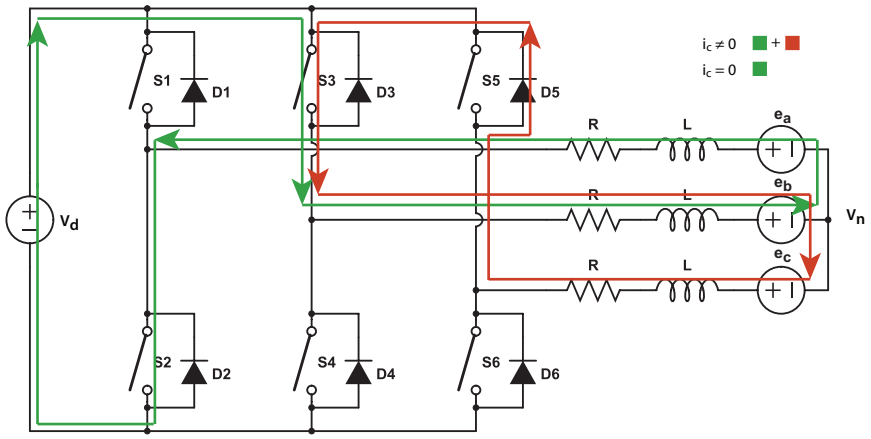

Figure A.5: 1Current path through the three phase inverter for the interval $180 - 240°$ where the green path represents the current through the active phases and the red path represents the commutating current from the previous switching sequence

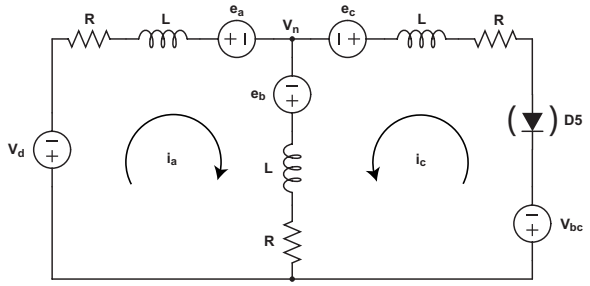

Figure A.6: Circuit topology for the case $180 - 240°$, where V_{bc} represents the voltage over a reversed biased diode

$i_c \neq 0$

$$V_{ab} = -V_d \tag{A.23}$$

$$V_{bc} = 0 \tag{A.24}$$

$$V_{ca} = V_d \tag{A.25}$$

When $i_c = 0$ Kirchhoff's voltage law are applied around each mesh in Figure A.6 to obtain the three phase-to-phase voltages

$$-V_d - Ri_a - L\frac{di_a}{dt} - e_a + e_b - L\frac{d(i_a + i_c)}{dt} - R(i_a + i_c) = 0 \tag{A.26}$$

$$-V_{bc} - Ri_c - L\frac{di_c}{dt} - e_c + e_b - L\frac{d(i_a + i_c)}{dt} - R(i_a + i_c) = 0 \tag{A.27}$$

when $i_c = 0$

$$-V_d - 2Ri - 2L\frac{di}{dt} - e_a + e_b = 0 \tag{A.28}$$

$$-V_{bc} - e_c + e_b - L\frac{di}{dt} - Ri = 0 \tag{A.29}$$

(A.28) and (A.29) gives

$$V_{bc} = \frac{1}{2}(V_d + e_a + e_b - 2e_c) \tag{A.30}$$

so the three phase-to-phase voltages will be

$$V_{ab} = -V_d \tag{A.31}$$

$$V_{bc} = \frac{1}{2}(V_d + e_a + e_b - 2e_c) \tag{A.32}$$

$$V_{ca} = \frac{1}{2}(V_d - e_a - e_b + 2e_c) \tag{A.33}$$

A.4 Case $240 - 300°$

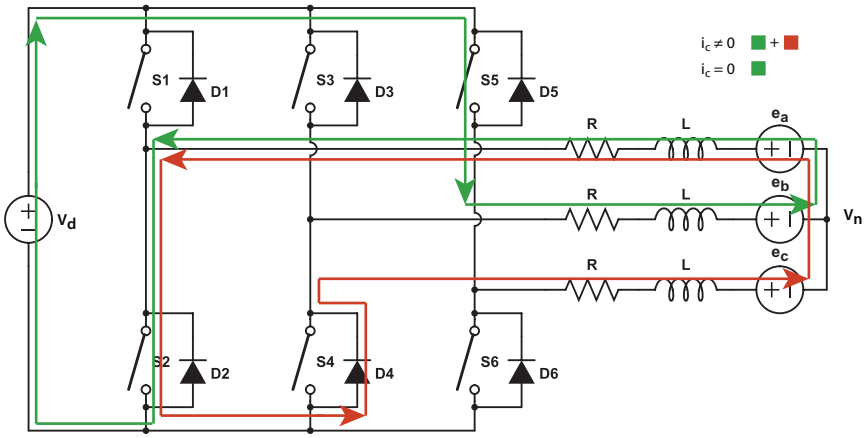

Figure A.7: Current path through the three phase inverter for the interval $240 - 300°$ where the green path represents the current through the active phases and the red path represents the commutating current from the previous switching sequence

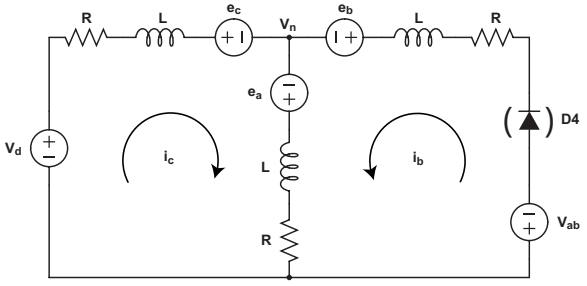

Figure A.8: Circuit topology for the case $240 - 300°$, where V_{bc} represents the voltage over a reversed biased diode

$i_b \neq 0$

$$V_{ab} = 0 \tag{A.34}$$

$$V_{bc} = -V_d \tag{A.35}$$

$$V_{ca} = V_d \tag{A.36}$$

When $i_b = 0$ Kirchhoff's voltage law are applied around each mesh in Figure A.8 to obtain the three phase-to-phase voltages

$$V_d - Ri_c - L\frac{di_c}{dt} - e_c + e_a - L\frac{d(i_c + i_b)}{dt} - R(i_c + i_b) = 0 \tag{A.37}$$

$$-V_{ab} - Ri_b - L\frac{di_b}{dt} - e_b + e_a - L\frac{d(i_c + i_b)}{dt} - R(i_c + i_b) = 0 \tag{A.38}$$

when $i_b = 0$

$$V_d - 2Ri - 2L\frac{di}{dt} - e_c + e_a = 0 \tag{A.39}$$

$$-V_{ab} - e_b + e_a - L\frac{di}{dt} - Ri = 0 \tag{A.40}$$

(A.39) and (A.40) gives

$$V_{ab} = \frac{1}{2}(-V_d + e_c + e_a - 2e_b) \tag{A.41}$$

so the three phase-to-phase voltages will be

$$V_{ab} = \frac{1}{2}(-V_d + e_c + e_a - 2e_b) \tag{A.42}$$

$$V_{bc} = \frac{1}{2}(-V_d - e_c - e_a + 2e_b) \tag{A.43}$$

$$V_{ca} = V_d \tag{A.44}$$

A.5 Case $300 - 360°$

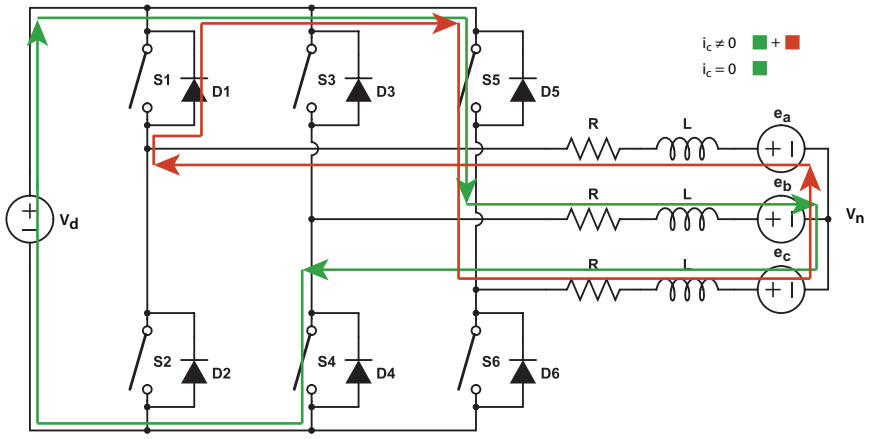

Figure A.9: Current path through the three phase inverter for the interval $300 - 360°$ where the green path represents the current through the active phases and the red path represents the commutating current from the previous switching sequence

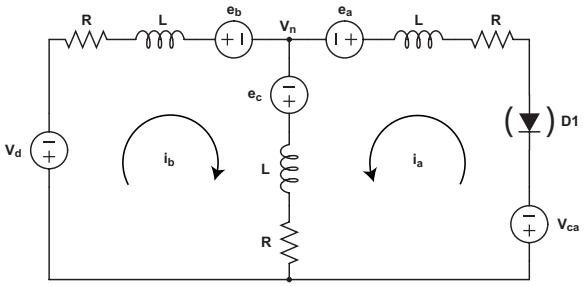

Figure A.10: Circuit topology for the case $300 - 360°$, where V_{bc} represents the voltage over a reversed biased diode

$i_a \neq 0$

$$V_{ab} = V_d \tag{A.45}$$

$$V_{bc} = -V_d \tag{A.46}$$

$$V_{ca} = 0 \tag{A.47}$$

When $i_a = 0$ Kirchhoff's voltage law are applied around each mesh in Figure A.10 to obtain the three phase-to-phase voltages

$$-V_d - Ri_b - L\frac{di_b}{dt} - e_b + e_c - L\frac{d(i_b + i_a)}{dt} - R(i_b + i_a) = 0 \tag{A.48}$$

$$-V_{ca} - Ri_a - L\frac{di_a}{dt} - e_a + e_c - L\frac{d(i_b + i_a)}{dt} - R(i_b + i_a) = 0 \tag{A.49}$$

when $i_a = 0$

$$-V_d - 2Ri - 2L\frac{di}{dt} - e_b + e_c = 0 \tag{A.50}$$

$$-V_{ca} - e_a + e_c - L\frac{di}{dt} - Ri = 0 \tag{A.51}$$

(A.50) and (A.51) gives

$$V_{ca} = \frac{1}{2}(V_d + e_b + e_c - 2e_a) \tag{A.52}$$

so the three phase-to-phase voltages will be

$$V_{ab} = \frac{1}{2}(V_d - e_b - e_c + 2e_a) \tag{A.53}$$

$$V_{bc} = -V_d \tag{A.54}$$

$$V_{ca} = \frac{1}{2}(V_d + e_b + e_c - 2e_a) \tag{A.55}$$

B Control PCB Schematic

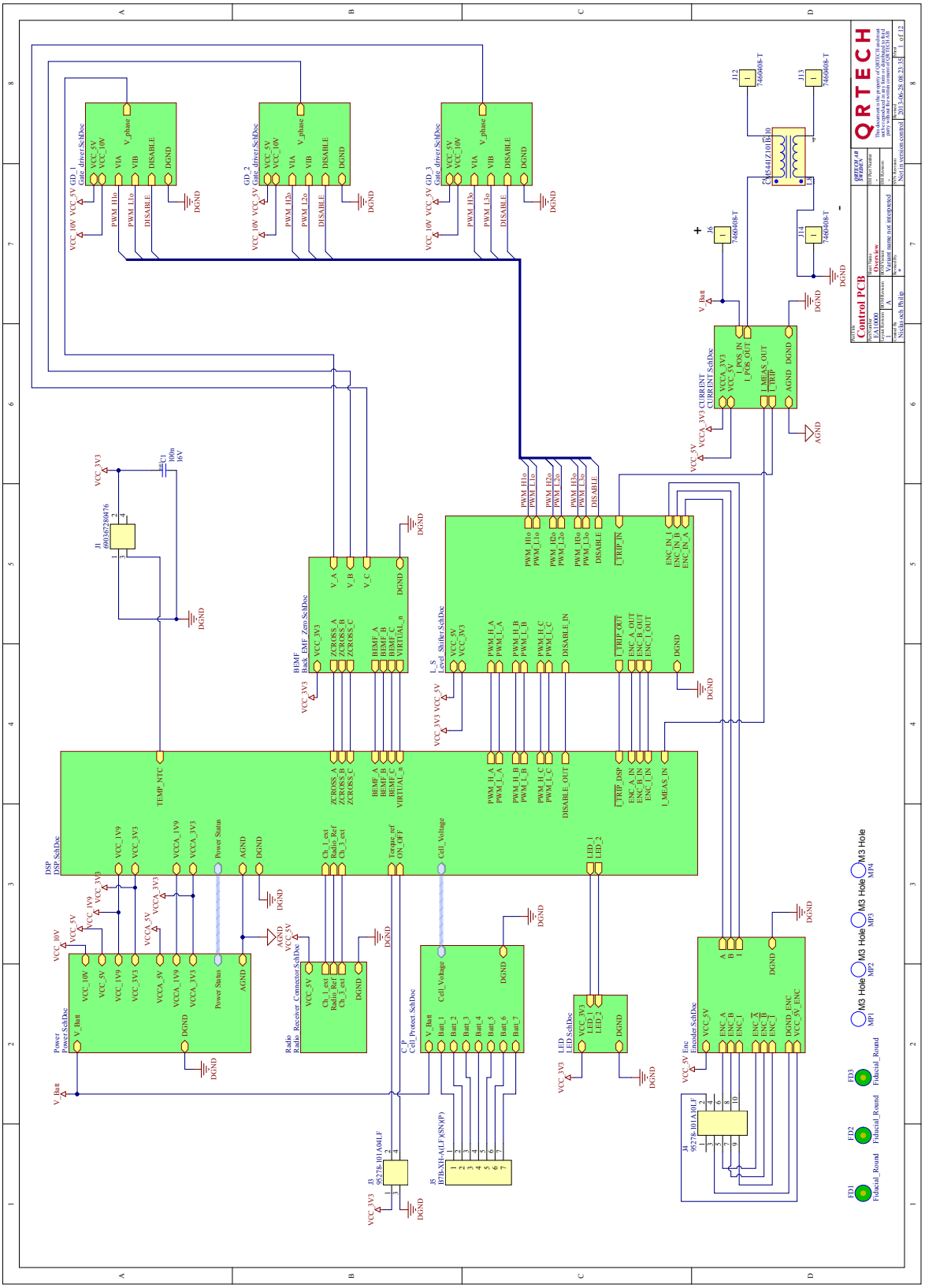

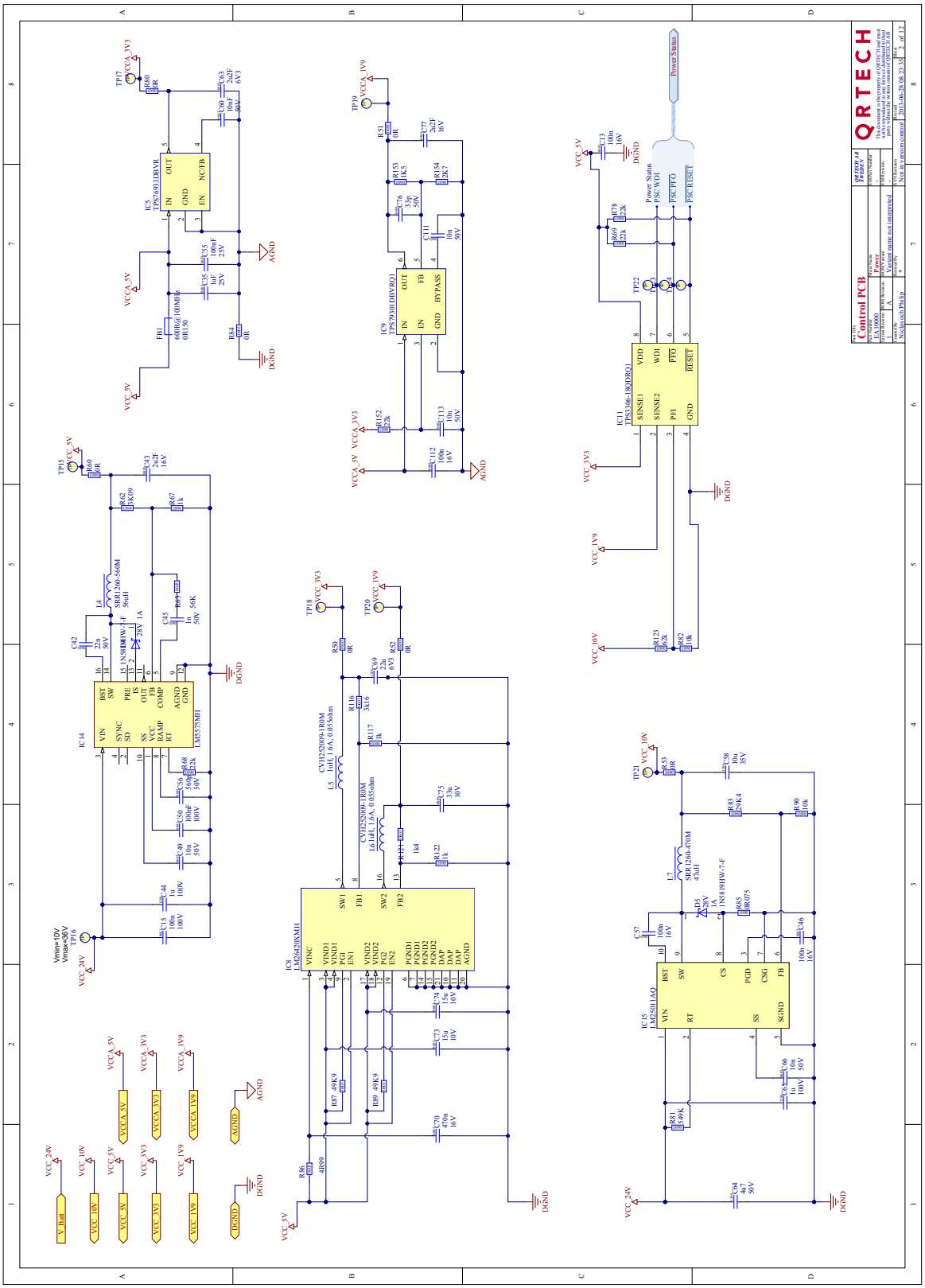
Control PCB
QRTECH
Power Status
VCC_5V
VCC_3V3
VCC_1V9
VCC_10V
VCC_24V
VCCA_5V
VCCA_3V3
VCCA_1V9
DGND
AGND
PSC_WDI
PSC_PFO
PSC_RESET
IC5 TPS7691DBVR
IC9 TPS79301DBVRQ1
IC11 TPS3106-18QDRQ1
IC14 LM5575MH
IC8 LM25620XMH
IC15 LM25011AQ

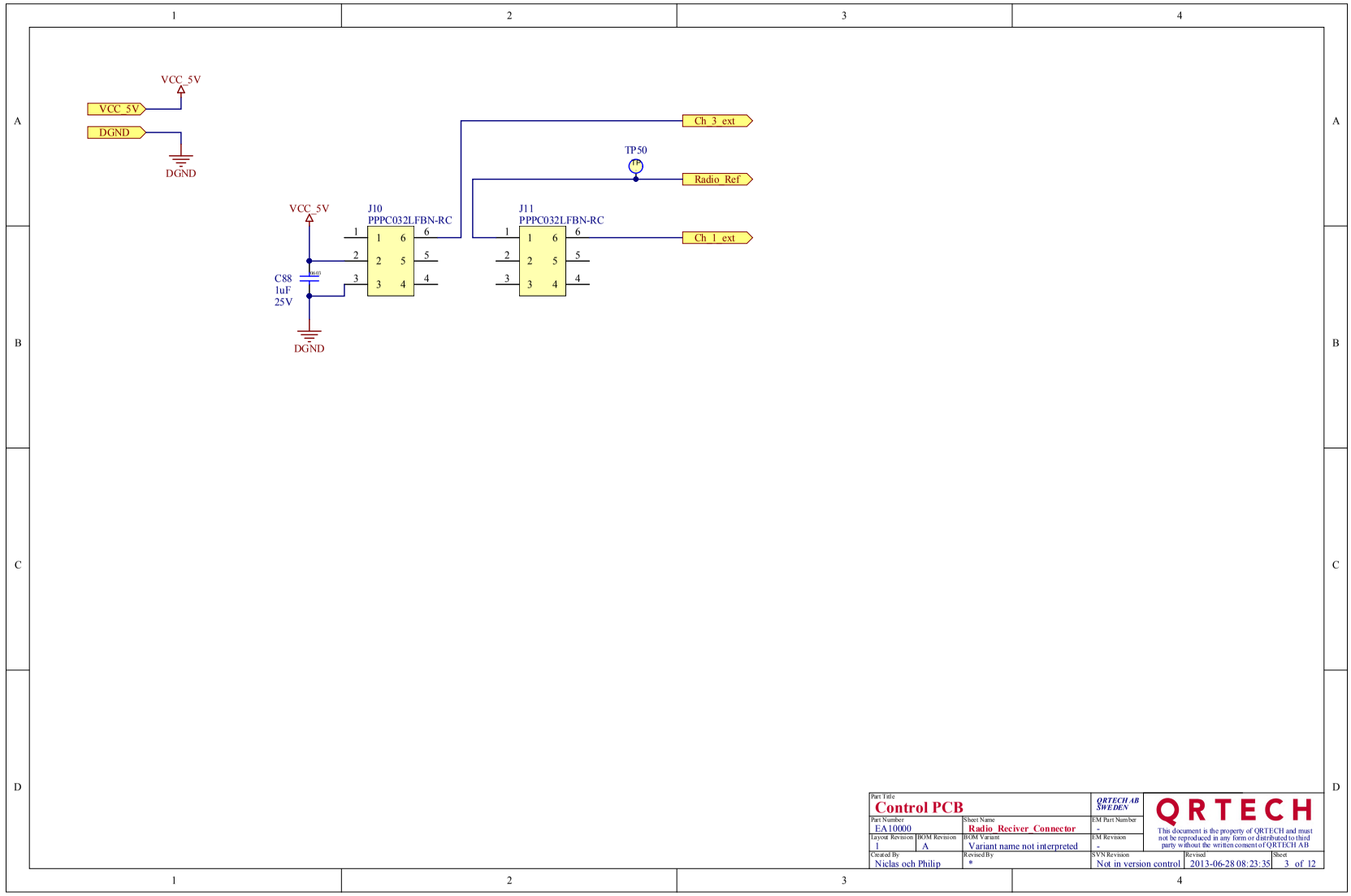
VCC_5V
VCC_5V
DGND
DGND
VCC_5V
J10
PPPC032LFBN-RC
J11
PPPC032LFBN-RC
C88
1uF
25V
DGND
TP50
Ch_3_ext
Radio_Ref
Ch_1_ext
Part Title
Control PCB
QRTECH AB SWEDEN
QRTECH
Part Number
EA10000
Sheet Name
Radio_Reciver_Connector
EM Part Number
-
Layout Revision
1
BOM Revision
A
BOM Variant
Variant name not interpreted
EM Revision
-
Created By
Niclas och Philip
Revised By
*
SVN Revision
Not in version control
Revised
2013-06-28 08:23:35
Sheet
3 of 12
This document is the property of QRTECH and must not be reproduced in any form or distributed to third party without the written coment of QRTECH AB

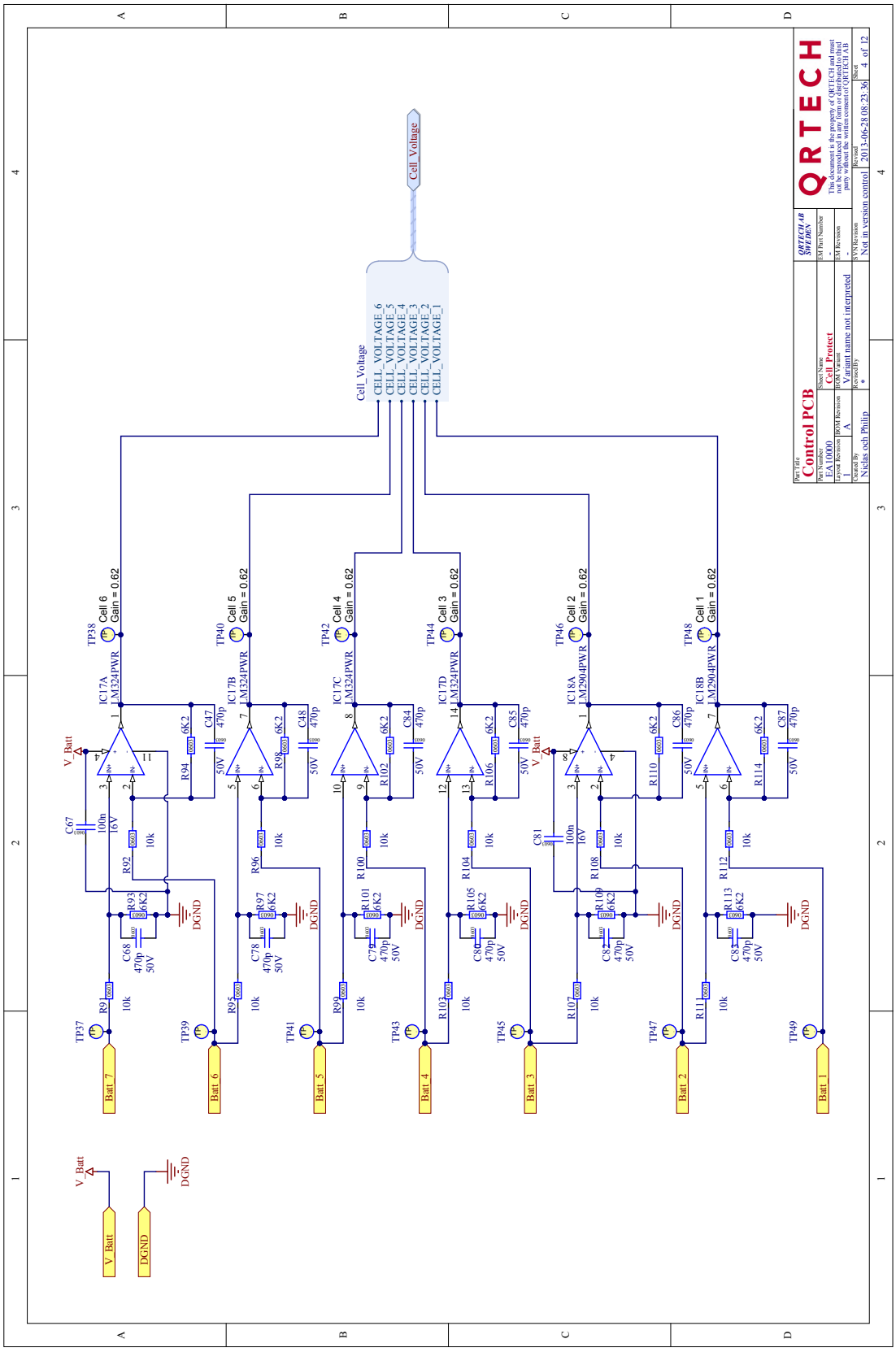
Cell_Voltage
CELL_VOLTAGE_6
CELL_VOLTAGE_5
CELL_VOLTAGE_4
CELL_VOLTAGE_3
CELL_VOLTAGE_2
CELL_VOLTAGE_1
V_Batt
DGND
Batt_7
Batt_6
Batt_5
Batt_4
Batt_3
Batt_2
Batt_1
Cell 6 Gain = 0.62
Cell 5 Gain = 0.62
Cell 4 Gain = 0.62
Cell 3 Gain = 0.62
Cell 2 Gain = 0.62
Cell 1 Gain = 0.62
LM324PWR
LM2904PWR
Part Title
Control PCB
Part Number
EA 10000
Drawn By
Niclas och Philip
Sheet Name
Cell_Protect
Variant name not interpreted
Not in version control
QRTECH
2013-06-28 08:23:36
4 of 12

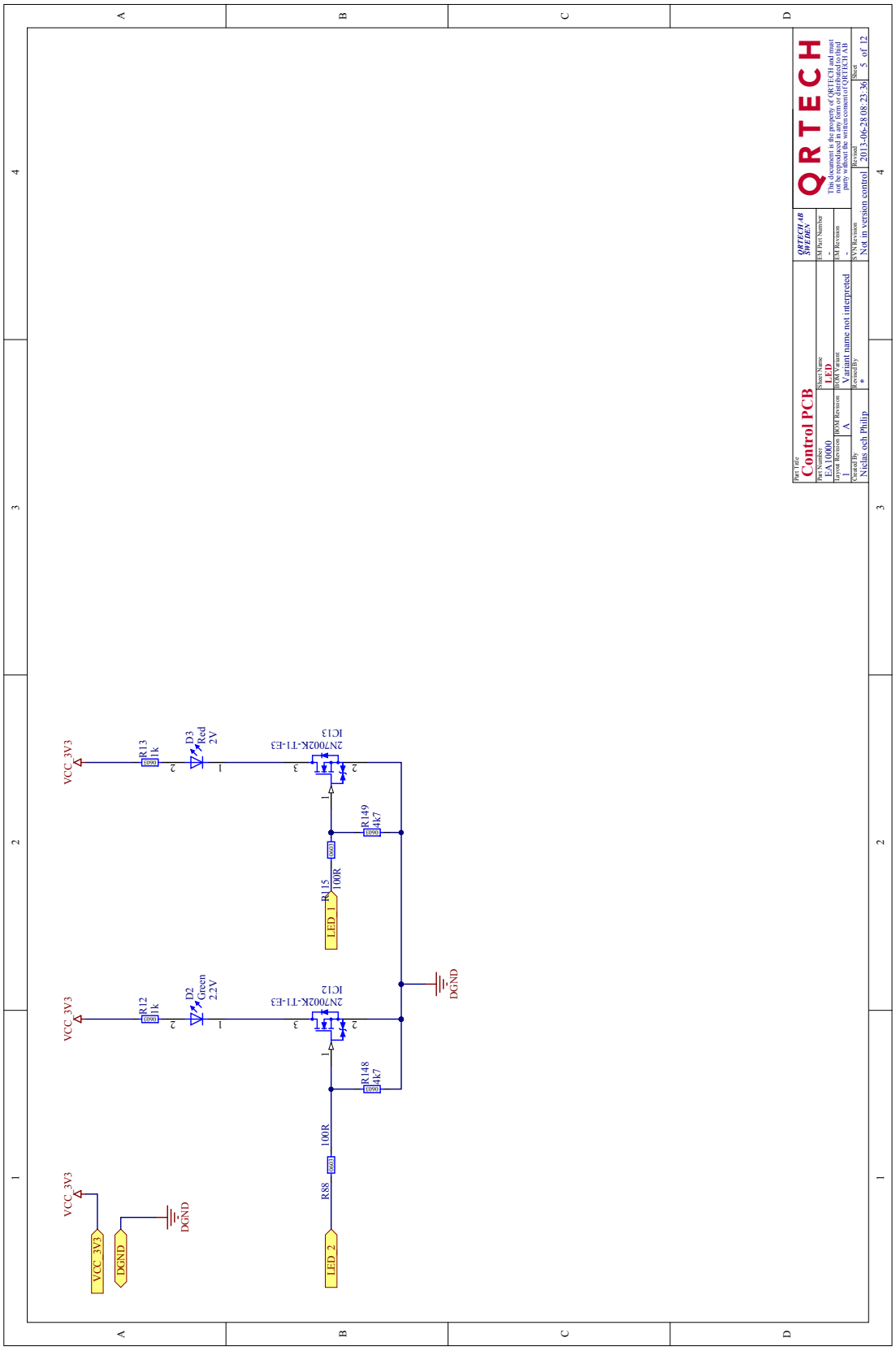
VCC_3V3
R13
1k
D3
Red
2V
IC13
2N7002K-T1-E3
R149
4k7
R115
100R
LED 1
VCC_3V3
R12
1k
D2
Green
2.2V
IC12
2N7002K-T1-E3
R148
4k7
DGND
100R
R88
LED 2
VCC_3V3
VCC_3V3
DGND
DGND
Part Title
Control PCB
Part Number
EA 10000
Layout Revision
1
Created By
Niclas och Philip
Sheet Name
LED
BOM Variante
Variant name not interpreted
BOM Revision
A
RevisedBy
*
QRTECH AB SWEDEN
IM Part Number
-
IM Revision
-
SVN Revision
Not in version control
QRTECH
This document is the property of QRTECH and must not be copied or distributed to any third party without the written consent of QRTECH AB
Revised
2013-06-28 08:23:36
Sheet
5 of 12

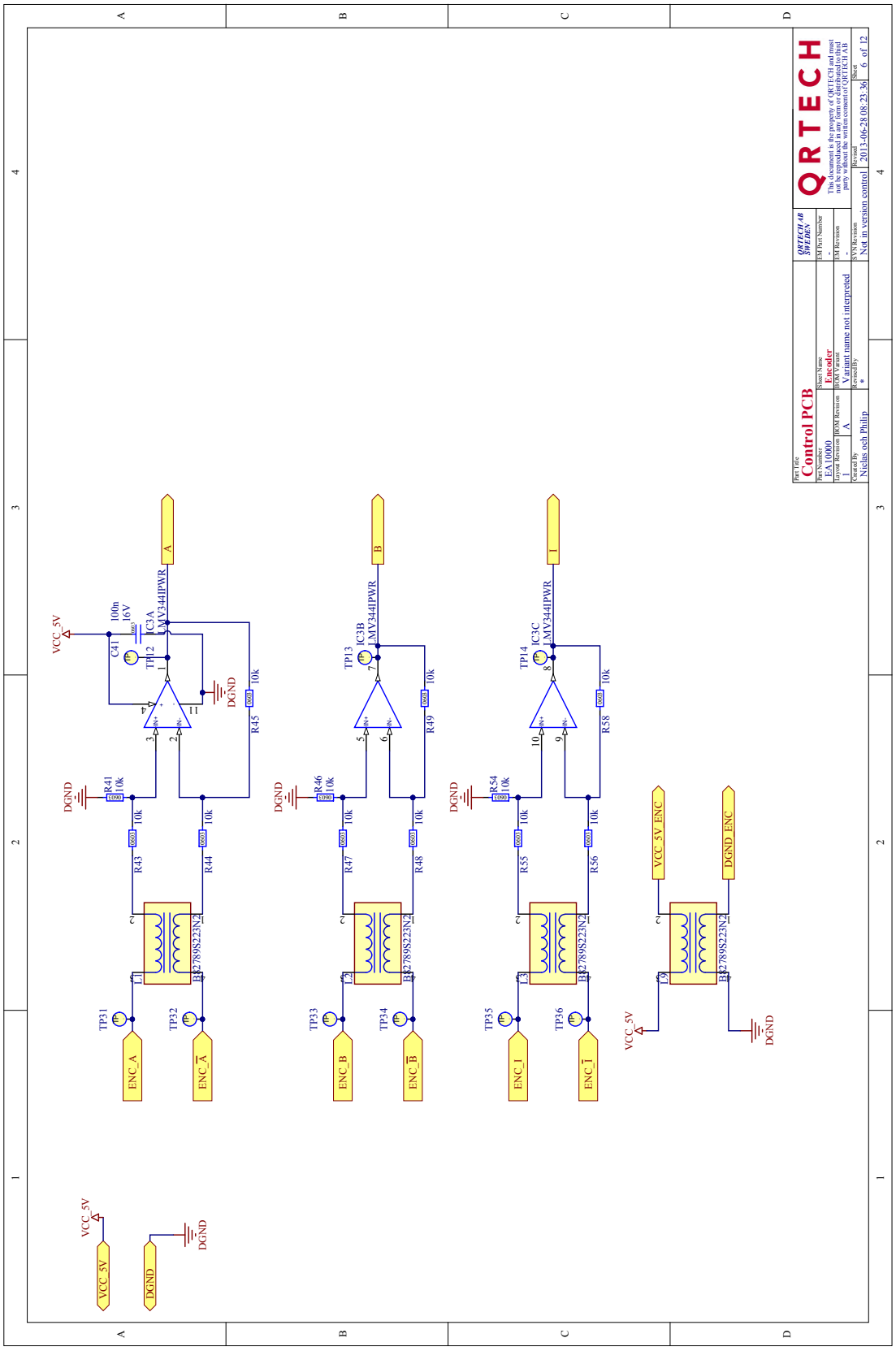
QRTECH
Control PCB
EA 10000
Encoder
Variant name not interpreted
Not in version control
Niclas och Philip
2013-06-28 08:23:36
6 of 12
VCC_5V
DGND
ENC_A
ENC_Ā
ENC_B
ENC_B̄
ENC_I
ENC_Ī
VCC_5V_ENC
DGND_ENC
IC3A LMV344IPWR
IC3B LMV344IPWR
IC3C LMV344IPWR
B82789S223N2
100n 16V
10k

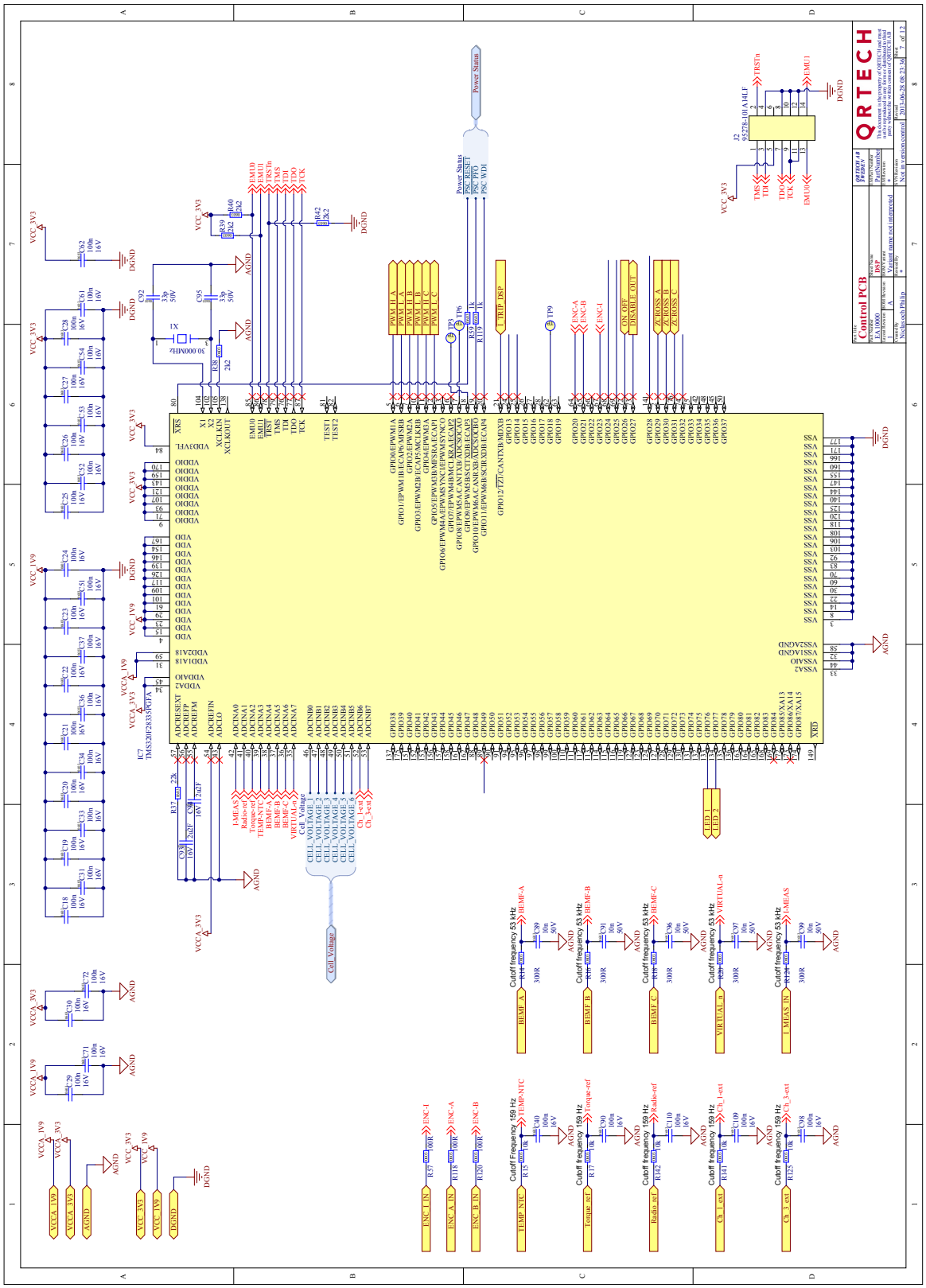
Control PCB
QRTECH
IC7
TMS320F28335PGFA
Cell_Voltage
Power Status
Cutoff frequency 159 Hz
Cutoff frequency 53 kHz
BEMF_A
BEMF_B
BEMF_C
VIRTUAL_n
I_MEAS_IN
TEMP_NTC
Torque_ref
Radio_ref
Ch_1_ext
Ch_3_ext
ENC_A_IN
ENC_B_IN
ENC_I_IN
VCC_3V3
VCCA_3V3
VCC_1V9
VCCA_1V9
AGND
DGND

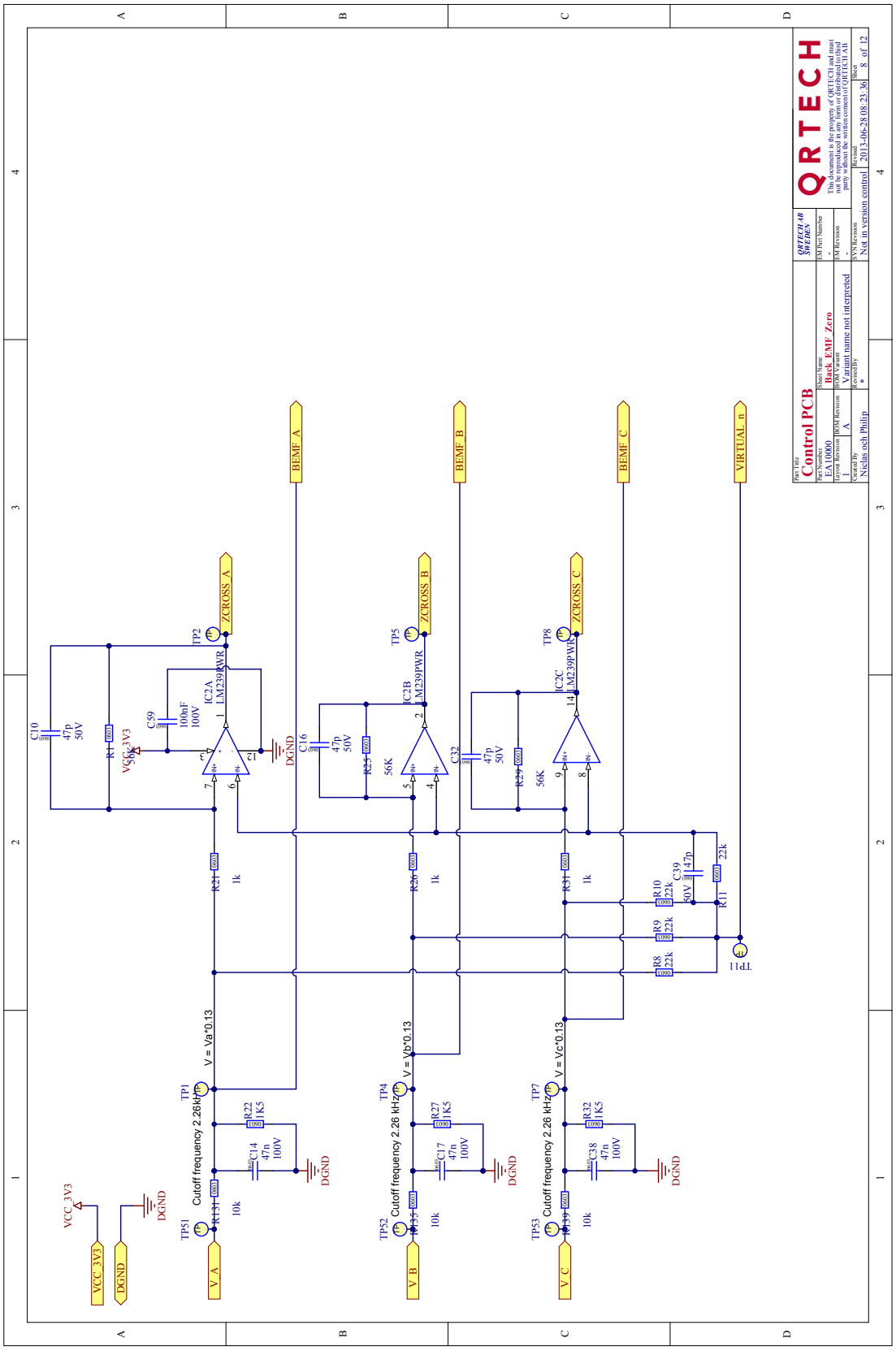
Part Title
Control PCB
Part Number
EA 10000
Layout Revision
1
Created By
Niclas och Philip
IKOM Revision
A
Revised By
*
Sheet Name
Back_EMF_Zero
IKOM Variant
Variant name not interpreted
QRTECH AB SWEDEN
IKM Part Number
IKM Revision
-
SVN Revision
Not in version control
Revised
2013-06-28 08:23:36
Sheet
8 of 12
QRTECH
This document is the property of QRTECH and must not be copied or distributed to any third party or made accessible to third parties without the written consent of QRTECH AB
VCC_3V3
DGND
V_A
V_B
V_C
Cutoff frequency 2.26kHz
V = Va*0.13
V = Vb*0.13
V = Vc*0.13
ZCROSS_A
ZCROSS_B
ZCROSS_C
BEMF_A
BEMF_B
BEMF_C
VIRTUAL_n
IC2A LM239PWR
IC2B LM239PWR
IC2C LM239PWR
R1 56K
R21 1k
R26 1k
R31 1k
R22 1K5
R27 1K5
R32 1K5
R33 10k
R34 10k
R35 10k
R8 22k
R9 22k
R10 22k
R11 22k
C10 47p 50V
C59 100nF 100V
C16 47p 50V
C32 47p 50V
C14 47n 100V
C17 47n 100V
C38 47n 100V
C39 147n 50V
TP1
TP2
TP4
TP5
TP7
TP8
TP51
TP52
TP53
TP11

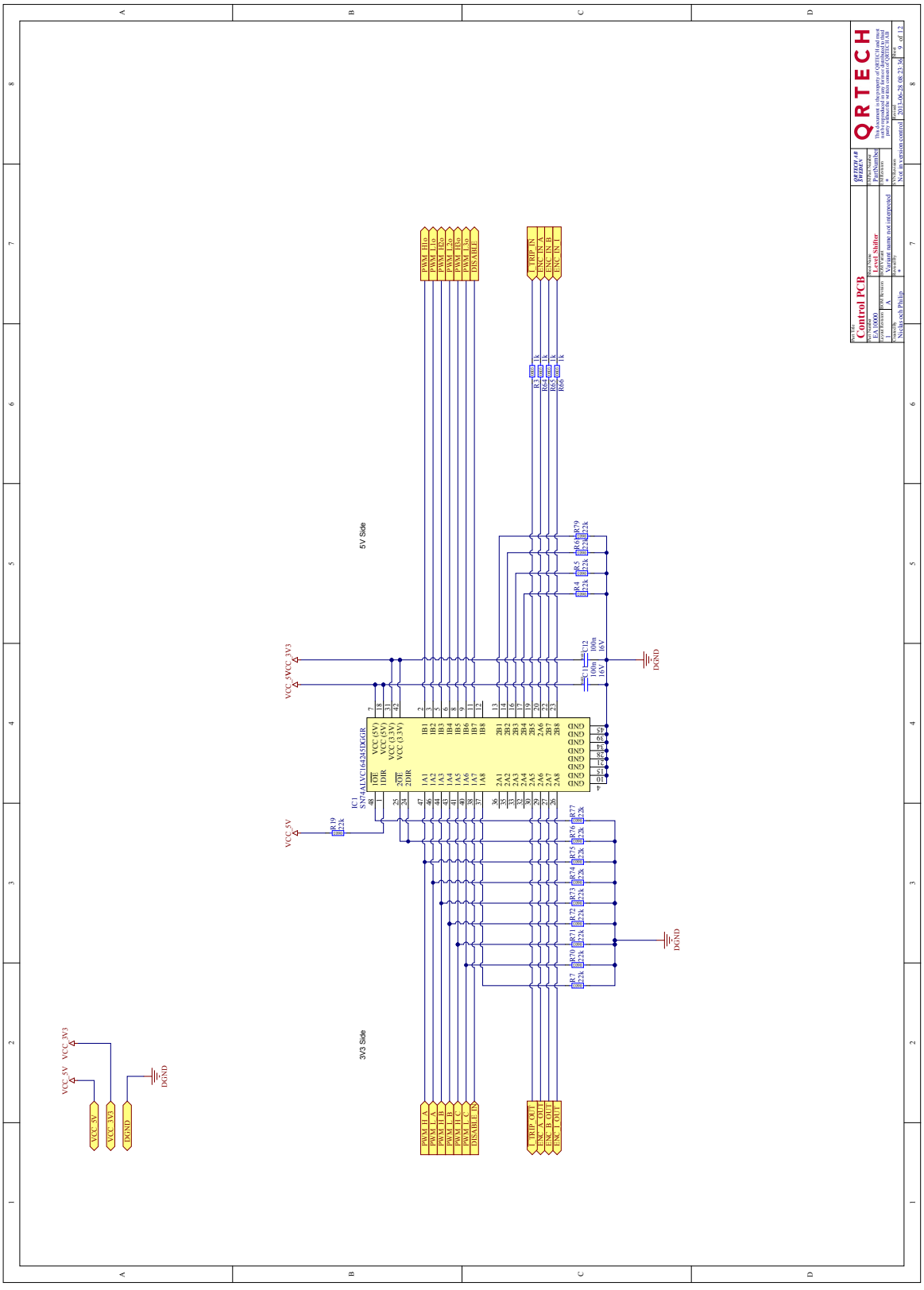
Control PCB
QRTECH
5V Side
3V3 Side
IC1
SN74ALVC164245DGGR
VCC_5V
VCC_3V3
DGND
PWM_H1o
PWM_L1o
PWM_H2o
PWM_L2o
PWM_H3o
PWM_L3o
DISABLE
T_TRIP_IN
INC_IN_A
INC_IN_B
INC_IN_T
PWM_H_A
PWM_L_A
PWM_H_B
PWM_L_B
PWM_H_C
PWM_L_C
DISABLE_IN
T_TRIP_OUT
INC_A_OUT
INC_B_OUT
INC_T_OUT

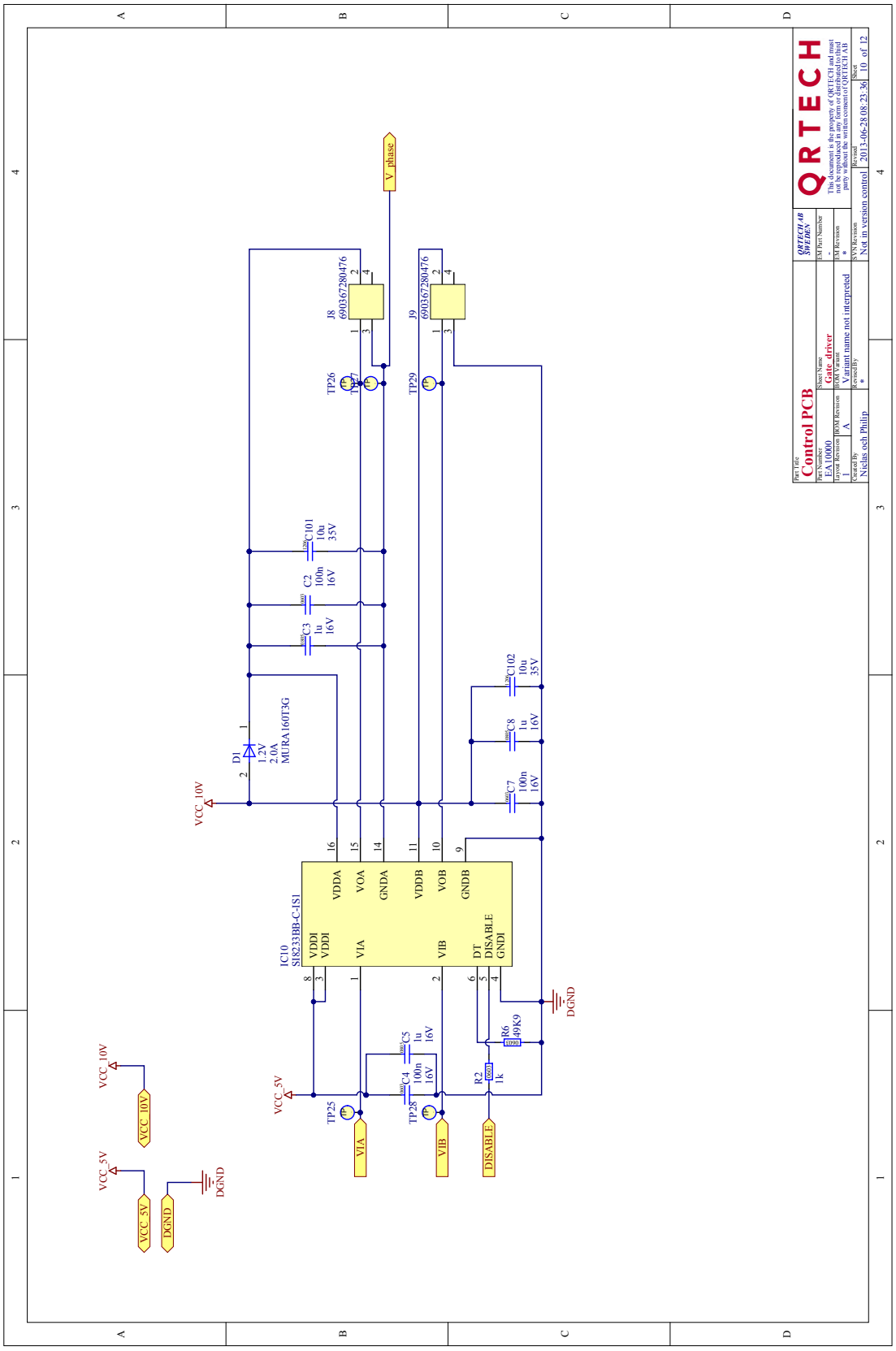
Part Title
Control PCB
Part Number
EA 10000
Layout Revision
1
Created By
Niclas och Philip
QRTECH AB SWEDEN
IM Part Number
IM Revision
A
Revised By
*
Sheet Name
Gate driver
PWA Number
PWA Revision
Variant name not interpreted
SVN Revision
*
QRTECH
This document is the property of QRTECH and must not be copied or disclosed to a third party or used for any purpose without the written consent of QRTECH AB
Revised
2013-06-28 08:23:36
Not in version control
Sheet
10 of 12
V phase
VCC_10V
VCC_5V
DGND
VIA
VIB
DISABLE
J8
69036728047G
J9
69036728047G
TP26
TP27
TP29
TP25
TP28
D1
1.2V
2.0A
MURA160T3G
C101
10u
35V
C2
100n
16V
C3
1u
16V
C102
10u
35V
C8
1u
16V
C7
100n
16V
C5
1u
16V
C4
100n
16V
R2
1k
R6
69K9
IC10
SI8233BB-C-IS1
VDDI
VDDI
VIA
VIB
DT
DISABLE
GNDI
VDDA
VOA
GNDA
VDDB
VOB
GNDB

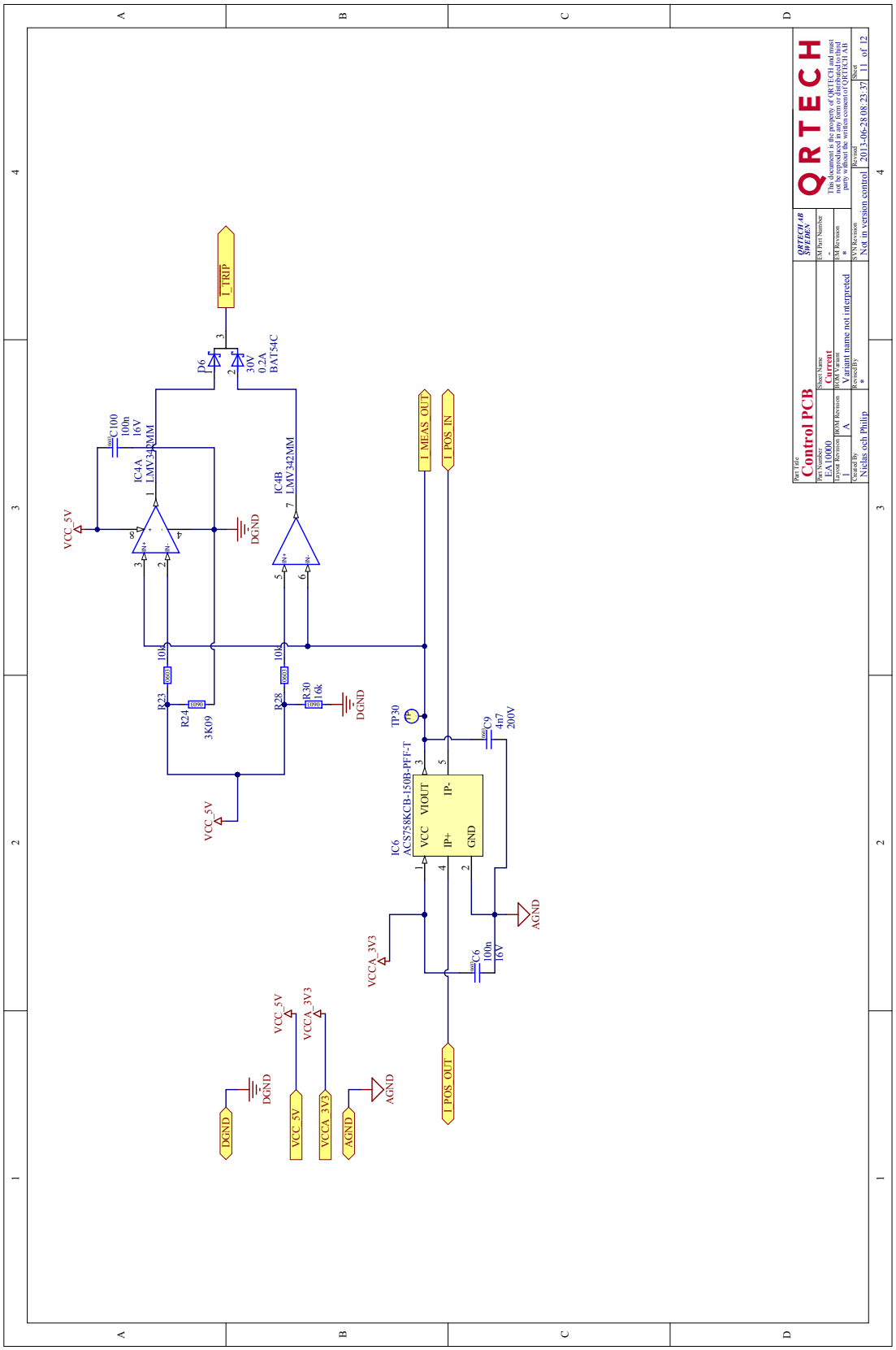
I_TRIP
D6
30V
0.2A
BAT54C
C100
100n
16V
IC4A
LMV342MM
IC4B
LMV342MM
VCC_5V
DGND
I_MEAS_OUT
I_POS_IN
R23
10k
0603
R24
3K09
1%
R28
10k
0603
R30
16k
1%
TP30
IC6
ACS758KCB-150B-PFF-T
VCC
VIOUT
IP+
GND
IP-
C9
4n7
200V
C6
100n
16V
VCCA_3V3
AGND
I_POS_OUT
Part Title
Control PCB
Part Number
EA 10000
Layout Revision
1
Created By
Niclas och Philip
IKM Part Number
IKM Revision
A
Revised By
*
Sheet Name
Current
IKM Revision
Variant name not interpreted
SVN Revision
*
QRTECH AB
SWEDEN
IXM Part Number
IXM Revision
*
SVN Revision
Not in version control
QRTECH
This document is the property of QRTECH and must
not be copied or disclosed to a third party or used for any third
party without the written consent of QRTECH AB
Revised
2013-06-28 08:23:37
Sheet
11 of 12

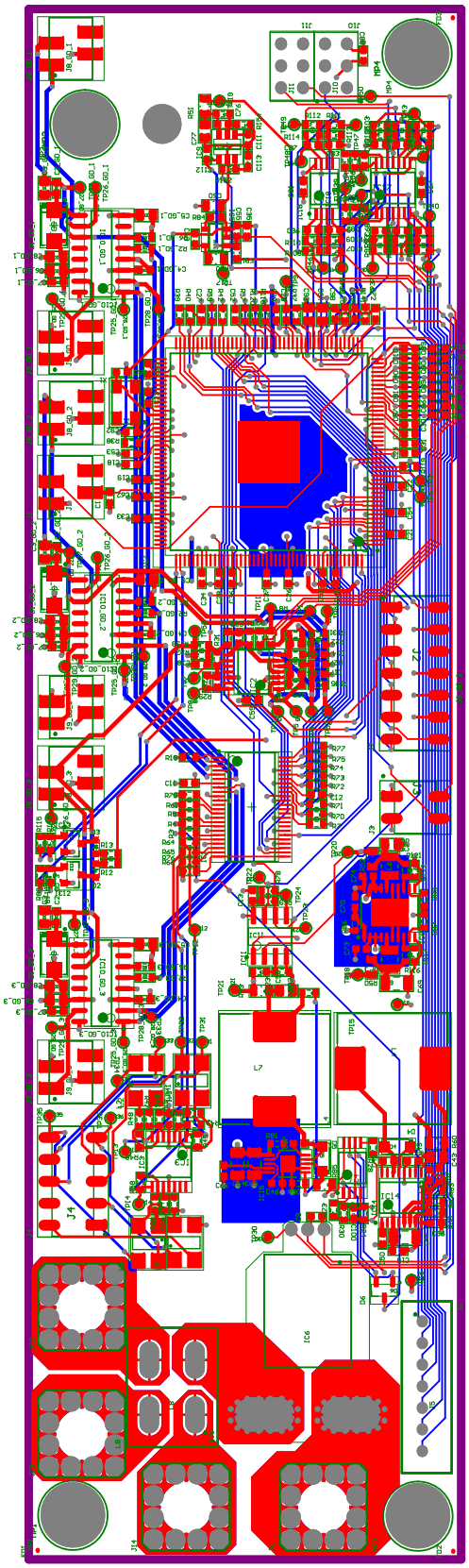

C Power PCB Schematic

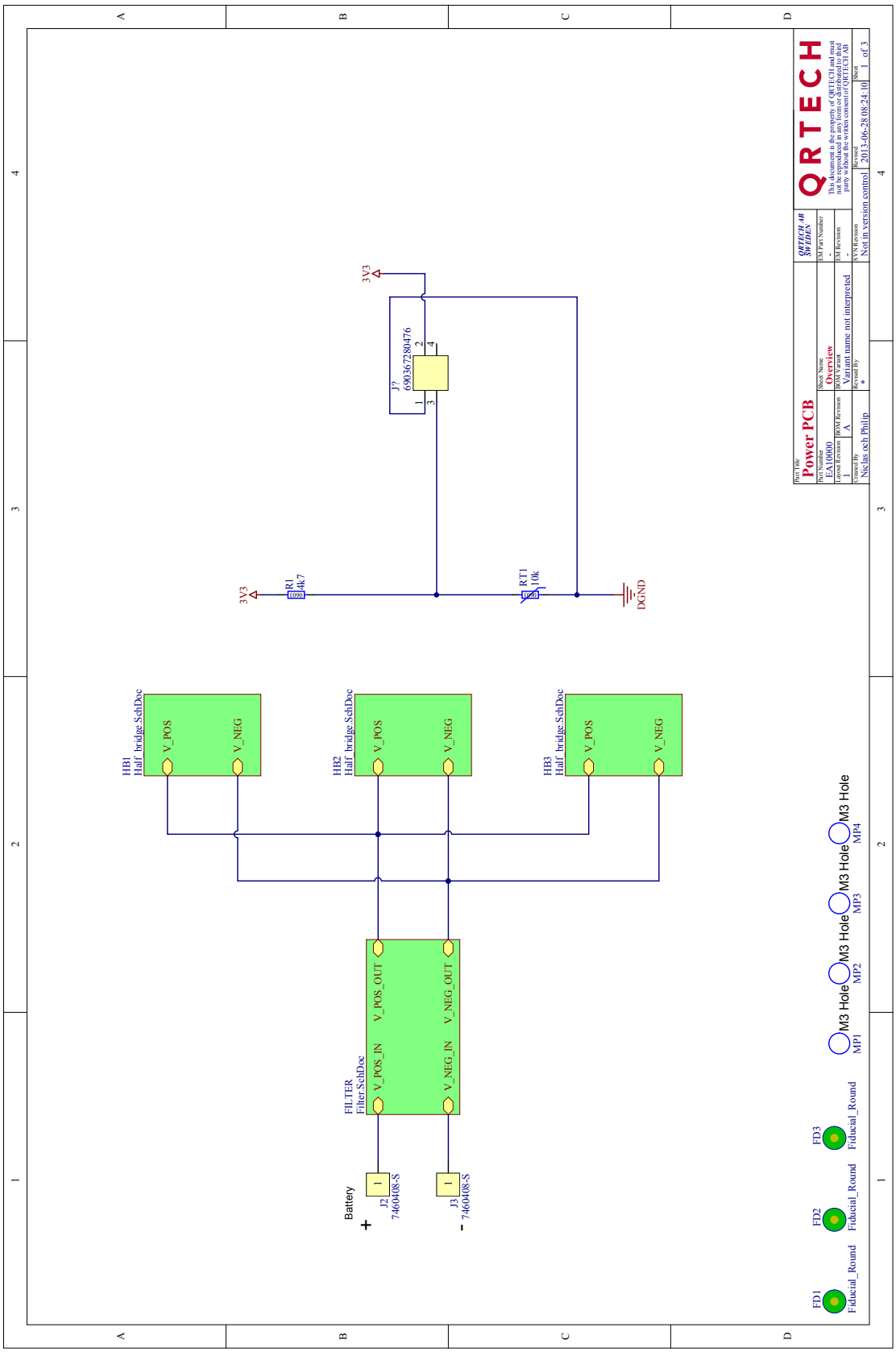

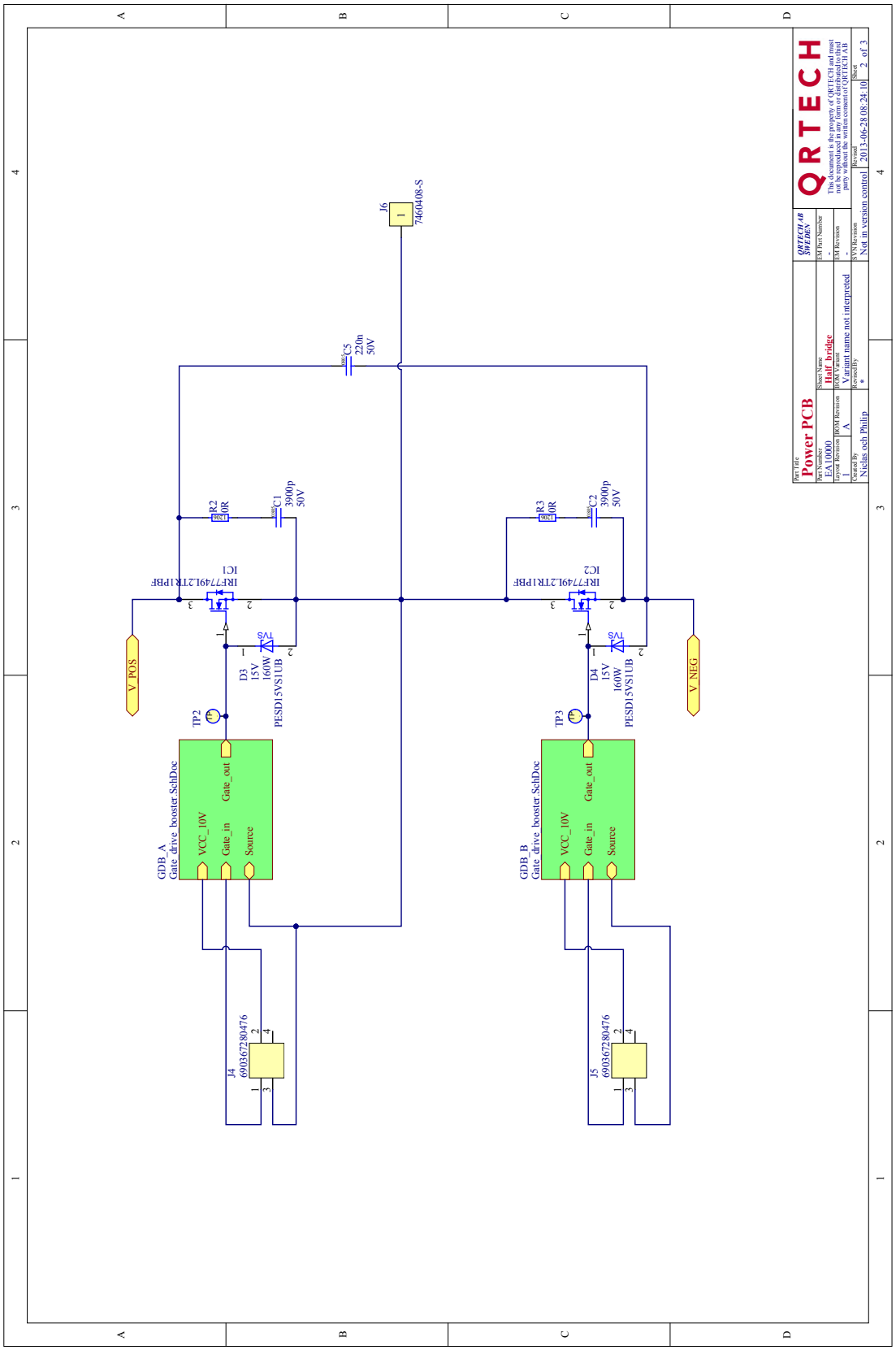
QRTECH
Power PCB
Half_bridge
Variant name not interpreted
Not in version control
2013-06-28 08:24:10
2_of_3
Nielas och Philip
V_POS
V_NEG
J6
74604108-S
C5
220n
50V
R2
10R
C1
3900p
50V
R3
10R
C2
3900p
50V
IC1
IRF7749L2TR1PBF
IC2
IRF7749L2TR1PBF
D3
15V
160W
PESD15VS1UB
D4
15V
160W
PESD15VS1UB
TP2
TP3
GDB_A
Gate_drive_booster.SchDoc
GDB_B
Gate_drive_booster.SchDoc
VCC_10V
Gate_in
Gate_out
Source
J4
690367280476
J5
690367280476

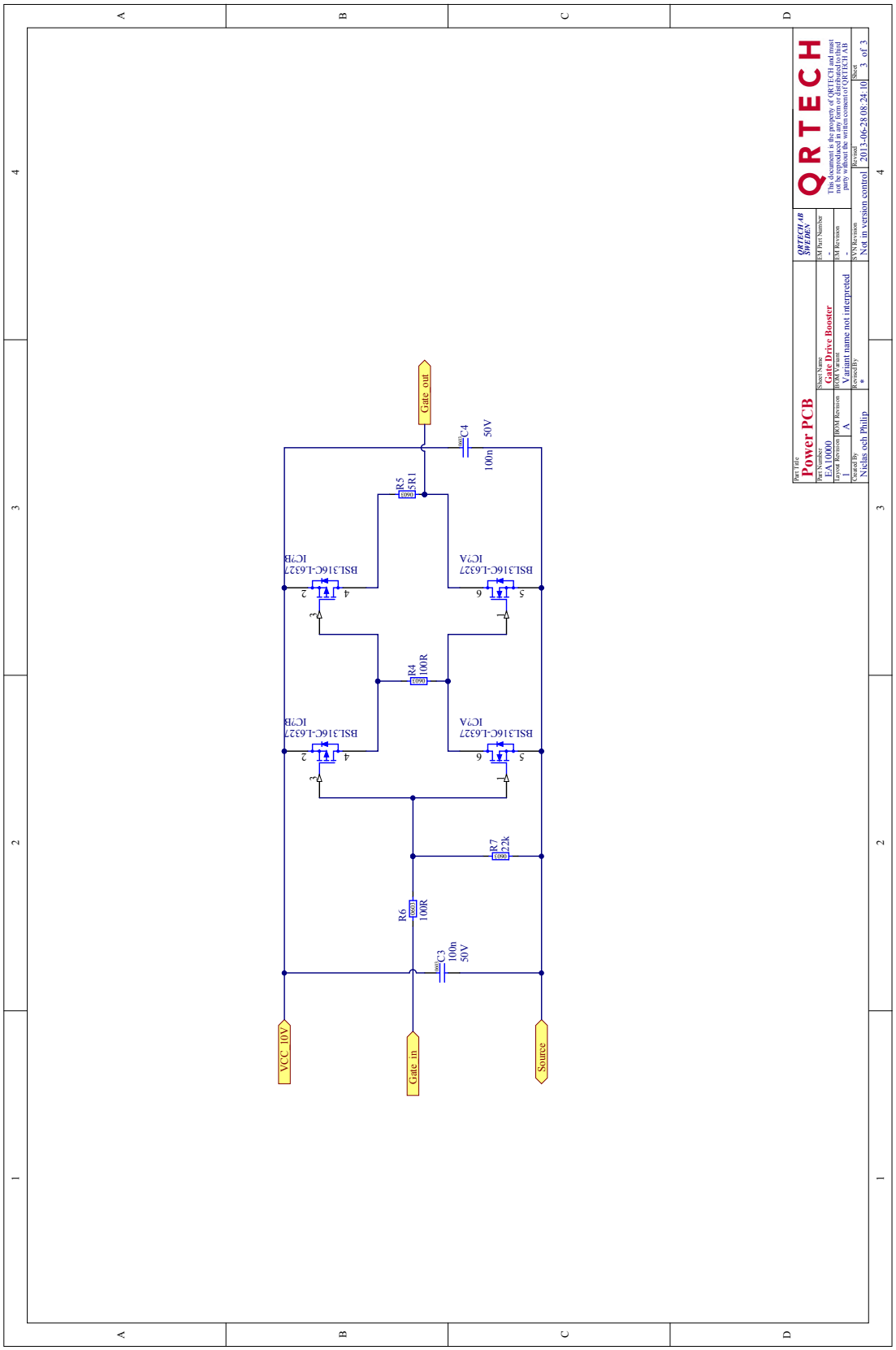
Gate out
C4
100n
50V
R5
5R1
BSL316C-L6327
IC?A
BSL316C-L6327
IC?B
R4
100R
R7
22k
R6
100R
C3
100n
50V
VCC 10V
Gate in
Source
Part Title
Power PCB
Part Number
EA 10000
Last Revision
1
Created By
Niclas och Philip
Sheet Name
Gate Drive Booster
BOM Variant
Variant name not interpreted
BOM Revision
A
RevisedBy
*
QRTECH AB SWEDEN
EM Part Number
EA Revision
-
SVN Revision
Not in version control
QRTECH
This document is the property of QRTECH and must not be copied or distributed to any third party without the written consent of QRTECH AB
Revised
2013-06-28 08:24:10
Sheet
3 of 3

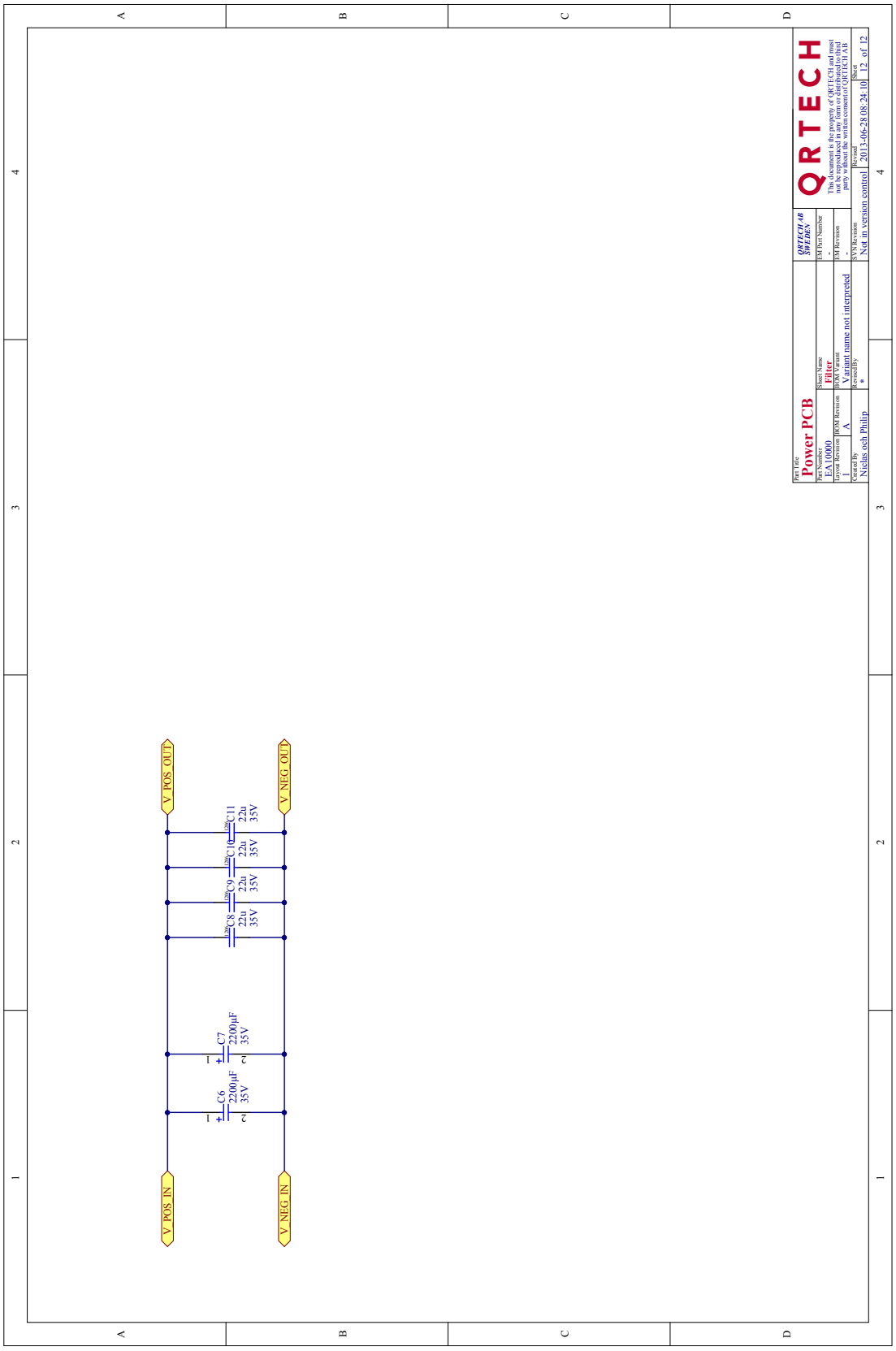
V_POS_OUT
V_NEG_OUT
V_POS_IN
V_NEG_IN
C6
2200µF
35V
C7
2200µF
35V
C8
22u
35V
C9
22u
35V
C10
22u
35V
C11
22u
35V
Part Title
Power PCB
Part Number
EA 10000
Layer Revision
1
IBOM Revision
A
Created By
Niclas och Philip
Sheet Name
Filter
IBOM Variant
Variant name not interpreted
Revised By
*
QRTECH AB SWEDEN
EM Part Number
EA 10000
EM Revision
-
SVN Revision
Not in version control
QRTECH
This document is the property of QRTECH and must not be copied or distributed to any third party without the written consent of QRTECH AB
Revised
2013-06-28 08:24:10
Sheet
12 of 12